ANALYSIS AND SIMULATION OF ACTIVE VIBRATION DAMPENING USING CONSTRAINED MODAL SPACE OPTIMAL CONTROL APPROACH

A Thesis Submitted to the College of

Graduate Studies and Research

In Partial Fulfillment of the Requirements

For the Degree of Masters of Science

In the Department of Mechanical Engineering

University of Saskatchewan

Saskatoon, SK

By

Simon Patrick Woods

PERMISSION TO USE

In presenting this thesis in partial fulfilment of the requirements for a Master's degree from the University of Saskatchewan, I agree that the Libraries of this University may make it freely available for inspection. I further agree that permission for copying of this thesis in any manner, in whole or in part, for scholarly purposes may be granted by the professor or professors who supervised my thesis work or, in their absence, by the Head of the Department or the Dean of the College in which my thesis work was done. It is understood that any copying or publication or use of this thesis or parts thereof for financial gain shall not be allowed without my written permission. It is also understood that due recognition shall be given to me and to the University of Saskatchewan in any scholarly use which may be made of any material in my thesis.

Requests for permission to copy or to make other use of material in this thesis in whole or part should be addressed to:

Head of the Department of Mechanical Engineering

University of Saskatchewan

Saskatoon, Saskatchewan

ABSTRACT

The active vibration attenuation of linearly elastic structures modeled by the finite element method, with a possibly large number of degrees of freedom, is considered. The approach, formulated in modal space, applies mathematical optimization to obtain exact solutions to systems that may involve any number of modes to be controlled by an equal or smaller number of discrete actuators. Such systems are under-actuated and generally involve second-order non-holonomic constraints that impose limitations on the dynamically admissible motions that the system can be made to follow. The approach presented in this thesis has value as a tool for the designing and analyzing active vibration attenuation in structures under idealized conditions, but does not replace traditional control approaches are necessary for practical implementation of such systems.

The optimal attenuation of the structure subject to any initial disturbance is obtained by applying Pontryagin's principle to solve for the minimum solution to a quadratic performance index subject to additional under-actuated constraints that are satisfied by the introduction of time-dependant Lagrange multipliers. The optimality conditions are derived in a compact form and solved by applying symbolic differential operators. The approach uses commercial finite element analysis software and symbolic mathematical software to obtain the optimal actuation forces required by each discrete actuator and the trajectory that the system will undergo.

The approach, which is called the constrained modal space optimal control method involves three primary stages in the solution process. The first stage –the structural stage – involves the transformation of any system modeled by finite elements into a sufficient number of

modal variables and selection of the number and positioning of potential actuator locations. In this stage any problems with poor controllability can be quickly assessed and mitigated prior to proceeding with the next solution stage – the control stage. In the control stage the optimal control problem is solved and all unknown system forces and trajectories are obtained. System gains for the closed loop system can also be obtained in this stage. In the third stage – the verification stage – the actuation forces obtained in the control stage are tested on a transient time-integrated finite element model to evaluate if the system will respond as expected. Any potential spillover effects on higher modes of vibration not considered in the control can be observed in the verification stage.

ACKNOWLEDGMENTS

My heartfelt gratitude goes to my supervisor Dr. Walerian Szyszkowski, for his continuous support in the completion of this thesis. Special thanks to my advisory committee Dr. Reza Fotouhi and Dr. Richard Burton. To all the professors and support personnel in the department of mechanical engineering that have enabled me to complete this work, my sincere thanks.

Thank you to the Department of Mechanical Engineering, the Natural Science and Engineering Research Council (NSERC), and Kova Engineering (Saskatchewan) Ltd. for the scholarships and financial support over the years.

And finally, I must acknowledge the love and encouragement from my family and wife. Their support has been instrumental in the completion of this work.

DEDICATION

This thesis is dedicated to my son

Evan Alexander Woods

TABLE OF CONTENTS

LIST OF FIGURES

LIST OF TABLES

LIST OF ABREVIATIONS

Abbreviation/symbol	Meaning
a	coefficient weighting strain energy in the performance index, or distance
$\boldsymbol{A}$	matrix of modal constraints, $\boldsymbol{A} = [\boldsymbol{A_a} \quad \boldsymbol{A_r}]$
$\overline{\boldsymbol{A}}$	normalized matrix of constraints, $\overline{\boldsymbol{A}} = [\overline{\boldsymbol{A}}_{\boldsymbol{a}} \quad \overline{\boldsymbol{A}}_{\boldsymbol{r}}]$
$\boldsymbol{A_a}$	bottom left sub-matrix of matrix of $\widehat{\boldsymbol{B}}^{-1}$
$\boldsymbol{A_r}$	bottom right sub-matrix of matrix of $\widehat{\boldsymbol{B}}^{-1}$
b	coefficient weighting kinetic energy in the performance index
$\boldsymbol{B}$	actuator configuration matrix
$\widehat{\boldsymbol{B}}$	matrix relating actuators to modal controls
$\overline{\boldsymbol{B}}_{\boldsymbol{a}}$	pseudo-transfer matrix for under-actuated system
$\widetilde{\boldsymbol{B}}_{\boldsymbol{a}}$	top left sub-matrix of matrix of $\widehat{\boldsymbol{B}}^{-1}$
$\widetilde{\boldsymbol{B}}_{\boldsymbol{r}}$	top right sub-matrix of matrix of $\widehat{\boldsymbol{B}}^{-1}$
c	coefficient weighting actuator input energy
$\boldsymbol{C}$	Rayleigh natural damping matrix with component C_{ij}, or sensor positioning matrix
c_{kj}^{i}	integration constant
CMSOC	constrained modal space optimal control
d_i^p	displacement of point p along axis i
D	differential operator
DOF(s)	degree(s) of freedom
E	elastic modulus
$\boldsymbol{E_p}$	matrix differential operator consisting of submatrices $\boldsymbol{E}$, $\breve{\boldsymbol{E}}$, $\widehat{\boldsymbol{E}}$
f	penalty function
f_i	natural frequency
$\boldsymbol{F}$	nodal force vector with components F_i
$\boldsymbol{F_a}$	actuator force vector with components F_{a_i}
$\boldsymbol{F_d}$	vector of dummy actuators
FEM	finite element method
g	gravitational constant
$\boldsymbol{G}$	matrix of gains
$\boldsymbol{G_d}$, $\boldsymbol{G_v}$	gains related to positions and velocities respectively

$\boldsymbol{h}$ ..... vector of constraint equations

H ..... Hamiltonian

$\boldsymbol{I}$ ..... identity matrix

IMSC ..... independent modal space control

J ..... performance index

$\boldsymbol{K}$ ..... stiffness matrix with component K_{ij}

L ..... length

LQR ..... linear quadratic regulator

$\boldsymbol{M}$ ..... mass matrix with component M_{ij}

n ..... number of DOFs

n_a ..... number of actuators

n_c ..... number of constraints

n_m ..... number of modes

n_s ..... number of sensors

n_t ..... number of modes and constraints

$\boldsymbol{P_d}$ ..... vector of costates

$\boldsymbol{P_v}$ ..... vector of costates

$\boldsymbol{q}$ ..... vector of DOFs with components q_i

$\boldsymbol{q_a}$ ..... vector of 'actuated' DOFs

$\boldsymbol{q_c}$ ..... vector of 'constrained' DOFs

$\boldsymbol{q_{int}}$ ..... vector DOFs obtained from direct integration

$\boldsymbol{q_0}$ ..... vector of initial DOFs at $t = 0$

t ..... time

t_{ef} ..... effective settling time

t_f ..... final time

$t_k^{3\%}$ ..... three-percent settling time

Δt ..... time increment

T ..... matrix transpose

$\boldsymbol{U}$ ..... vector of modal controls with components u_i

$\boldsymbol{U_a}$ ..... vector of 'independent' modal controls

$\boldsymbol{U_r}$ ..... vector of 'redundant' modal controls

$\boldsymbol{\nu}$ ..... vector of Lagrange multipliers with components ν_i

$\boldsymbol{Q_d}$ ..... modal weighting matrix with diagonal terms $Q_{d_{ii}}$

$\boldsymbol{Q_v}$ ..... modal weighting matrix with diagonal terms $Q_{v_{ii}}$

r ..... auxiliary variable

r_l ..l-th root of characteristic equation with real component α_k and imajinary component β_k

$\boldsymbol{R}$ ..... modal weighting matrix with diagonal terms R_{ii}

x ..... position from a datum

$\boldsymbol{y}$ ..... output vector

$\boldsymbol{Y}$ ..... vector modal varibles and Lagrange multipliers with components Y_j

$\boldsymbol{z}$ ..... vector of states

$\boldsymbol{\Delta}$ ..... modal natural damping matrix with diagonal terms $\Delta_{ii} = 2\zeta_i\omega_i$

$\boldsymbol{\Phi}$ ..... modal shape matrix involving concatenation of modal shape vectors $\boldsymbol{\phi}_i$

ρ ..... density

λ ..... rate parameter

κ ..... effort parameter

$\boldsymbol{\eta}$ ..... vector of modal variables with components η_i

$\boldsymbol{\eta_a}$ ..... vector of 'independent' modal variables

$\boldsymbol{\eta_r}$ ..... vector of 'redundant' modal variables

θ ..... angle

ξ_k ..... active modal damping ratio of mode k

ω_i ..... frequency of mode i

$\boldsymbol{\Omega}$ ..... diagonal matrix of ordered frequencies

ζ_i ..... passive modal damping ratios for mode i

1. INTRODUCTION

1.1 Motivation

This work aims to formulate and demonstrate a method for analyzing and simulating active control systems for attenuating vibrations in linear elastic structures. These *actively dampened structures* are mechanical systems combining sensors, actuators, and a processor to attenuate the effects of external disturbances as a closed-loop system. Applications for actively dampened structures include: satellites, telescopes, antennas, and other systems that are adversely affected by vibrations and, for practical implementation, cannot be built with sufficient stiffness and/or passive damping properties to keep vibrations to an acceptable level.

Two potential applications for actively dampened structures are shown in Figures 1-1 and 1-2. Figure 1-1 shows an example of a mast type structure that utilizes two piezoelectric actuators located at its base to attenuate vibrations. This type of structure could be implemented to support a vibration sensitive component at its tip. In Chapter 6 the dynamics of this actively controlled structure is considered using the approach presented in this thesis. Figure 1-2 shows a long span cable stayed bridge located in Normandy, France. Due to its length and flexibility, it is vulnerable to wind-induced vibrations and flutter. In [2] it was proposed that the situation could be improved by incorporating active tendons (control cables) in the structure to attenuate the harmful vibrations.

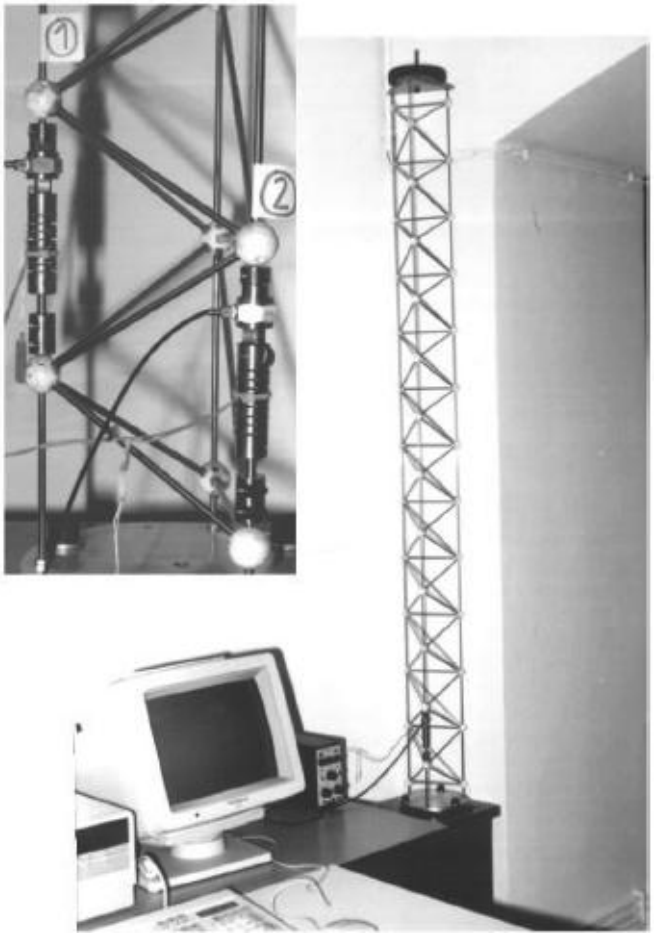

Figure 1-1. Experimental active truss structure at the Free University of Brussels (source: [1]).

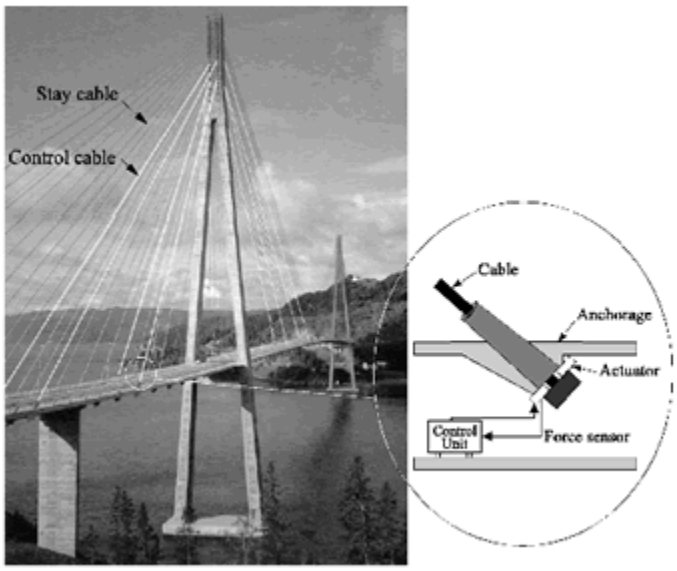

Figure 1-2. Normandy Bridge in France, with proposed active control cables to attenuate wind-induced vibrations (source: [2]).

There are several questions to be considered in the design of actively dampened structures. Some of these include: how many actuators will be required and where should they be located to best attenuate undesired vibrations? What actuation forces will be required to dampen expected disturbances? At what frequencies will the actuators operate and what forces will they produce? How will the active system respond and how quickly will the disturbance be eliminated? Will the actuators alter the passive dynamic properties of the structure or will their actions produce unwanted vibrations in modes not considered in the control? The method presented in this work will address these questions by combining concepts from computational mechanics and mathematical optimization.

The approach in this work is distinct from others published in literature because it applies to general actively dampened systems that are *under-actuated*. Under-actuated systems have more degrees of freedom (DOFs) than actuators to control them [3], meaning that some DOFs are not directly manipulated by an actuator and are referred to as redundant. This property distinguishes them from *fully-actuated* systems which have actuators controlling all DOFs. In under-actuated systems, the motions of redundant DOFs (as well as directly manipulated DOFs) are governed by non-integrable constraints arising from the governing equations of motion. These constraints are non-integrable because they generally involve accelerations and velocities of the DOFs.

In a control analysis, under-actuated systems are more complicated than fully-actuated systems because of the additional non-integral constraints affecting the dynamics. A control analysis requires that the actuation forces producing a desired system trajectory be determined through the *inverse dynamics*, but only trajectories that satisfy the set of non-integrable constraints can be physically realized, or in other words, are *dynamically admissible* [4].

Therefore, a given trajectory may not be dynamically admissible; this limitation complicates the synthesis of the control forces.

In several literature references ([3] and [5] for example) control of under-actuated systems is associated with 'non-minimum phase features' that lead to unbounded behavior. This is mostly due to the inverse dynamics becoming unstable (generating unstable zeros) when attempting to follow desired trajectories that do not satisfy the non-integrable constraints [6]. To avoid the unstable inverse dynamics, so-called 'non-causal' methods were proposed and applied mainly to under-actuated flexible manipulators in [7-9]. These methods appear to have ignored the physical restrictions that the non-integrable constraints represent, leading to violations in the general rules of dynamics. Some under-actuated problems, related mostly to tracking problems, have been analyzed by first eliminating the redundant DOFs and then solving the reduced fully-actuated problem, with a number of actuators controlling the same number of independent DOFs [10-16]. This approach is limited to cases where the elimination of redundant DOFs is possible (exactly or approximately) and typically requires extensive analytical effort.

Theoretically, all actively dampened structures that include continuous elements such as beams, plates, shells and solids are under-actuated systems because they are defined by an infinite number of DOFs. In practice, the dynamics of such systems can be adequately approximated using the modal superposition method where the infinite DOFs are replaced by a handful of *dynamically significant* modes of vibration [17]. This property is exploited in the area of active structures because they typically can be modeled with a small number of modes that can feasibly be controlled by the same number of actuators; hence the non-integrable constraints associated with under-actuated systems are avoided. This approach is referred to as *independent modal space control* (IMSC) and is widely used in research in the area of actively dampened

structures. Its main advantage is that each modal variable is directly related to a corresponding modal control that can be subsequently converted into the actions of properly placed actuators [18]. The methodology presented in this thesis is referred to as *constrained modal space optimal control* (CMSOC) to distinguish it from the IMSC. Most importantly, CMSOC allows the number of modes of vibration included in modeling the system dynamics to be greater than the number of actuators in the system (under-actuated systems) because it accounts for the resulting non-integrable constraints. Since the constraints are always satisfied, the problem of unstable inverse dynamics is eliminated and the stability of the control system is guaranteed.

Using the CMSOC method, solutions for active structures are obtained in the 'output space' with the problem size equal to the number of vibration modes considered. *Dummy actuators*, which produce zero force, are added to the system to make the number of actuators equal to the number of dynamically significant modes instead of attempting to eliminate redundant modes (or redundant DOFs). The dummy actuators are subsequently eliminated by applying the under-actuated constraints, which take a convenient algebraic form when written in terms of modal controls. This algebraic form may be written as a matrix equation from which one can obtain the *matrix of constraints*, which is populated with terms reflecting the system's controllability and attenuation characteristics. The active controls are solved by mathematically formulating the attenuation process as a constrained optimization problem involving a set of time-dependent Lagrange multipliers that ensure all constraints are satisfied. A set of optimality equations are derived that involve all modal variables and Lagrange multipliers and are solved by applying symbolic differential operators to obtain the optimal actuation forces (inputs) and system responses (outputs). Finally, the solution can be verified by directly applying the actuation forces to a transient model of the system, which may contain additional modes not

considered in the control analysis to detect possible *spillover effects* of the controls on these higher modes.

The mathematical foundations for this method were introduced in [19]; however the contribution of this thesis work, some of which is contained in [20-22], was to generalize and formalize the methodology and implement it on a variety of geometrically complex structures. This work studied and formally identified the link between controllability and actuator positioning as well as a formal method of obtaining gains for implementation of a feedback control system. Also, an automated solution program was written in MAPLE to effectively deal with a wide variety of problems that required minimal user input (see Appendix A for example) and a method of verifying the solution using the ANSYS program was successfully implemented on several different examples (see Appendix C).

The CMSOC method is intended to be used as a tool in the design of actively dampened structures as it provides insight that may enable the designer to select good locations for positioning actuators in a given structure. For an idealized structure, information can be obtained on what actuation forces will be required to obtain a target rate of active dampening and how the system will respond. However, the CMSOC method is limited to idealized structures that undergo small displacement vibrations or similar linear motions. It is not a replacement for other control system analysis and design techniques that are essential for practical controls implementation on 'real world' structures, but is rather a complimentary tool for understanding the physical behavior of actively dampened structures, particularly for systems that may be considered under-actuated.

1.2 Outline

The information presented in this thesis is organized as follows:

- Chapter 2 contains the mathematical background related to controlling under-actuated systems and optimal active vibration attenuation.

- Chapter 3 contains the mathematical formulation for CMSOC, including the derivation and solution to the optimality conditions, implementation for closed loop feedback, and discussion on the methodology of the three main stages involved in the procedure.

- Chapter 4 contains an example demonstrating the CMSOC approach on a simple problem involving a gantry crane. The results are compared with those obtained and published in [3] for the same system. Emphasis is given to the individual steps in the solution process and how selection of certain optimization parameters can be expected to alter the system response.

- Chapter 5 contains an example demonstrating the CMSOC approach on a plane frame structure. Emphasis is given to how various actuator configurations and various degrees of under-actuation impact the dynamic response of the system and how controllability problems can be detected early in the solution process. The three main stages of the procedure are covered.

- Chapter 6 contains an example demonstrating the CMSOC approach on a three-dimensional mast problem (model based on that shown in Figure 1-1). Controllability issues are discussed for various configurations and numbers of actuators and their dynamic behavior is compared.

- Chapter 7 contains some general conclusions regarding the CMSOC approach.

2. MATHEMATICAL BACKGROUND

2.1 Control of Under-actuated Systems

Continuous (or discrete) mechanical systems may be represented by a sufficiently large number of n DOFs using the Finite Element Method (FEM) to obtain a model that is governed by a set of second-order differential equations. These equations define the system's dynamics and require that the sum of all inertial, damping, and restoring forces in a system balance the external forces applied to it. Mathematically they take the form:

$$\boldsymbol{M\ddot{q} + C\dot{q} + Kq = BF_a = F} \tag{2.1}$$

Note that equation (2.1) does not include any external disturbing forces acting on the structure as attenuation of free vibrations is of interest. There are n independent equations in (2.1) involving n DOFs that describe the system's motion. The displacements, velocities, and accelerations (or rotation, rotational velocity, and rotational acceleration) of these DOFs are represented by the time varying components contained in the vectors $\boldsymbol{q} = [q_1(t) \quad ... \quad q_n(t)]^T$, $\boldsymbol{\dot{q}} = [\dot{q}_1(t) \quad ... \quad \dot{q}_n(t)]^T$, and $\boldsymbol{\ddot{q}} = [\ddot{q}_1(t) \quad ... \quad \ddot{q}_n(t)]^T$ respectively (the superscript T denotes the matrix transpose operation). From a control perspective, systems described in the form (2.1) contain $2n$ states corresponding to the positions and velocities of each DOF and are contained in state vector $\boldsymbol{z} = [\boldsymbol{q}^T \quad \boldsymbol{\dot{q}}^T]^T$.

Matrices $\boldsymbol{M}$, $\boldsymbol{C}$, and $\boldsymbol{K}$ are of size $n \times n$ with respective components M_{ij}, C_{ij}, K_{ij} ($i = 1, \dots, n$ and $j = 1, \dots, n$) that may generally be state dependent and represent the distribution of masses, natural damping, and stiffness respectively. The nodal force vector

$\boldsymbol{F} = [F_1(t) \quad ... \quad F_n(t)]^T$ contains individual time varying forces F_i that are assigned directly to corresponding DOFs q_i $(i = 1, ..., n)$. The matrix $\boldsymbol{B}$ of size $n \times n_a$ is called the actuator configuration matrix because it assigns n_a discrete actuation forces contained in vector $\boldsymbol{F_a} = \left[F_{a_1}(t) \quad ... \quad F_{a_{n_a}}(t)\right]^T$ to the system of n DOFs as shown on the right hand side of (2.1).

For many practical systems the number of independent actuation forces contained in vector $\boldsymbol{F_a}$ is smaller than the number of DOFs that define the system ($n > n_a$) and so they are considered under-actuated. If the number of independent actuation forces is equal to the number of DOFs ($n = n_a$) then the system is considered fully-actuated. The distinction between these system classifications is of particular importance for control analyses because it affects the steps involved in their solution [4].

Equations of motion in the form (2.1) may be used in calculating the unknown motions described by vector $\boldsymbol{q}$ for a given set of applied forces in vector $\boldsymbol{F_a}$. This calculation is referred to as the *direct dynamics* and is routinely handled by commercial FEM software. Calculating the direct dynamics is straightforward for both under-actuated and fully-actuated systems by using a direct numerical integration method such as the Newmark Procedure [17]. However, a control analysis requires the inverse dynamics solution because the independent applied forces in vector $\boldsymbol{F_a}$ are unknown and their actions, producing a particular system response (described by vectors $\boldsymbol{q}$), are to be determined. As previously mentioned this solution poses a computational challenge for under-actuated systems due to the presence of non-integrable constraints governing possible motions [3].

Inverse dynamics solutions for a fully-actuated systems are straightforward because any desirable trajectories in vector $\boldsymbol{q}$ may be followed provided that it is 'smooth' so it can be differentiated to obtain the corresponding velocities and accelerations in vectors $\dot{\boldsymbol{q}}$ and $\ddot{\boldsymbol{q}}$, which

can be substituted into equations (2.1) to yield required nodal force vector $\boldsymbol{F}$. The vector $\boldsymbol{F}$ can then be transformed into the actuation force vector $\boldsymbol{F_a}$ through the inverse operation on the right hand side of equations (2.1) which takes the form: $\boldsymbol{F_a} = \boldsymbol{B}^{-1}\boldsymbol{F}$. For any fully-actuated system the inverse operation is permissible because $\boldsymbol{B}$ is a square $n \times n$ matrix (provided that $\boldsymbol{B}$ is non-singular).

In contrast, the inverse dynamics solution for under-actuated systems is complicated by $n_c = n - n_a$ additional constraints present in the system (that must be satisfied). For demonstration, consider the two DOFs spring-mass system shown in Figure 2-1. For this particular example, passive damping effects are ignored and the mass and stiffness matrices are assumed constant (independent of states). The governing equations for the system in the form of equation (2.1) are included in Figure 2-1.

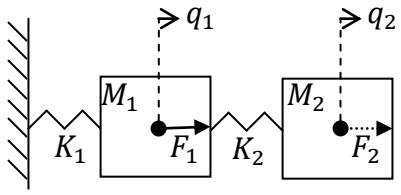

Governing Equations:

$$\begin{bmatrix} M_1 & 0 \\ 0 & M_2 \end{bmatrix}\begin{bmatrix} \ddot{q}_1 \\ \ddot{q}_2 \end{bmatrix} + \begin{bmatrix} K_1 + K_2 & -K_2 \\ -K_2 & K_2 \end{bmatrix}\begin{bmatrix} q_1 \\ q_2 \end{bmatrix} = \begin{bmatrix} F_1 \\ F_2 \end{bmatrix}$$

Figure 2-1. Two-DOF Spring-Mass System.

First consider the fully-actuated case where both F_1 and F_2 are used to perform a maneuver. To calculate the inverse dynamics, any system trajectory, described by vector $\boldsymbol{q} = [q_1(t) \quad q_2(t)]^T$, can be proposed and the corresponding forces in vector $\boldsymbol{F} = [F_1(t) \quad F_2(t)]^T$ can be determined through differentiation and direct substitution into the governing equations (see Figure 2-1). In contrast, if the force F_2 is removed ($F_2 = 0$), then the second row of the governing equations becomes a constraint that limits the set of dynamically

admissible motions described by vector $\boldsymbol{q}$. Only the motions that satisfy this constraint (dynamically admissible motions) can be used to determine the corresponding time varying force F_1. Written explicitly, this constraint on admissible trajectories takes the form:

$$M_2\ddot{q}_2 + K_2(q_2 - q_1) = 0 \tag{2.2}$$

Constraint (2.2) mathematically describes what is intuitively known – that one cannot arbitrarily produce any motion of masses M_1 and M_2 by applying only the force F_1. The motion of the uncontrolled mass M_2 will always be coupled to the motion of the controlled mass M_1 through the equation (2.2). In this example, q_1 is directly controlled by F_1 and so it is considered to be an *actuated* DOF, while q_2 is indirectly controlled and so it is referred to as a *constrained* DOF.

For general under-actuated systems the equations in (2.1) may be grouped and written to distinguish between actuated and constrained DOFs in the form:

$$\begin{bmatrix} \boldsymbol{M_{aa}} & \boldsymbol{M_{ac}} \\ \boldsymbol{M_{ca}} & \boldsymbol{M_{cc}} \end{bmatrix} \begin{bmatrix} \ddot{\boldsymbol{q}}_{\boldsymbol{a}} \\ \ddot{\boldsymbol{q}}_{\boldsymbol{c}} \end{bmatrix} + \begin{bmatrix} \boldsymbol{C_{aa}} & \boldsymbol{C_{ac}} \\ \boldsymbol{C_{ca}} & \boldsymbol{C_{cc}} \end{bmatrix} \begin{bmatrix} \dot{\boldsymbol{q}}_{\boldsymbol{a}} \\ \dot{\boldsymbol{q}}_{\boldsymbol{c}} \end{bmatrix} + \begin{bmatrix} \boldsymbol{K_{aa}} & \boldsymbol{K_{ac}} \\ \boldsymbol{K_{ca}} & \boldsymbol{K_{cc}} \end{bmatrix} \begin{bmatrix} \boldsymbol{q_a} \\ \boldsymbol{q_c} \end{bmatrix} = \begin{bmatrix} \boldsymbol{F_a} \\ \boldsymbol{0} \end{bmatrix} \tag{2.3}$$

The top n_a components of the nodal force vector in (2.3) contain the independent actuation forces in vector $\boldsymbol{F_a}$ and the remaining n_c zero-valued components are contained in the null vector $\boldsymbol{0}$. The vectors of nodal displacements, velocities, and accelerations are grouped so that the top n_a components (considered actuated) contained in vectors $\boldsymbol{q_a}$, $\dot{\boldsymbol{q}}_{\boldsymbol{a}}$, and $\ddot{\boldsymbol{q}}_{\boldsymbol{a}}$ are separated from the bottom n_c components (considered constrained) in vectors $\boldsymbol{q_c}$, $\dot{\boldsymbol{q}}_{\boldsymbol{c}}$, and $\ddot{\boldsymbol{q}}_{\boldsymbol{c}}$ [4]. Referring to the spring-mass system in Figure 2-1, formally $q_1 = \boldsymbol{q_a}$ and $q_2 = \boldsymbol{q_c}$.

Any requested trajectories in vector $\boldsymbol{q} = [\boldsymbol{q}_{\boldsymbol{a}}^T \quad \boldsymbol{q}_{\boldsymbol{c}}^T]^T$ and their corresponding derivatives must satisfy the lower n_c equations in (2.3), and the initial and final boundary conditions, for them to be considered a dynamically admissible. If the solution is dynamically admissible, then

the corresponding actuation forces in vector $\boldsymbol{F_a}$ can be determined. Written explicitly, the constraints from (2.3) take the form:

$$\boldsymbol{h}(\boldsymbol{q}, \dot{\boldsymbol{q}}, \ddot{\boldsymbol{q}}) = \boldsymbol{M_{ca}}\ddot{\boldsymbol{q}}_{\boldsymbol{a}} + \boldsymbol{C_{ca}}\dot{\boldsymbol{q}}_{\boldsymbol{a}} + \boldsymbol{K_{ca}}\boldsymbol{q_a} + \boldsymbol{M_{cc}}\ddot{\boldsymbol{q}}_{\boldsymbol{c}} + \boldsymbol{C_{cc}}\dot{\boldsymbol{q}}_{\boldsymbol{c}} + \boldsymbol{K_{cc}}\boldsymbol{q_c} = \boldsymbol{0} \tag{2.4}$$

The vector of constraints $\boldsymbol{h}$ constitutes a set of n_c equations that contain functions of the positions, velocities, and accelerations of all DOFs; hence they are non-integrable and belong to an extended class of non-holonomic constraints [3]. This means that, in general, equations (2.4) cannot be used to provide a set of equations in the form $\boldsymbol{q_c} = \boldsymbol{f}(\boldsymbol{q_a})$ to eliminate the constrained DOFs in vector $\boldsymbol{q_c}$ so that the applied forces in vector $\boldsymbol{F_a}$ could be obtained from only the top n_a equations in (2.3). Written explicitly, the actuation forces in vector $\boldsymbol{F_a}$ from equations (2.3) take the form:

$$\boldsymbol{F_a} = \boldsymbol{M_{aa}}\ddot{\boldsymbol{q}}_{\boldsymbol{a}} + \boldsymbol{C_{aa}}\dot{\boldsymbol{q}}_{\boldsymbol{a}} + \boldsymbol{K_{aa}}\boldsymbol{q_a} + \boldsymbol{M_{ac}}\ddot{\boldsymbol{q}}_{\boldsymbol{c}} + \boldsymbol{C_{ac}}\dot{\boldsymbol{q}}_{\boldsymbol{c}} + \boldsymbol{K_{ac}}\boldsymbol{q_c} \tag{2.5}$$

The objective in control design is to determine the actuation forces in vector $\boldsymbol{F_a}$ that will produce a system trajectory $\boldsymbol{q}$ that satisfies all constraints in vector $\boldsymbol{h}$ as well as the initial and final boundary conditions. However, a potentially infinite number of trajectories and the corresponding actuation forces can be generated to meet this objective. The *optimal* control aims at selecting one trajectory that satisfies a more specific objective, which can be found by applying mathematical optimization techniques. The mathematical objective of the CMSOC methodology is to obtain a unique solution for all trajectories in vector $\boldsymbol{q}$ and control forces in vector $\boldsymbol{F_a}$ that will minimize a selected quadratic performance index and be dynamically admissible (i.e. satisfying equation (2.4)). Selecting 'desirable' trajectories becomes a matter of weighting and selection of various performance index parameters (penalty functions) relating to

the systems energy, control effort, or the error between requested trajectories and the 'closest' dynamically admissible ones [4].

A typical performance index incorporates a penalty function f such as:

$$J = \int_{t_1}^{t_2} f(\boldsymbol{q}, \dot{\boldsymbol{q}}, \boldsymbol{F}))dt \rightarrow min \tag{2.6}$$

The penalty function f (quadratic in terms of $\boldsymbol{q}$, $\dot{\boldsymbol{q}}$, and $\boldsymbol{F}$) may be chosen to obtain system trajectories that minimize control input energy, reduce potential energy and/or kinetic energy levels, minimize control time, and/or minimize deviations from a particular reference trajectory. The issue of the dynamically admissibility of requested trajectories is mathematically handled in the optimization procedure. In this thesis, such optimization-based methods of dealing with under-actuated problems are applied to simulate and analyze active vibration attenuation in geometrically complex linear elastic structural systems modeled by the FEM.

2.2 Optimal Active Vibration Attenuation

The objective in optimal active vibration control is to actively dampen, or attenuate, vibrations in structural systems using a finite, and possibly *small*, number of actuators, or active members. Typical structures are composed of continuous members, such as beams, columns, plates, and shells that are comprised of a theoretically infinite number DOFs. Using FEM such systems are accurately simulated using a finite, but often *large* number of DOFs that are governed by equations of motion of the form (2.1). The direct dynamics calculation for systems with a large number of DOFs is routinely handled by commercial FEM software; however, it may become increasingly numerically complex with an increasing number of DOFs. Fortunately, the motion of linear elastic structural models can be simplified by transforming the problem from a vector-space containing a large number of DOFs to a reduced space containing only a handful

of modes of vibration. This can be done through a routine modal analysis as presented later in this section [17].

Graphically, the task of vibration control for systems approximated by n equations (2.1) is represented in Figure 2-2, which shows the system brought from some disturbed non-zero initial state to the origin and at rest. Note that the path along which the system is brought to rest is not prescribed, but it must be dynamically admissible. The disturbed structure is described by the $2n$ initial conditions in the form of displacements $\boldsymbol{q_0}$ and velocities $\dot{\boldsymbol{q}}_{\boldsymbol{0}}$ at time $t = 0$. By time $t = t_f$ (where t_f is the maneuver time) all disturbances are attenuated. Mathematically, the initial and final boundary conditions shown in Figure 2-2 are written in the form:

$$\boldsymbol{q}(0) = \boldsymbol{q_0},\ \dot{\boldsymbol{q}}(0) = \dot{\boldsymbol{q}}_{\boldsymbol{0}},\ \boldsymbol{q}(t_f) = \mathbf{0},\ \dot{\boldsymbol{q}}(t_f) = \mathbf{0} \tag{2.7}$$

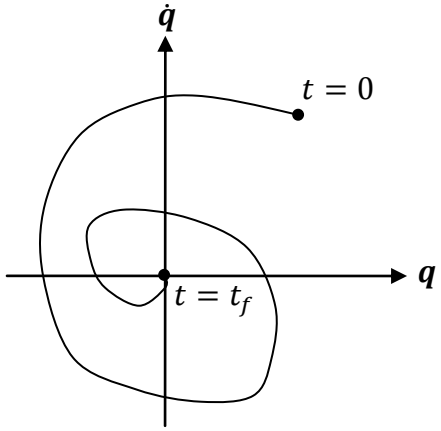

Figure 2-2. Vibration attenuation problem shown in terms of state variables.

Actively dampened structures typically use a closed-loop control system to allow the structure to adapt to sensory feedback in order to continuously eliminate vibrations. If the maneuver interval approaches infinity ($t_f \to \infty$) the problem becomes *time invariant* because the maneuver's

feedback (gains) does not depend on time nor on initial conditions. The control task for time invariant problems is to continuously attenuate the vibrating motion.

Various control schemes can be analyzed by using mathematical optimization. The linear optimal control for a vibration attenuation problem is based on a quadratic performance index that takes the form:

$$J = 1/2 \int_0^{t_f} (a\boldsymbol{q}^T\boldsymbol{K}\boldsymbol{q} + b\dot{\boldsymbol{q}}^T\boldsymbol{M}\dot{\boldsymbol{q}} + c\boldsymbol{F}^T\boldsymbol{K}^{-1}\boldsymbol{F})dt \rightarrow min \tag{2.8}$$

Weighting coefficients a, b, and c are assigned to terms that represent a system's potential energy (elastic), kinetic energy, and work of the actuation forces respectively. This type of quadratic performance index is routinely used in vibration control of flexible structures [23].

The optimization problem defined by a set of linear governing equations in the form (2.1) and a performance index in the form (2.8) is an example of a linear quadratic regulator (LQR) problem with $2n$ states and n_a controls. The standard approach to such problems involves the solution of nonlinear algebraic Riccati equations for the unknown terms of a symmetric matrix of size $2n$ containing a total of $2n^2 + n$ unknowns [23]. For example, a structure having 100 DOFs, will require the solution of 20,100 unknowns. The approach presented in this thesis does not require solving the Riccati equations and so avoids the large number of unknowns and non-linear equations.

FEM models may be transformed from the *DOF-space* into the *modal-space* to simplify their handling. When the problem defined by equations (2.1) is mapped into modal-space, the displacement variables in vector $\boldsymbol{q}$, of size n, are transformed to an equivalent system defined in terms of an equal or smaller sized vector of modal variables $\boldsymbol{\eta} = [\eta_1 \quad \cdots \quad \eta_{n_m}]^T$ ($n_m \leq n$). Similarly, force vector $\boldsymbol{F}$ is transformed into an equal or smaller sized vector of modal controls $\boldsymbol{U} = [u_1 \quad \cdots \quad u_{n_m}]^T$. The mapping between the DOF-space and modal-space variables

represents an exact transformation if their size is equal ($n_m = n$), otherwise the transformation is an approximation ($n_m < n$). The transformation mapping between DOF-space and modal-space takes the form:

$$\boldsymbol{q} = \boldsymbol{\Phi\eta} \tag{2.9a}$$

$$\boldsymbol{U} = \boldsymbol{\Phi}^T\boldsymbol{F} = \boldsymbol{\Phi}^T\boldsymbol{B}\boldsymbol{F_a} = \widehat{\boldsymbol{B}}\boldsymbol{F_a} \tag{2.9b}$$

In the transformation (2.9*b*), matrix $\widehat{\boldsymbol{B}} = \boldsymbol{\Phi^T B}$ of size $n_m \times n_a$ defines the mapping between vectors $\boldsymbol{F_a}$ and $\boldsymbol{U}$, and the modal shape matrix $\boldsymbol{\Phi} = [\boldsymbol{\phi}_1 \quad \cdots \quad \boldsymbol{\phi}_{n_m}]$ defines the mapping between vectors $\boldsymbol{q}$ and $\boldsymbol{\eta}$. The modal shape matrix $\boldsymbol{\Phi}$ contains n_m modal shape vectors $\boldsymbol{\phi}_i$ that for computational convenience are made to satisfy the orthogonality conditions:

$$\boldsymbol{\Phi}^T\boldsymbol{M\Phi} = \boldsymbol{I} \tag{2.10a}$$

$$\boldsymbol{\Phi}^T\boldsymbol{K\Phi} = \boldsymbol{\Omega} \tag{2.10b}$$

Matrix $\boldsymbol{I}$ is the unitary matrix ($I_{ii} = 1$) and matrix $\boldsymbol{\Omega}$ is the diagonal matrix of ordered modal frequencies with the terms $\Omega_{ii} = \omega_i^2$, where $i = 1, \dots, n_m$. Each modal shape vector $\boldsymbol{\phi}_i$ and frequency ω_i are solutions to the standard eigenvalues problem for an elastic system in the form [17]:

$$(\boldsymbol{K} - \omega_i^2)\boldsymbol{\phi}_i = \boldsymbol{0} \quad \text{for } i = 1, \dots, n_m \tag{2.11}$$

If the damping matrix $\boldsymbol{C}$ in equation (2.1) is assumed to take the form of the Rayleigh damping matrix, the equations of motion become completely uncoupled by applying the transformations (2.9*a*), (2.9*b*), and the orthogonality conditions (2.10*a*), and (2.10*b*). The resulting n_m equations of motion are obtained in the modal-space form as [17]:

$$\boldsymbol{I\ddot{\eta}} + \boldsymbol{\Delta\dot{\eta}} + \boldsymbol{\Omega\eta} = \boldsymbol{U} \tag{2.12}$$

Modal damping matrix $\boldsymbol{\Delta}$ contains the diagonal terms $\Delta_{ii} = 2\zeta_i\omega_i$, where $\zeta_i = \boldsymbol{\phi}_i^T \boldsymbol{C} \boldsymbol{\phi}_i/(2\omega_i)$ are passive modal damping ratios for $i = 1, \ldots, n_m$.

The two advantages of modal-space modeling is that, the governing equations (2.1) uncouple when written in the form (2.12), and it is possible to obtain acceptable solutions for systems with a large number (or infinite) number of DOFs by considering only a small number of n_m modal variables that are considered *dynamically significant* [17]. The number of dynamically significant modes that might be considered for a system is related to the accuracy requirements, physical characteristics, and the dynamic characteristics of potential disturbances.

The equations of motion (2.12) in modal-space have an equal number of modal variables in vector $\boldsymbol{\eta}$ and modal controls in vector $\boldsymbol{U}$ so it is always possible to compute both the direct ($\boldsymbol{U} \rightarrow \boldsymbol{\eta}$) and inverse ($\boldsymbol{\eta} \rightarrow \boldsymbol{U}$) operations. In standard computational mechanics, the direct operation is required to obtain a system's response. Hence, modal controls in vector $\boldsymbol{U}$ correspond to the applied control forces in vector $\boldsymbol{F_a}$ directly through transformation (2.9*b*) and the modal variable responses in vector $\boldsymbol{\eta}$ are subsequently obtained through equation (2.12).

Active vibration control requires calculation of the inverse dynamics because the modal controls vector $\boldsymbol{U}$ must be obtained through the inverse of operation (2.12) and then the real actuation forces in vector $\boldsymbol{F_a}$ must be determined from the inverse operation of equation (2.9*b*). This last operation poses a problem when the sizes of vectors $\boldsymbol{F_a}$ and $\boldsymbol{U}$ are inconsistent because the system is formally under-actuated ($n_m > n_a$).

In modal-space, if the number of significant modes of vibration n_m is equal to the number of actuators n_a then problem is considered fully-actuated and theoretically any modal trajectories defined by vector $\boldsymbol{\eta}$ are realizable provided that matrix $\widehat{\boldsymbol{B}}$ in equation (2.9b) is non-singular. This property is exploited in the IMSC method, proposed in [24,25] and used

extensively in numerous applications [18,26,27]. The advantage of dealing with fully-actuated modal-space systems using the IMSC approach lies in the fact that modal controls can be obtained for all controlled modes and subsequently transformed into the actions of an equal number discrete actuators controlling the system. However, if the number of n_m significant modes of vibration that are needed to adequately model a system's dynamics exceeds the number of n_a discrete actuators controlling them, then the problem is formally under-actuated and similar to under-actuated systems in the DOF-space, performing the inverse dynamics is complicated by non-holonomic constraints.

A modified approach must be adopted to deal with under-actuated problems. The CMSOC method presented in this thesis is capable of dealing with some of these problems. The CMSOC method can be viewed as an extension of the IMSC method for dealing with under-actuated vibration control problems. The IMSC approach requires that the size of the system to control must be equal to the number of actuators (inputs) and for this reason the problem is said to be solved in the *input space*. On the other hand the CMSOC approach allows the system size (i.e. number of output variables) to exceed the number of actuators, hence the problem is said to be solved in the *output space*. Solutions obtained using the CMSOC method are consistent with those obtained using the IMSC method when the system is fully-actuated.

3. CONSTRAINED MODAL SPACE OPTIMAL CONTROL (CMSOC)

3.1 Overview of CMSOC

The CMSOC approach consists of three distinct stages: the *structural stage*, the *control stage*, and a *verification stage* as shown in Figure 3-1. In this figure, the three distinct stages of the solution process are enclosed by the heavy lined boxes and the computational steps involved in each stage are enclosed by the smaller shaded boxes. The software that was used in each step is denoted in brackets in the small boxes where applicable. The details of the structural stage, control stage, and verification stage are covered in Section 3.2, Section 3.3, and Section 3.4 respectively.

In the *structural stage*, a system is modeled by the FEM and a routine modal analysis is performed to obtain modal frequencies contained in the matrix $\boldsymbol{\Omega}$ and the corresponding mode shapes contained in matrix $\boldsymbol{\Phi}$. This process is efficiently handled using the ANSYS FEM software. The next step is to choose a potential actuator configuration for the system and assemble the corresponding actuator positioning matrix $\boldsymbol{B}$. Also the sensor configuration matrix $\boldsymbol{C}$ may also be assembled based on the positions of sensors. These parameters are input into a worksheet using the MAPLE software to perform a number of matrix manipulations that are necessary for assessing the controllability of the actuator configuration and for performing calculations in subsequent stages.

In the *control stage* the results of the structural stage are required to solve the optimization problem, obtain the optimal control forces for each actuator, and calculate the expected dynamic response of the system. The constant gains for a closed-loop system control

system meeting the observability requirements may also be solved (if applicable). The control stage is efficiently handled and automated using the MAPLE software, which is capable of the necessary symbolic computations (see Appendix A for an example MAPLE code).

In the *verification stage* the solution obtained in the control stage is checked for accuracy and for any potential *spillover effects*. This check, which is performed using the ANSYS, applies the actuator forces obtained in the control stage to the FEM model in a transient direct dynamic analysis to verify how closely the system response matches that obtained in the control stage. Since the control stage solution may generally involve a smaller number of n_m significant modes of vibration than the total number of n modes, spillover effects involving higher modes of vibration (that were not considered in the system modeling) can be detected. Essentially, this check is performed to ensure that the applied actuator forces do not excite higher modes of vibration that were not included in the dynamic model considered in the control stage.

Another benefit of the verification stage is that one can check that the physical presence of actuators in the system will not significantly impact the dynamics of the structure. It was assumed in the structural stage that the actuator masses and stiffnesses were negligible. These parameters could have been incorporated into the FEM model in the structural stage to mitigate errors due to the above mentioned assumptions; however, this would require that the FEM model be modified every time that a new actuator configuration is to be investigated, making it difficult to quickly assess a variety of configurations. The procedure presented in this work assumes that actuators have no mass or stiffness – an assumption that is later checked and updated if necessary.

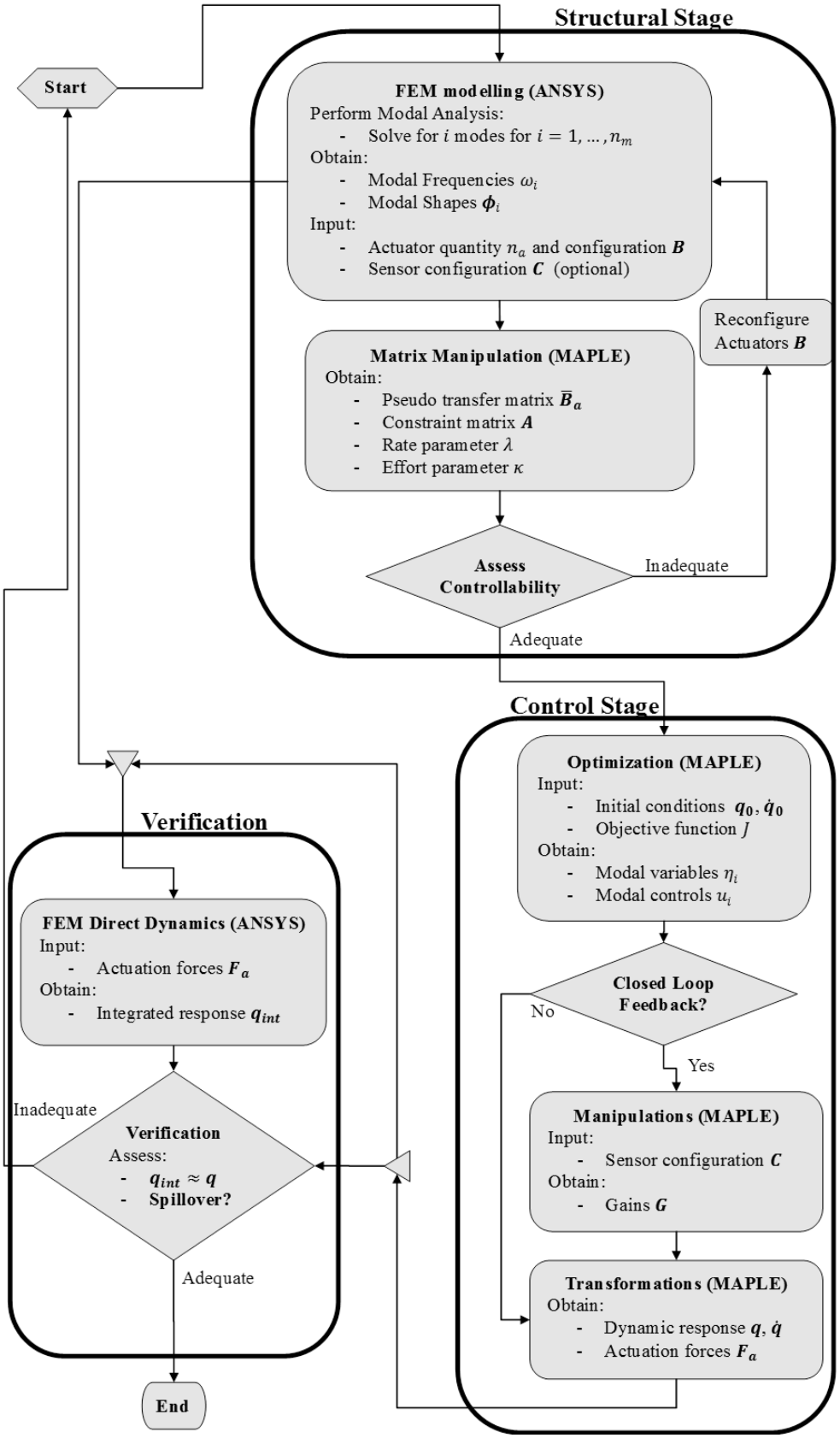

Figure 3-1. Flowchart of CMSOC Approach.

The flow of the solution process shown in Figure 3-1 involves some iteration in the structural stage to determine an effective configuration of actuators because it will be shown that any choice of actuator positions can be conveniently related to controllability prior to engaging in subsequent computational steps. The entire solution process may involve multiple iterations, as the verification stage may indicate unacceptably large modeling errors or spillover effects that require model refinement and repeating the solution process. The CMSOC procedure ends when the control provides a satisfactory response with minimal modeling errors and spillover effects. In the following sections the calculations and operations involved in each step of the procedure (see Figure 3-1) are explained in detail.

3.2 Structural Stage

The structural stage is represented in the topmost box of the flowchart in Figure 3-1. It consists of three main steps: creating the FEM model and performing the modal analysis (previously discussed in Section 2.2), performing several matrix operations as discussed in Section 3.2.1, and assessing the controllability indicators as discussed in Section 3.2.2.

3.2.1 Matrix Operations

The analysis of under-actuated systems in modal-space is complicated by the fact that n_m modal controls contained in vector $\boldsymbol{U}$ must be transformed into a smaller number of n_a actuation forces contained in vector $\boldsymbol{F_a}$ ($n_m > n_a$). This operation requires the inverse of transformation (2.9*b*) which is permitted only if matrix $\widehat{\boldsymbol{B}}$ is 'invertible'. This poses a problem if matrix $\widehat{\boldsymbol{B}}$ is of size $n_m \times n_a$ ($n_m > n_a$) because matrix $\widehat{\boldsymbol{B}}^{-1}$ will not exist, so vector $\boldsymbol{U}$ cannot be obtained from (2.9*b*) directly. To calculate the inverse dynamics in modal-space $n_c = n_m - n_a$ redundant modal variables must be determined from n_c additional constraints. These constraints can be explicitly derived by sequentially eliminating the n_a components of vector $\boldsymbol{F_a}$ from equation

(2.9*b*) to obtain the extra conditions to be satisfied by all n_m components of vector $\boldsymbol{U}$. However, eliminating these variables to obtain the constraints can be challenging and is not easily automated to obtain the solution using mathematical software.

In this thesis a different approach is used to obtain the under-actuated constraints. Instead of eliminating redundant modal variables, the vector of applied actuation forces $\boldsymbol{F_a}$ is augmented by $n_c = n_m - n_a$ *dummy* (zero-valued) *actuators* forces contained in vector $\boldsymbol{F_d}$ ($\widehat{\boldsymbol{F}} = [\boldsymbol{F_a}^T \quad \boldsymbol{F_d}^T]^T$). These dummy actuators are arbitrarily configured in the system to 'artificially' convert the under-actuated problem into an equivalent fully-actuated problem for which $\widehat{\boldsymbol{B}}^{-1}$ does exist. Hence, the inverse of the operation (2.9*b*) can be performed with the augmented actuation force vector $\widehat{\boldsymbol{F}}$ replacing vector $\boldsymbol{F_a}$ in this transformation. The only restriction on the dummy actuator configuration is that it produces a non-singular square matrix $\widehat{\boldsymbol{B}}$. The inverted augmented system can be partitioned to better distinguish between those elements contributing to the mapping of real actuation forces and those elements mapping the dummy actuation forces whose actions are null valued ($\boldsymbol{F_d} = [0 \quad \cdots \quad 0]^T$). The partitioned inverse operation (2.9*b*) with augmented force vector takes the form:

$$\widehat{\boldsymbol{F}} = \widehat{\boldsymbol{B}}^{-1}\boldsymbol{U} \quad \Rightarrow \quad \begin{bmatrix} \boldsymbol{F_a} \\ \boldsymbol{F_d} \end{bmatrix} = \begin{bmatrix} \widetilde{\boldsymbol{B}}_{\boldsymbol{a}} & \widetilde{\boldsymbol{B}}_{\boldsymbol{r}} \\ \boldsymbol{A_a} & \boldsymbol{A_r} \end{bmatrix} \begin{bmatrix} \boldsymbol{U_a} \\ \boldsymbol{U_r} \end{bmatrix} \tag{3.1}$$

The expression on the left and right of the arrow in (3.1) are equivalent, only the expression on the right is written in the partitioned form. Square sub-matrices $\widetilde{\boldsymbol{B}}_{\boldsymbol{a}}$ and $\boldsymbol{A_r}$ have the dimensions $n_a \times n_a$ and $n_c \times n_c$ respectively. The vector of modal controls $\boldsymbol{U}$ is divided into two sub-vectors $\boldsymbol{U_a} = [u_1 \quad \cdots \quad u_{n_a}]^T$ and $\boldsymbol{U_r} = [u_{n_a+1} \quad \cdots \quad u_{n_m}]^T$ which contain the *independent* and *redundant* modal controls respectively. To be consistent with this naming convention, the modal variables in vector $\boldsymbol{\eta}$ are similarly divided into their independent and redundant components in

sub-vectors $\boldsymbol{\eta_a} = [\eta_1 \quad \cdots \quad \eta_{n_a}]^T$ and $\boldsymbol{\eta_r} = [\eta_{n_a+1} \quad \cdots \quad \eta_{n_m}]^T$ respectively. Though all modal controls are required to solve for the system motion described by vector $\boldsymbol{\eta}$, only the components in vector $\boldsymbol{U_a}$ are required to determine the actuation forces in vector $\boldsymbol{F_a}$ from equation (3.1).

The lower partition in (3.1), involving the zero-valued dummy actuator forces $\boldsymbol{F_d} = [0 \quad \cdots \quad 0]^T$, define a set of n_c constraints that are linear in terms of modal controls and may written in the form:

$$\boldsymbol{A_a U_a + A_r U_r = AU = 0} \tag{3.2}$$

Matrix $\boldsymbol{A} = [\boldsymbol{A_a} \quad \boldsymbol{A_r}]$ of size $n_c \times n_m$ will be referred to as the matrix of constraints and defines the constraints arising due to under-actuation in terms of a modal controls in vector $\boldsymbol{U}$. The matrix of constraints contains $n_c n_m$ nonzero coefficients $A_{i,j}$. Since the equations in set (3.2) are homogeneous, the terms in matrix $\boldsymbol{A}$ can be normalized such that $A_{i,i} = 1$, $A_{k,i} = 0$ for $k < i$ (left bottom corner), and $A_{k,n_a+1+k} = 0$ for $1 \le k \le n_c - 1$ (right upper corner). The normalized matrix of constraints is denoted by $\overline{\boldsymbol{A}}$ (formally $\overline{\boldsymbol{A}} = \boldsymbol{A}$) and it can also be partitioned such that $\overline{\boldsymbol{A}} = [\overline{\boldsymbol{A}}_{\boldsymbol{a}} \quad \overline{\boldsymbol{A}}_{\boldsymbol{r}}]$, which takes the form:

$$\overline{\boldsymbol{A}} = \left[\begin{array}{ccccccc|ccccc} 1 & \bar{A}_{12} & \bar{A}_{13} & \cdots & \bar{A}_{1,n_c} & \cdots & \bar{A}_{1,n_a} & \bar{A}_{1,n_a+1} & & & & \\ & 1 & \bar{A}_{23} & \cdots & \bar{A}_{2,n_c} & \cdots & \bar{A}_{2,n_a} & \bar{A}_{2,n_a+1} & \bar{A}_{2,n_a+2} & & & \\ & & 1 & \cdots & \bar{A}_{3,n_c} & \cdots & \bar{A}_{3,n_a} & \bar{A}_{3,n_a+1} & \bar{A}_{3,n_a+2} & \bar{A}_{3,n_a+3} & & \\ & & & \ddots & \vdots & \cdots & \vdots & \vdots & \vdots & \vdots & \ddots & \\ & & & & 1 & \cdots & \bar{A}_{n_c,n_a} & \bar{A}_{n_c,n_a+1} & \bar{A}_{n_c,n_a+2} & \bar{A}_{n_c,n_a+3} & \cdots & \bar{A}_{n_c,n_m} \end{array}\right] \tag{3.3}$$

In the normalized form (3.3), the sub-matrix $\overline{\boldsymbol{A}}_{\boldsymbol{a}}$ appears on the left of the vertical line divider and sub-matrix $\overline{\boldsymbol{A}}_{\boldsymbol{r}}$ appears on the right.

The normalized matrix of modal constraints $\overline{\boldsymbol{A}}$ is independent of the location of the dummy actuators in the system, as the dummy actuators were only added to facilitate the application of the constraints in determining the actuator forces in vector $\boldsymbol{F_a}$ from equation (3.1).

In the normalized form (3.3), the matrix of constraints serves as a means of comparing the effectiveness of different configurations of actuators placed in a system. In other words, it is a means of evaluating the controllability of a given under-actuated system with different actuator configurations.

The actuation forces in vector $\boldsymbol{F_a}$ are functions of both the independent modal controls in vector $\boldsymbol{U_a}$ and the redundant modal controls in vector $\boldsymbol{U_r}$ in accordance with the upper partition in the equation (3.1). However, by applying the constraint (3.2) the redundant modal controls in vector $\boldsymbol{U_r}$ can be eliminated and the real actuation forces can be obtained in terms of the components in of the independent modal controls in vector $\boldsymbol{U_a}$ through the equations:

$$\boldsymbol{F_a = \bar{B}_a U_a = \left(\tilde{B}_a - \tilde{B}_r A_r^{-1} A_a\right) U_a} \tag{3.4}$$

The square matrix $\boldsymbol{\bar{B}_a = \tilde{B}_a - \tilde{B}_r A_r^{-1} A_a}$ has the dimensions $n_a \times n_a$ and is referred to as the *pseudo-transfer matrix* because it has a similar physical interpretation as the transfer matrix $\boldsymbol{\hat{B}}$ for fully-actuated systems. Note that a fully-actuated problem (i.e. $n_m = n_a$) has the property: $\boldsymbol{\bar{B}_a = \tilde{B}_a = \hat{B}}$. The matrix $\boldsymbol{\bar{B}_a}$ is independent of the location of dummy actuators in the system and, similar to matrix $\boldsymbol{\bar{A}}$, is an indicator for comparing the controllability for a system with different actuator configurations. Equation (3.4) requires that matrix $\boldsymbol{A_r}$ is non-singular; otherwise, the operation is impossible.

3.2.2 Controllability Indicators

Matrices $\boldsymbol{\bar{A}_r}$ and $\boldsymbol{\bar{B}_a}$ are indicators of an under-actuated system's controllability for particular actuator configurations (note that the normalized matrix $\boldsymbol{\bar{A}_r}$ is required to give a meaningful indicator). These indicators help to effectively position actuators in a system to dampen the vibrations of all dynamically significant modes. Effective placement of actuators is critical to the performance of an actively attenuated system. To illustrate this point consider

Figure 3-2, which shows a standard simply supported beam of length *L* and its modal shapes in the first two modes of vibration. The single active force $F_{a_1}(t)$ acts perpendicular to the beam axis and can be located at any location *x* along the beams length.

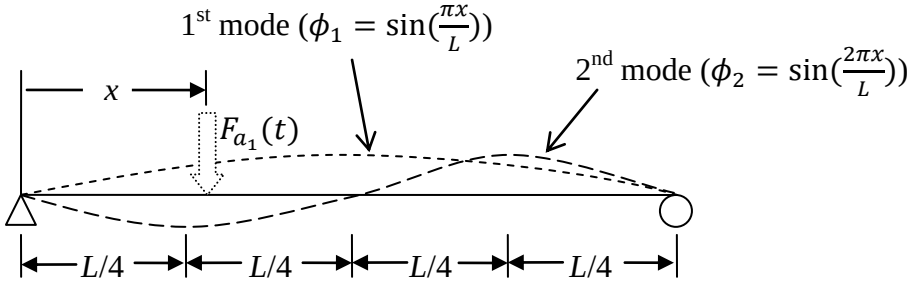

Figure 3-2. Actuator configuration and controllability for a vibrating beam.

At what location *x* should the actuator $F_{a_1}(t)$ be located to best attenuate the two vibration modes? Intuitively, one can see that placing an actuator at the midpoint of the beam at $x = L/2$ would leave the second mode uncontrollable because this location essentially does not 'see' the second mode of vibration. Also at the terminal points $x = 0$ and $x = L$, one would expect that the both modes would be completely uncontrollable. A better actuator position would be some location between the middle of the beam and the end points. As it will be demonstrated, the method presented in this thesis can help to address what is the 'best' location for placing the actuator in the structural stage.

The 'best' actuator position is reflected in the transformation (3.4) and more specifically the matrices $\overline{\boldsymbol{A}}_{\boldsymbol{r}}$ and $\overline{\boldsymbol{B}}_{\boldsymbol{a}}$. It will be shown that, for under-actuated systems, the magnitude of components in the matrix $\overline{\boldsymbol{A}}_{\boldsymbol{r}}$ and $\overline{\boldsymbol{B}}_{\boldsymbol{a}}$ reflect the expected rate of attenuation of the slowest dampened mode of vibration and the peak force amplitudes required by the actuator(s), respectively. Both qualities are indicators of system controllability given a particular actuator

configuration. Two scalar measures are adopted as quantitative measures of these qualities – the *rate parameter* λ and *effort parameter* κ, which are defined as:

$$\lambda = |\det \bar{\boldsymbol{A}}_{\boldsymbol{r}}| \tag{3.5a}$$

$$\kappa = |\det \bar{\boldsymbol{B}}_{\boldsymbol{a}}| \tag{3.5b}$$

As their naming suggests, the rate parameter λ indicates the rate at which the slowest damped mode(s) of vibration will be attenuated and the effort parameter κ indicates the magnitude of required actuation forces. Note that the controllability parameters in (3.5*a*) and (3.5*b*) only serve to compare the effectiveness of different configurations of actuators for a particular under-actuated mechanical system and not as an objective measure of general control effectiveness for all systems.

Matrix $\bar{\boldsymbol{A}}_{\boldsymbol{r}}$ contains the last n_c columns of the normalized matrix $\bar{\boldsymbol{A}}$ and is triangular such that: $\det(\bar{\boldsymbol{A}}_{\boldsymbol{r}}) = \bar{A}_{1,n_a+1}\, \bar{A}_{2,n_a+2} \cdots \bar{A}_{n_c,n_m}$. The most uniform rate of attenuation of all modes considered is achieved if all non-zero elements of matrix $\bar{\boldsymbol{A}}_{\boldsymbol{r}}$ have a value of unity such that: $\lambda = |\det \boldsymbol{A}_{\boldsymbol{r}}| = 1$. Systems with a rate parameter λ close to unity have redundant modal controls in vector $\boldsymbol{U}_{\boldsymbol{r}}$ similar in magnitude to the independent modal controls in vector $\boldsymbol{U}_{\boldsymbol{a}}$. This means redundant modal variables in vector $\boldsymbol{\eta}_{\boldsymbol{r}}$ are attenuated at similar rates as the independent modal variables in vector $\boldsymbol{\eta}_{\boldsymbol{a}}$ in accordance with relation (2.12).

The pseudo-transfer matrix $\bar{\boldsymbol{B}}_{\boldsymbol{a}}$ transfers the independent modal controls in vector $\boldsymbol{U}_{\boldsymbol{a}}$ to the real actuation forces in vector $\boldsymbol{F}_{\boldsymbol{a}}$ through equation (3.4). Therefore, for the same system, smaller values of the effort parameter $\kappa = |\det \bar{\boldsymbol{B}}_{\boldsymbol{a}}|$ correspond to actuator configurations that will have smaller force amplitude requirements than actuator configurations that produce larger values of κ.

Returning the simply supported beam example in Figure 3-2 one can assume that a second dummy actuator is applied at a distance y along the beam length; therefore by applying equation (2.9*b*) with appropriate substitutions of the modal shapes in Figure 3-2 one can obtain the transformation matrix $\widehat{\boldsymbol{B}} = \begin{bmatrix} sin(\frac{\pi x}{L}) & sin(\frac{\pi y}{L}) \\ sin(\frac{2\pi x}{L}) & sin(\frac{2\pi y}{L}) \end{bmatrix}$. Then by taking the inverse of this matrix and performing the partitioning in accordance with equation (3.1) the controllability indicators in (3.5*a*) and (3.5*b*) can be solved to obtain: $\lambda = 1/\left(2\cos(\frac{\pi x}{L})\right)$ and $\kappa = 1/\left(sin(\frac{\pi x}{L})\right)$ (which are completely independent of the assumed location of the dummy actuator location y). Using these indicators the "best" position x of the actuator F_{a_1} for attenuating the two dominant modes of vibration can be evaluated. In Figure 3-3 the values of λ and κ are plotted as a function of actuator position x along the length of the beam L. The figure demonstrates that as the location of the actuator approaches the midpoint of the beam ($x = L/2$) the value of the rate parameter approaches infinity ($\lambda \to \infty$) and as it nears the endpoints ($x = 0$, $x = L$) the effort parameter approaches infinity ($\kappa \to \infty$). These singularity points correspond to actuator locations that result in an uncontrollable system.

Recall that a value of $\lambda \approx 1$ and a "small" value of κ is most desirable for good controllability. As shown in Figure 3-3, the rate parameter is equal to unity ($\lambda = 1$) when the actuator is positioned at $x = L/3$ and $x = 2L/3$ (one third positions), indicating that these locations will provide similar damping rates for both modes of vibration. Any change in position from the one third positions towards the beam midpoint will marginally decrease the effort parameter value, but rapidly increase the rate parameter value because control over the second mode of vibration rapidly decreases. Conversely, any repositioning towards the endpoints will increase the effort parameter and reduce the rate parameter. For practical purposes the third

points of the beam represent the "best" location for positioning the single actuator F_{a_1} for attenuating the first two modes of vibration.

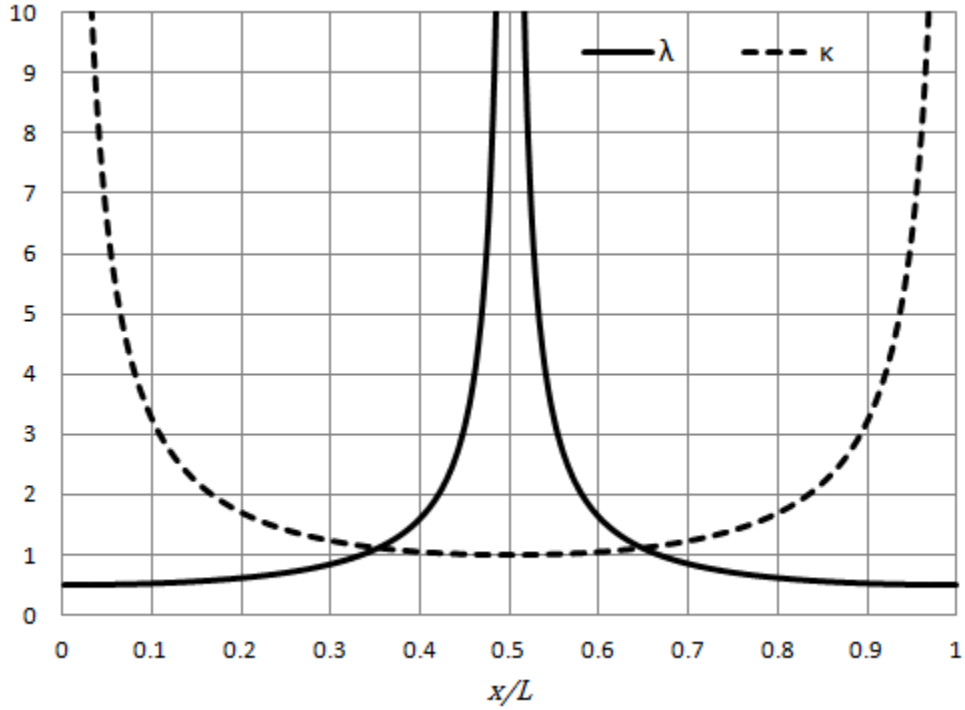

Figure 3-3. Rate parameter λ and effort parameter κ as functions of actuator position x along beam length L.

By observing the controllability indicators, potential actuator configurations can be quickly assessed prior to proceeding with the more computationally intensive control stage described in Section 3.3. Hence, several iterations of the structural stage may be required, as shown in Figure 3-1, in search of the "best" actuator configuration for a given system. When a sufficiently "good" actuator configuration is obtained (determining the "best" configuration may be difficult or impossible for geometrically complex systems involving several modes of vibration and multiple actuators) the structural stage is completed. The next stage of the CMSOC procedure is the control stage which is covered in Section 3.3.

3.3 Control Stage

The control stage is represented in the lower right-hand box of flowchart in Figure 3-1. It involves three main steps: selecting initial and final boundary conditions and performance criteria as discussed in Section 3.3.1, solving the optimality conditions as discussed in Section 3.3.3, and obtaining the closed loop feedback gains as discussed in Section 3.3.4. The derivation of the optimality conditions is covered in detail in Section 3.3.2.

3.3.1 Boundary Conditions and Performance Criteria

The initial and final boundary conditions defined in the DOF-space in (2.7) may be transformed to modal-space through transformation (2.9*a*) along with the appropriate substitution from orthogonality condition (2.10*a*), to obtain:

$$\boldsymbol{\eta}(0) = \boldsymbol{\Phi}^T \boldsymbol{M}\boldsymbol{q}(0) = \boldsymbol{\eta_0}, \qquad \dot{\boldsymbol{\eta}}(0) = \boldsymbol{\Phi}^T \boldsymbol{M}\dot{\boldsymbol{q}}(0) = \dot{\boldsymbol{\eta}}_{\boldsymbol{0}} \tag{3.6a}$$

$$\boldsymbol{\eta}(t_f) = \mathbf{0}, \qquad \dot{\boldsymbol{\eta}}(t_f) = \mathbf{0} \tag{3.6b}$$

Note that operation (3.6*a*) is formally equivalent to the inverse of operation (2.9*a*) for a fully-actuated system only. The time-invariant close-loop control solution ($t_f \to \infty$) is of primary interest for actively dampened structures and is typically dealt with in this thesis. Formally the initial conditions are not required to obtain feedback gains for a closed-loop system; however for convenience, an arbitrary set of initial conditions (3.6*a*) can be assumed for obtaining the gains in a later step (Section 3.3.4).

The modal-space equivalent of the performance index (2.8) is obtained by substituting (2.9*a*) and (2.9*b*) into equation (2.8) and applying the orthogonality conditions (2.10*a*) and (2.10*b*) to obtain:

$$J = 1/2 \int_0^\infty (\boldsymbol{\eta}^T \boldsymbol{Q_d}\boldsymbol{\eta} + \dot{\boldsymbol{\eta}}^T \boldsymbol{Q_v}\dot{\boldsymbol{\eta}} + \boldsymbol{U}^T \boldsymbol{R}\boldsymbol{U})dt \to min \tag{3.7}$$

Formally, the performance indices J in (3.7) and (2.8) are equivalent if the weighting matrices appearing in (3.7) are diagonal and equal to $\boldsymbol{Q_d} = a\boldsymbol{\Omega}$, $\boldsymbol{Q_v} = b\boldsymbol{I}$, and $\boldsymbol{R} = c\boldsymbol{\Omega}^{-1}$ where a, b, and c are constant weighting terms that were previously defined in (2.8). However, the diagonal weighting terms $Q_{d_{ii}}$, $Q_{v_{ii}}$, and R_{ii} $(i = 1, \dots, n_m)$ in matrices $\boldsymbol{Q_d}$, $\boldsymbol{Q_v}$, and $\boldsymbol{R}$ may be chosen arbitrarily as design parameters to "tune" the resulting system dynamics to produce a desired system response.

3.3.2 Deriving Optimality Conditions

The optimization problem with n_a independent actuators acting upon n_m modal variables is defined by equations of motion (2.12), with constraints (3.2), and performance index (3.7). The optimality conditions for this problem are derived from Pontryagin's principle [28]. The modal variables in vector $\boldsymbol{\eta}$ and their corresponding velocities in vector $\dot{\boldsymbol{\eta}}$ are treated as system state variables so the system's Hamiltonian H takes the form:

$$H = 1/2(\boldsymbol{\eta}^T\boldsymbol{Q_d}\boldsymbol{\eta} + \dot{\boldsymbol{\eta}}^T\boldsymbol{Q_v}\dot{\boldsymbol{\eta}} + \boldsymbol{U}^T\boldsymbol{R}\boldsymbol{U}) + \boldsymbol{P_d}^T\dot{\boldsymbol{\eta}} + \boldsymbol{P_v}^T(-\boldsymbol{\Delta}\dot{\boldsymbol{\eta}} - \boldsymbol{\Omega}\boldsymbol{\eta} + \boldsymbol{U}) + \boldsymbol{\nu}^T\boldsymbol{A}\boldsymbol{U} \qquad (3.8)$$

The first bracketed term contains the integrand of the performance index (3.7), the second and third terms contain the system states related through equation (2.12), and the last term contains the constraint equations (3.2) arising due to under-actuation. Vectors $\boldsymbol{P_d}$ and $\boldsymbol{P_v}$ are standard costate vectors that account for the modal states represented by vectors $\boldsymbol{\eta}$ and $\dot{\boldsymbol{\eta}}$ respectively. Vector $\boldsymbol{\nu}^T = [\nu_1 \quad \cdots \quad \nu_{n_c}]$ represents a set of n_c time-varying Lagrange multipliers introduced to satisfy the constraints (3.2). Pontryagin's theorem states that for an optimal system motion the Hamiltonian H must be stationary with respect the states, costates, and modal controls [28]. Following Pontryagin's formulation, the costate equations take the form:

$$\dot{\boldsymbol{P}}_{\boldsymbol{d}} = {}^{\partial H}/_{\partial \boldsymbol{\eta}} = \boldsymbol{Q_d}\boldsymbol{\eta} + \boldsymbol{\Omega}\boldsymbol{P_v} \qquad (3.9a)$$

$$\dot{\boldsymbol{P}}_{\boldsymbol{v}} = {}^{\partial H}/_{\partial \dot{\boldsymbol{\eta}}} = \boldsymbol{Q}_{\boldsymbol{v}}\dot{\boldsymbol{\eta}} - \boldsymbol{P}_{\boldsymbol{d}} + \boldsymbol{\Delta P}_{\boldsymbol{v}} \tag{3.9b}$$

The Hamiltonian is stationary with respect to the modal controls if:

$${}^{\partial H}/_{\partial \boldsymbol{U}} = -\boldsymbol{RU} + \boldsymbol{P}_{\boldsymbol{v}} + \boldsymbol{A}^{T}\boldsymbol{\nu} = \boldsymbol{0} \tag{3.10}$$

The costate vector $\boldsymbol{P}_{\boldsymbol{v}}$ is obtained in terms of the modal variables in vector $\boldsymbol{\eta}$ and the Lagrange multipliers in vector $\boldsymbol{\nu}$ by rearranging (3.10) and making the appropriate substitution from (2.12) to obtain:

$$\boldsymbol{P}_{\boldsymbol{v}} = \boldsymbol{R}(\boldsymbol{I}\ddot{\boldsymbol{\eta}} + \boldsymbol{\Delta}\dot{\boldsymbol{\eta}} + \boldsymbol{\Omega\eta}) - \boldsymbol{A}^{T}\boldsymbol{\nu} \tag{3.11}$$

By substituting vector $\boldsymbol{P}_{\boldsymbol{v}}$ from (3.11) into (3.9*b*) the costate vector $\boldsymbol{P}_{\boldsymbol{d}}$ is obtained in terms of vectors $\boldsymbol{\eta}$ and $\boldsymbol{\upsilon}$ in the form:

$$\boldsymbol{P}_{\boldsymbol{d}} = \boldsymbol{Q}_{\boldsymbol{v}}\dot{\boldsymbol{\eta}} - \boldsymbol{R}(\boldsymbol{I}\dddot{\boldsymbol{\eta}} + \boldsymbol{\Delta}\ddot{\boldsymbol{\eta}} + \boldsymbol{\Omega}\dot{\boldsymbol{\eta}}) + \boldsymbol{\Delta R}(\boldsymbol{I}\ddot{\boldsymbol{\eta}} + \boldsymbol{\Delta}\dot{\boldsymbol{\eta}} + \boldsymbol{\Omega\eta}) + \boldsymbol{A}^{T}\dot{\boldsymbol{\nu}} - \boldsymbol{\Delta A}^{T}\boldsymbol{\nu} \tag{3.12}$$

A set of optimality conditions defined in terms of modal variables and Lagrange multipliers is obtained by substitution of (3.12) into (3.9*a*) to obtain:

$$\boldsymbol{R}\ddot{\ddot{\boldsymbol{\eta}}} + (\boldsymbol{2\Omega R} - \boldsymbol{Q}_{\boldsymbol{v}} - \boldsymbol{R\Delta}^{2})\ddot{\boldsymbol{\eta}} + (\boldsymbol{R\Omega}^{2} + \boldsymbol{Q}_{\boldsymbol{d}})\boldsymbol{\eta} - (\boldsymbol{A}^{T}\ddot{\boldsymbol{\nu}} - \boldsymbol{\Delta A}^{T}\dot{\boldsymbol{\nu}} + \boldsymbol{\Omega A}^{T}\boldsymbol{\nu}) = \boldsymbol{0} \tag{3.13}$$

The n_m optimality equations (3.13) contain n_m unknown components in the vector of modal variables $\boldsymbol{\eta}$ and an additional n_c unknown components in the vector of Lagrange multipliers $\boldsymbol{\nu}$. To solve for the total number of $n_t = n_m + n_c$ unknowns in (3.13) the n_c additional constraint equations in the form (3.2) must be solved simultaneously with the equations (3.13). However, the constraints must be written as a function of modal variables in vector $\boldsymbol{\eta}$ by substituting (2.12), so that the algebraic form in (3.2) is replaced by the differential form written as:

$$\boldsymbol{A}(\boldsymbol{I}\ddot{\boldsymbol{\eta}} + \boldsymbol{\Delta}\dot{\boldsymbol{\eta}} + \boldsymbol{\Omega\eta}) = \boldsymbol{0} \tag{3.14}$$

The modal variables in equations (3.14) are coupled by higher time derivatives. Unlike the independent and redundant components of controls $\boldsymbol{U}$ that are related via equation (3.2), the independent components of modal variables in vector $\boldsymbol{\eta_a}$ cannot be separated analytically from the redundant modal variables in vector $\boldsymbol{\eta_r}$. In other words constraints (3.14) are formally non-holonomic. The total number of n_t equations in the form of (3.13) and (3.14) is equal to the number of unknowns in vectors $\boldsymbol{\eta}$ and $\boldsymbol{\nu}$, and may therefore be solved. Formally only the independent modal variables are required to determine the actuation forces through equation (3.4) with the necessary substitution from (2.12). However, all modal variables are needed to determine the motion of any particular DOF from transformation (2.9*a*).

In summary, under-actuated systems are governed by the set of equations (3.13) and (3.14). These equations are handled numerically by the CMSOC procedure and the details of the solution are discussed in the next section.

3.3.3 Solving Optimality Conditions in the Control Stage

The solution to the optimality equations (3.13) and the system constraints (3.14) is obtained using standard methods for obtaining exact solutions to dynamic systems involving higher order differential equations. The symbolic differential operator $D^j = d^j/dt^j$ is used to transform the system equations to a characteristic polynomial equation. The differential operator is substituted into equations (3.13) and (3.14) and the result is organized into a compact matrix notation in the form:

$$\boldsymbol{E_p Y} = \mathbf{0} \;\Rightarrow\; \begin{bmatrix} \boldsymbol{E} & -\widehat{\boldsymbol{E}}^T \\ \breve{\boldsymbol{E}} & \mathbf{0} \end{bmatrix} \begin{bmatrix} \boldsymbol{\eta} \\ \boldsymbol{\nu} \end{bmatrix} = \mathbf{0} \tag{3.15}$$

The expressions on both sides of the arrow in (3.15) are equivalent, but the expression on the right is shown in a partitioned form. The vector $\boldsymbol{Y} = [\boldsymbol{\eta}^T \quad \boldsymbol{\nu}^T]^T$ contains n_t ($n_t = n_m + n_c$)

unknown modal variables in vector $\boldsymbol{\eta}$ and Lagrange multipliers in vector $\boldsymbol{\nu}$. The matrix $\boldsymbol{E_p}$ is partitioned into the upper-left sub-matrix $\boldsymbol{E}$ with diagonal terms E_{ii}, the upper-right sub-matrix $\widehat{\boldsymbol{E}}$ with terms $\widehat{E}_{ij}$, and the lower-left sub-matrix $\breve{\boldsymbol{E}}$ with terms $\breve{E}_{ji}$ ($i = 1, \dots, n_m$ and $j = 1, \dots, n_c$). The lower right sub-matrix in $\boldsymbol{E_p}$ is of size $n_c \times n_c$ and populated with zero-valued components. These partitioned sub-matrices are defined as:

$$\boldsymbol{E} = \boldsymbol{R}D^4 + (\boldsymbol{2\Omega R} - \boldsymbol{Q_v} - \boldsymbol{R\Delta}^2)D^2 + (\boldsymbol{R\Omega}^2 + \boldsymbol{Q_d})D \tag{3.16a}$$

$$\widehat{\boldsymbol{E}} = \boldsymbol{A}(\boldsymbol{I}D^2 + \boldsymbol{\Delta}D + \boldsymbol{\Omega}) \tag{3.16b}$$

$$\breve{\boldsymbol{E}} = \boldsymbol{A}(\boldsymbol{I}D^2 - \boldsymbol{\Delta}D + \boldsymbol{\Omega}) \tag{3.16c}$$

Fully-actuated problems do not contain the sub-matrices $\widehat{\boldsymbol{E}}$ and $\breve{\boldsymbol{E}}$ defined in (3.16*b*) and (3.16*c*) respectively. Such problems have matrix $\boldsymbol{E_p}$ equal to submatrix $\boldsymbol{E}$ and there are no Lagrange multipliers required, so equation (3.15) reduces to $\boldsymbol{E\eta} = \boldsymbol{0}$. Furthermore, the diagonal operator $\boldsymbol{E}$ provides all the necessary equations $E_{ii} = 0$ ($i = 1, \dots, n_m$) from which the four integration constants generated can be obtained directly from the boundary conditions (3.6*a*) and (3.6*b*) for the vibration mode under consideration. This is consistent with the IMSC approach where the vibration modes of fully-actuated problems can be solved independently of each other, one by one, directly from the boundary conditions and optimality conditions.

The characteristic equation for the system defined by (3.15) is a polynomial of r to the power of $4n_m$ (with the differential operator D replaced by an auxiliary variable r), which takes the form:

$$Det(\boldsymbol{E_p})\big|_{D\to r} = 0 \tag{3.17}$$

The solution to the characteristic equation (3.17) involves roots r_l ($l = 1, \dots, 4n_m$). The $4n_m$ roots of the characteristic equation may generally be complex numbers in the form:

$$r_l = \pm\alpha_k \pm i\beta_k, \qquad k = 1, \dots, n_m \; and \; l = 1, \dots, 4n_m \tag{3.18}$$

The positive real numbers α_k and β_k characterize the dynamics of the k-th mode of vibration. If all roots r_l are unique complex numbers in accordance with (3.18) than a general solution function for the unknown modal variables and Lagrange multipliers in vector $\boldsymbol{Y}$ is obtained in the below form:

$$Y_j = \sum_{k=1}^{n_m} \left\{ e^{-\alpha_k t} \left[c_{kj}^1 sin(\beta_k t) + c_{kj}^2 cos(\beta_k t) \right] + e^{\alpha_k t} \left[c_{kj}^3 sin(\beta_k t) + c_{kj}^4 cos(\beta_k t) \right] \right\} \tag{3.19}$$

Note that solution functions in the form (3.19) only apply to systems that have unique complex roots r_l in the form (3.18). For problems with repeating roots not lying in the complex plane, alternative solution functions must be used (see Chapter 4 for an example).

The solution function (3.19) is defined for each component Y_j and each contains $4n_m$ independent elementary functions. There are $j = 1, \dots, n_t$ solution functions Y_j that relate to a corresponding modal variable η or a Lagrange multiplier ν, such that $Y_j = \eta_j$ for $j = 1, \dots, n_m$ and $Y_j = \nu_{j-n_m}$ for $j = n_m, \dots, n_t$ (i.e. $\boldsymbol{Y} = [\eta_1 \quad \cdots \quad \eta_{n_m} \quad \nu_1 \quad \cdots \quad \nu_{n_c}]^T$). There are $4n_m n_t$ unknown integration constants c_{kj}^1, c_{kj}^2, c_{kj}^3, and c_{kj}^4 contained in the solution functions (3.19). Their values are obtained by substituting the assumed form into the optimality equations (3.13) and the constraint equations (3.14) and then applying the method of undetermined coefficients to generate n_t sets of $4n_m$ linear algebraic equations relating an equal number of unknown integration constants [29]. However, one differential equation, corresponding to $4n_m$ algebraic equations, in (3.13) and (3.14) must be replaced by the set of $4n_m$ boundary conditions in the form (3.6*a*) and (3.6*b*) to obtain a unique solution to the unknown integration constants.

In closed loop feedback control the motion of a system is continually driven to the null state, with zero displacements and velocities, in a time-invariant manner. This scenario is typical for actively dampened structures, where vibrations are observed by sensors and relayed to actuators that act to reduce disturbances. Therefore, the final boundary conditions are defined over an infinite maneuver time ($t_f \to \infty$) and the solution functions in vector $\boldsymbol{Y}$ must decay with increasing time. This requires that the value of the integration constants c_{kj}^3 and c_{kj}^4 in equation (3.19) be set to zero. This reduces the number of unknown integration constants defining the solution functions by half and the resulting solution functions, with $2n_m$ unknown integration constants, take the form:

$$Y_j = \sum_{k=1}^{n_m} e^{-\alpha_k t}\left[c_{kj}^1 sin(\beta_k t) + c_{kj}^2 cos(\beta_k t)\right], \qquad j = 1, \dots, n_t \tag{3.20}$$

The parameters β_k and α_k can be respectively interpreted as the vibration frequency and active damping associated with the k-th controlled mode corresponding to modal shape vector $\boldsymbol{\phi}_k$. Any vibrations with the frequency β_k will be reduced to approximately 3-percent of the initial value after a time period of $t_k^{3\%} = 3.5/\alpha_k$, referred to as the 3-percent settling time and corresponds to the k-th mode of vibration (i.e. $e^{-3.5} \cong 0.03$). The active modal damping ratio corresponding to the k-th mode is defined as $\xi_k = \alpha_k/\beta_k$ and reflects how many oscillations should be expected in the k-th vibration mode before it effectively decays below a certain threshold. As previously mentioned these steps are handled automatically using the MAPLE software and form the majority of the calculations involved in the control stage (as shown in the flowchart of Figure 3-1).

3.3.4 Closed Loop Feedback Gains

In closed loop feedback control, a system is equipped with a number of n_s sensors that relay output information on the system's states to a processor that signals system actuation forces

to correct the disturbances in these states. In general, the system's output vector $\boldsymbol{y}$ can have n_s components related to the positions and velocities of the DOFs in the form:

$$\boldsymbol{y} = \boldsymbol{C}\boldsymbol{z} = [\boldsymbol{C_d} \quad \boldsymbol{C_v}] \begin{bmatrix} \boldsymbol{q} \\ \dot{\boldsymbol{q}} \end{bmatrix} = \boldsymbol{C_d}\boldsymbol{q} + \boldsymbol{C_v}\dot{\boldsymbol{q}} \tag{3.21}$$

Matrix $\boldsymbol{C}$ is partitioned into matrices $\boldsymbol{C_d}$ and $\boldsymbol{C_v}$ that are each of size $n_s \times n$ and describe the placement of sensors related to position and velocity states in vector $\boldsymbol{z} = [\boldsymbol{q}^T \quad \dot{\boldsymbol{q}}^T]^T$ respectively.

A simple feedback controller relays the system outputs contained in vector $\boldsymbol{y}$ and multiplies them by a set of constant valued gains that generate the actuation forces in vector $\boldsymbol{F_a}$ in the form:

$$\boldsymbol{F_a} = -\boldsymbol{G}\boldsymbol{y} = -\boldsymbol{G}\boldsymbol{C_d}\boldsymbol{q} - \boldsymbol{G}\boldsymbol{C_v}\dot{\boldsymbol{q}} = -\boldsymbol{G_d}\boldsymbol{q} - \boldsymbol{G_v}\dot{\boldsymbol{q}} \tag{3.22}$$

Matrix $\boldsymbol{G}$, of size $n_a \times n_s$, contains constant valued gains that when multiplied by positioning matrices $\boldsymbol{C_d}$ and $\boldsymbol{C_v}$, each of size $n_s \times n$, produce matrices $\boldsymbol{G_d}$ and $\boldsymbol{G_v}$, each of size $n_a \times n$. The matrices $\boldsymbol{G_d}$ and $\boldsymbol{G_v}$ contain gains relating to positions and velocities, respectively. As shown in the flowchart in Figure 3-1, these gains are easily obtained using the MAPLE software. The process is simple because the actuator forces $\boldsymbol{F_a}$ and system response $\boldsymbol{q}$ were already obtained in the previous step of the control stage enabling the gains to be solved directly by using the method of undetermined coefficients on equation (3.22). Alternatively, the gains may be solved by writing out equation (3.22) at a sufficient number of instances in time and solving the resulting system of equations for the unknown gains.

The feedback relationship (3.22) may be substituted into the governing equations of motion (2.1) to obtain:

$$\boldsymbol{M}\ddot{\boldsymbol{q}} + (\boldsymbol{C} + \boldsymbol{B}\boldsymbol{G_v})\dot{\boldsymbol{q}} + (\boldsymbol{K} + \boldsymbol{B}\boldsymbol{G_d})\boldsymbol{q} = \boldsymbol{0} \tag{3.23}$$

In the form (3.23), the gains matrix $\boldsymbol{G_d}$ affects the system stiffness and frequencies and the matrix $\boldsymbol{G_v}$ affects the attenuation properties.

Appendix B contains further discussion on the methods of obtaining gains with and without assuming initial conditions. Also, a means of evaluating system observability for a given configuration of sensors in a system is discussed.

3.4 Verification Stage

The verification stage is represented in the bottom left hand box in the flowchart of Figure 3-1. It utilizes the FEM model created in the structural stage to verify the system response that is obtained in the control stage. The transient time-integrated responses of the DOFs subject to the attenuation forces $\boldsymbol{F_a}$ (obtained in the control stage), contained in vector $\boldsymbol{q_{int}}$, are obtained using the ANSYS program. The responses contained in $\boldsymbol{q_{int}}$ are then compared to the response $\boldsymbol{q}$ (obtained in the control stage) to ensure that the model is accurate and that the attenuating forces do not excite higher modes of vibration not considered in the control stage (spillover effects).

For example consider the vibrating beam system in Figure 3-2. Two modes were considered in the dynamics and they were to be controlled by the single actuator F_{a_1} located at the position x. In general, the system motion actually contains an infinite number of other modes of vibration that were neglected in the control stage of the analysis. Therefore the control stage cannot provide any information on how the third, fouth, and fifth, etc. modes would be affected by the actuation force F_{a_1}.

In the verification stage any number of these higher modes could be considered to determine the effect that the control force will have on them. Say for this example that in the verification stage, the first three modes of vibration were included. One could see that the time-

integrated response $\boldsymbol{q_{int}} \neq \boldsymbol{q}$ because the force F_{a_1} may excite vibrations related to the third vibration mode that will not be controlled. If the level of un-attenuated motion exceeds an acceptable threshold than a new model that contains the additional mode(s) should be considered in the structural and control stages.

The verification stage requires that the continuous time-varying functions $\boldsymbol{F_a}(t)$, obtained in the control stage, be converted to a discrete time function $\boldsymbol{F_a}(n\Delta t)$ that can be applied to the transient FEM model at corresponding time steps and load steps. This process is facilitated through an EXCEL spreadsheet that can be written to a text file that can be interpreted by the ANSYS software. The details of this data manipulation and other issues concerning the selection of time steps, load steps, and applying initial conditions are covered in more detail in Chapter 5.

4. OPTIMAL MANUEVERS FOR GANTRY CRANE OPERATIONS

4.1 Gantry Crane Model [22]

The gantry crane problem is a simple under-actuated mechanical system involving two DOFs ($n = 2$). It is used to explain some details of the *structural stage* and the *control stage* of the CMSOC procedure (see Figure 3-1). The DOFs that define the system are the linear translation of a trolley and the rotation of a suspended load. The translational DOF is actuated by a trolley driving force and the suspended load is free to rotate in a pendular motion ($n_a = 1, n_c = 1$). Any finite cart translations are permitted, but swings of the suspended load are assumed sufficiently small for a linear model to adequately represent the system dynamics. The system model, shown in Figure 4-1, is a practical model for analyzing the dynamics of overhead crane operations [3,10].

The model parameters include: the mass of the trolley M, the mass of the suspended load m, the swing angle of the load suspending cable θ, and the displacement of the cart x. The cable of length L is assumed to be massless and rigid and the gravitational acceleration g is assumed to act in the same plane and perpendicular to the direction of trolley travel. The control task is to maneuver the system from an initial resting state at a some non-zero horizontal distance at $x(0) = a$ and $\theta(0) = 0$ to a final resting equilibrium state at the datum $x(t_f) = 0$ and $\theta(t_f) = 0$. The maneuver is controlled by the time-varying trolley driving force F_a. A dummy actuator force F_d is assumed to act in the same direction of F_a but applied to the center-of-gravity of the suspended load to define the augmented gantry crane system.

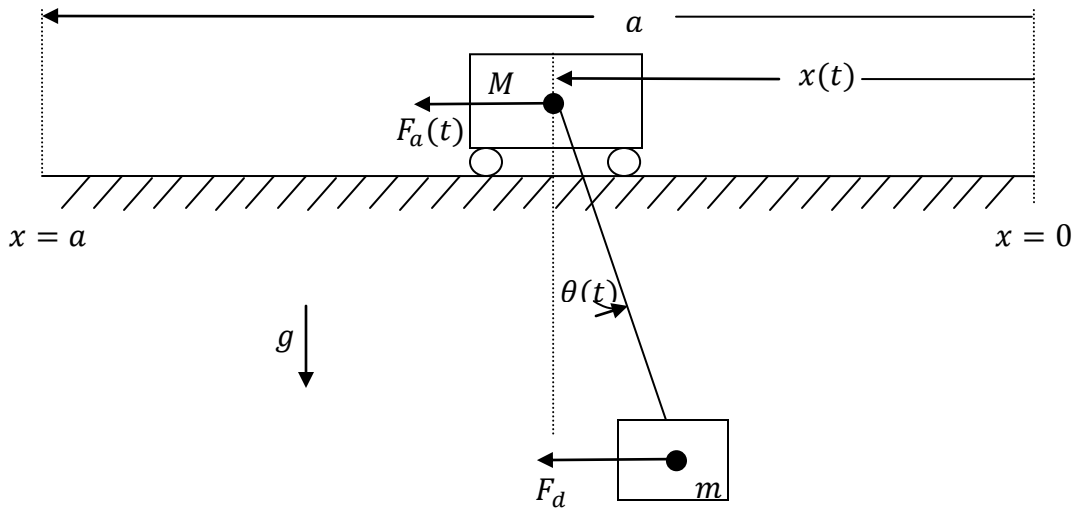

Figure 4-1. Gantry crane model.

This same gantry crane model was considered in many papers. In [3] a Lyapunov function was used to obtain an asymptotically stable (closed-loop) control (linear and non-linear) for attenuating disturbances (non-zero initial positions) in such a gantry crane system. The optimal control for this same system was analyzed in [10]. The CMSOC approach will be tested against the methods applied in these papers and the results will be compared. The gantry crane system shown Figure 4-1 and the coordinate system are chosen to be consistent with those used in [3]. The results and discussion presented in this chapter are more fully covered in [22].

The matrices and vectors characterizing the equations of motion (2.1) are:

$$\boldsymbol{M} = \begin{bmatrix} M+m & -m \\ -m & m \end{bmatrix}, \quad \boldsymbol{K} = \begin{bmatrix} 0 & 0 \\ 0 & \frac{mg}{L} \end{bmatrix}, \quad \boldsymbol{B} = \begin{bmatrix} 1 & 1 \\ 0 & -1 \end{bmatrix}, \quad \boldsymbol{q} = \begin{bmatrix} x \\ L\theta \end{bmatrix}, \quad \boldsymbol{F} = \begin{bmatrix} F_a \\ F_d \end{bmatrix} \tag{4.1}$$

To be consistent with the assumptions made in [3,10], and to concentrate on active damping characteristics, no dissipative effects are considered ($\boldsymbol{C} = \boldsymbol{O}$). The initial and final conditions are chosen to be consistent with the system considered in [3] and are:

$$\boldsymbol{q}(0) = \begin{bmatrix} a \\ 0 \end{bmatrix}, \qquad \dot{\boldsymbol{q}}(0) = \dot{\boldsymbol{q}}(t_f) = \boldsymbol{q}(t_f) = \begin{bmatrix} 0 \\ 0 \end{bmatrix} \tag{4.2}$$

The two system DOFs ($n = 2$) are related to two modal variables ($n_m = 2$) via equation (2.9*a*) with frequencies and modal shapes obtained from the eigenvalues problem (2.11) to obtain:

$$\boldsymbol{\Omega} = \begin{bmatrix} 0 & 0 \\ 0 & \left(1 + \frac{m}{M}\right)\frac{g}{L} \end{bmatrix}, \qquad \boldsymbol{\Phi} = \begin{bmatrix} \frac{1}{\sqrt{M+m}} & \sqrt{\frac{m}{M(M+m)}} \\ 0 & \sqrt{\frac{M+m}{Mm}} \end{bmatrix} \tag{4.3}$$

The first rigid body mode has a zero frequency ($\omega_1 = 0$) and the second pendular mode has the frequency $\omega_2 = \sqrt{\left(1 + \frac{m}{M}\right)\frac{g}{L}}$. The modal-space equation of motion (2.12) takes the uncoupled form written as:

$$\begin{bmatrix} 1 & 0 \\ 0 & 1 \end{bmatrix}\begin{bmatrix} \ddot{\eta}_1 \\ \ddot{\eta}_2 \end{bmatrix} + \begin{bmatrix} 0 & 0 \\ 0 & \left(1 + \frac{m}{M}\right)\frac{g}{L} \end{bmatrix}\begin{bmatrix} \eta_1 \\ \eta_2 \end{bmatrix} = \begin{bmatrix} u_1 \\ u_2 \end{bmatrix} \tag{4.4}$$

The transformation between the actuator forces (one real and one dummy) and modal controls in accordance with (2.9*b*) ($\widehat{\boldsymbol{B}} = \boldsymbol{\Phi}^{\boldsymbol{T}}\boldsymbol{B}$) may be obtained by making the appropriate substitutions from (4.1) and (4.3). The inverse transformation can be written in the form (3.1), as:

$$\begin{bmatrix} F_a \\ F_d \end{bmatrix} = \widehat{\boldsymbol{B}}^{-1}\boldsymbol{U} = \begin{bmatrix} \frac{M}{\sqrt{M+m}} & \sqrt{\frac{Mm}{M+m}} \\ \frac{m}{\sqrt{M+m}} & -\sqrt{\frac{Mm}{M+m}} \end{bmatrix}\begin{bmatrix} u_1 \\ u_2 \end{bmatrix} = \begin{bmatrix} F_a \\ 0 \end{bmatrix} \tag{4.5}$$

Modal controls u_1 and u_2 are considered independent and redundant respectively. The $n_c = 1$ constraint equation is obtained from the bottom row of matrix $\widehat{\boldsymbol{B}}^{-1}$ in (4.5) in accordance with (3.3) to obtain:

$$\begin{bmatrix} 1 & -\sqrt{\frac{M}{m}} \end{bmatrix}\begin{bmatrix} u_1 \\ u_2 \end{bmatrix} = u_1 - \sqrt{\frac{M}{m}}u_2 = 0 \tag{4.6}$$

The constraint equation (4.6) may be applied to eliminate the redundant modal control u_2 from the top row of operation (4.5) to obtain the drive force F_a as a function of only the independent modal control u_1 in accordance (3.4). This mapping, defined by the pseudo-transfer matrix $\bar{\boldsymbol{B}}_{\boldsymbol{a}} = \sqrt{M+m}$, takes the scalar form:

$$\boldsymbol{F_a} = F_a = \bar{\boldsymbol{B}}_{\boldsymbol{a}} \boldsymbol{U_a} = \sqrt{M+m}\, u_1 \tag{4.7}$$

The performance index for the gantry crane system is assumed to take a form which is consistent with the general form given in equation (3.7). The weighting matrices $\boldsymbol{Q_d}$, $\boldsymbol{Q_v}$, and $\boldsymbol{R}$ are assumed to have the diagonal weighting terms $Q_{d_{ii}}$, $Q_{v_{ii}}$, and R_{ii} $(i = 1, \dots, n_m)$ that penalize non-zero values of the system's four states $(\eta_1, \eta_2, \dot{\eta}_1, \dot{\eta}_2)$ and two modal controls (u_1, u_2) in the functional:

$$J = 1/2 \int_0^{t_f} \left(Q_{d_{11}}\eta_1^2 + Q_{d_{22}}\eta_2^2 + Q_{v_{11}}\dot{\eta}_1^2 + Q_{v_{22}}\dot{\eta}_2^2 + R_{11}u_1^2 + R_{22}u_2^2\right)dt \rightarrow min \tag{4.8}$$

The Hamiltonian is defined in accordance with equation (3.8) and Pontryagin's formalism is applied to obtain the set of $n_m = 2$ optimality equations in the form (3.13), written as:

$$R_{11}\dddot{\eta}_1 - Q_{v_{11}}\ddot{\eta}_1 + Q_{d_{11}}\eta_1 - \ddot{v}_1 = 0 \tag{4.9a}$$

$$R_{22}\dddot{\eta}_2 + \left(2R_{22}\omega_2^2 - Q_{v_{11}}\right)\ddot{\eta}_2 + \left(R_{22}\omega_2^4 + Q_{d_{22}}\right)\eta_2 + \sqrt{\tfrac{M}{m}}(\ddot{v}_1 + \omega_2^2 v_1) = 0 \tag{4.9b}$$

There is $n_c = 1$ Lagrange multiplier v_1 that accounts for the constraint (4.6). This constraint is written in accordance with (3.14), in the differential form:

$$\ddot{\eta}_1 - \sqrt{\tfrac{M}{m}}(\ddot{\eta}_2 + \omega_2^2\eta_2) = 0 \tag{4.10}$$

In modal-space the boundary conditions in the form (3.6a) and (3.6b), are:

$$\eta_1(0) = a\sqrt{M+m}, \qquad \eta_2(0) = \dot{\eta}_2(0) = \dot{\eta}_1(0) = 0$$

$$\eta_1(t_f) = \eta_2(t_f) = \dot{\eta}_1(t_f) = \dot{\eta}_2(t_f) = 0 \tag{4.11}$$

Substituting the differential operator $D^j = d^j/dt^j$ and adopting the matrix notation (3.15), the optimality conditions (4.9*a*) and (4.9*b*) and constraint equation (4.10) can be written as:

$$\boldsymbol{E_p Y} = \begin{bmatrix} \boldsymbol{E} & -\widehat{\boldsymbol{E}}^T \\ \check{\boldsymbol{E}} & \boldsymbol{0} \end{bmatrix} \begin{bmatrix} \boldsymbol{\eta} \\ \boldsymbol{v} \end{bmatrix} = \begin{bmatrix} E_1 & 0 & -\hat{E}_{11} \\ 0 & E_2 & -\hat{E}_{21} \\ \check{E}_{11} & \check{E}_{12} & 0 \end{bmatrix} \begin{bmatrix} \eta_1 \\ \eta_2 \\ v_1 \end{bmatrix} = \boldsymbol{0} \tag{4.12}$$

The components contained in (4.12), consistent with equations (3.16*a*), (3.16*b*), and (3.16*c*), take the form:

$$E_1 = R_{11}D^4 - Q_{v_{11}}D^2 + Q_{d_{11}}, \tag{4.13a}$$

$$E_2 = R_{22}D^4 + \left(2R_{22}\omega_2^2 - Q_{v_{11}}\right)D^2 + \left(R_{22}\omega_2^4 + Q_{d_{22}}\right) \tag{4.13b}$$

$$\hat{E}_{11} = \check{E}_{11} = D^2, \quad \hat{E}_{21} = \check{E}_{12} = -\sqrt{\tfrac{M}{m}}(D^2 + \omega_2^2) \tag{4.13c}$$

The characteristic equation (3.17) for the gantry crane system is an eighth order ($4n_m$) polynomial equation in the form:

$$Det\left(\boldsymbol{E_p}\right)\Big|_{D\to r} = E_1\hat{E}_{21}^2\check{E}_{12}^2 + E_2\hat{E}_{11}^2\check{E}_{11}^2\Big|_{D\to r} = 0 \tag{4.14}$$

$$= \tfrac{M}{m}\left(R_{11}r^4 - Q_{v_{11}}r^2 + Q_{d_{11}}\right)(r^2+\omega_2^2)^2 + r^4\left(R_{22}r^4 + \left(2R_{22}\omega_2^2 - Q_{v_{22}}\right)r^2 + \left(R_{22}\omega_2^4 + Q_{d_{22}}\right)\right) = 0$$

Eight roots are obtained from the characteristic equation (4.14). The solution functions take the form of equation (3.19) when the roots are complex in the form (3.18). This only applies to time-invariant problems where the maneuver time approaches infinity ($t_f \to \infty$). For maneuvers executed over a fixed time interval, zero valued roots are obtained and the solution functions

require modifications from that shown in (3.19) (see Section 4.2 for further explanation). Note that maneuvers executed over a finite time cannot be implemented in a closed-loop control system, as they depend on the initial conditions.

There are three solution functions that are assumed for the unknowns η_1, η_2, and ν_1. They depend on twenty-four unknown integration constants that are to be determined by substitution into optimality equations (4.9*a*) and (4.9*b*), and the constraint equation (4.10). By relating the coefficients corresponding to each of the eight independent elementary functions (i.e. in (3.19) these take the form $e^{(\pm\alpha_k \pm i\beta_k)t}$) one obtains eight algebraic equations for each differential equation in the set (4.9*a*), (4.9*b*) and (4.10). This gives a total of twenty-four linear algebraic equations relating the twenty-four unknown integration constants c_{kj}^{i} to be solved. However, these twenty-four equations are linearly dependant. To solve for the unknown constants, one complete set of eight algebraic equations (of the three obtained from (4.9*a*), (4.9*b*), or (4.10)) must be discarded and replaced with the complete set of eight boundary conditions (4.11).

In this example, the CMSOC method will be used to obtain the optimal actuation forces needed to drive the gantry crane from the resting position at a non-zero translational position ($x = a, \theta = 0$) to a resting position at the origin ($x = 0, \theta = 0$). Four cases will be examined:

A. An open-loop, fixed time interval maneuver that minimizes actuation forces.

B. A time-invariant, closed-loop maneuver that reproduces the control presented in [3].

C. A time-invariant, closed-loop maneuver with improved response.

D. A time-invariant, closed-loop maneuver of the fully-actuated system.

For each case, the numerical values for the physical constants defining the gantry crane system are assumed to be: $M = m = 1kg$, $L = 1m$, $g = 9.8\, m/s^2$, and $a = -5m$. These numerical assumptions are consistent with [3].

4.2 Case A: Open-loop, fixed time interval maneuver that minimizes actuation forces

Case A considers the optimal maneuver that brings the gantry crane model from rest at a known initial position ($x = a$, $\theta = 0$) to a resting position at the origin ($x = 0$, $\theta = 0$) in a finite time interval t_f. Controls operating over a finite time-interval must be implemented in an open-loop control system because the controls cannot be generated through sensor feedback. The performance index is chosen to be identical with that presented in [10], which is in the form (4.8) with the weighting parameter selections: $R_{11} = R_{22} = 1$, $Q_{d_{11}} = Q_{d_{22}} = Q_{v_{11}} = Q_{v_{22}} = 0$. For this case, the optimal control minimizes:

$$J = \int_0^{t_f} (u_1^2 + u_2^2)dt = \frac{1}{M}\int_0^{t_f} F_a^2 dt \rightarrow min \tag{4.15}$$

The expression on the right of (4.15) is obtained by substitutions from equations (4.6) and (4.7). In qualitative terms, the performance index (4.15) favors controls that perform the maneuver using the smallest possible forces in the finite time t_f. For this case, the maneuver time is somewhat arbitrarily chosen as $t_f = 4s$.

For this case, the characteristic polynomial equation from equation (4.14) reduces to:

$$\left(1 + \frac{M}{m}\right)(r^2 + \omega_2^2)^2 r^4 = 0 \tag{4.16}$$

The eight roots of equation (4.16) are: $r_1, \ldots, r_8 = 0,0,0,0, \pm i\omega_2, \pm i\omega_2$. These roots correspond to $\alpha_1 = \alpha_2 = \beta_1 = 0$ and $\beta_2 = \omega_2 = 4.43$ when written in the form (3.18). Due to the zero valued roots and repeating roots the solution functions in (3.19) must be modified to the form:

$$Y_j = c_{1j} + c_{2j}t + c_{3j}t^2 + c_{4j}t^3 + \left(c_{5j} + c_{7j}t\right)\sin(\omega_2 t) + \left(c_{6j} + c_{8j}t\right)\cos(\omega_2 t) \qquad (4.17)$$

Each solution function Y_j ($j = 1,2,3$ and recall that $Y_1 = \eta_1,\ Y_2 = \eta_2,\ Y_3 = \nu_1$) contains eight unknown integration constants c_{kj} ($k = 1, \ldots, 8$), which are obtained through the method of undetermined coefficients. Equation (4.17) is substituted into any two of three differential equations in the set (4.9*a*), (4.9*b*), or (4.10) and simultaneously solved with the eight boundary conditions (4.11). With the values of the integration constants obtained, the modal variables and Lagrange multiplier solutions are known functions. This stage of the solution was done automatically using MAPLE and yields the functions:

$$\eta_1 = -7.09 - 0.104t + 1.41t^2 - 0.235t^3 + 0.0235\sin(4.43t) + 0.0151\cos(4.43t) \qquad (4.18)$$

$$\eta_2 = \tfrac{1}{100}[14.4 - 7.19t + (0.451 - 3.33t)\sin(4.43t) + (-14.4 + 5.20t)\cos(4.43t)] \qquad (4.19)$$

$$\nu_1 = -2.82 + 1.41t - 0.460\sin(4.43t) - 0.295\cos(4.43t) \qquad (4.20)$$

The Lagrange multiplier function (4.20) is shown for completeness, but has no physical significance to the dynamics. The modal control u_1 is obtained by substitution of (4.18) into (4.4) to obtain:

$$u_1 = 2.82 - 1.41t - 0.460\sin(4.43t) - 0.295\cos(4.43t) \qquad (4.21)$$

The modal variable functions η_1 and η_2 in (4.18) and (4.19) are mapped to the DOFs x and θ by transformation (2.9*a*) with substitution of the modal shape matrix from (4.3). The actuation force F_a is obtained by substituting the modal control function u_1 from (4.21) into equation (4.7). These transformations take the form:

$$x = \tfrac{1}{\sqrt{2}}(\eta_1 + \eta_2), \quad \theta = \sqrt{2}(\eta_2), \quad F_a = \sqrt{2}u_1 \qquad (4.22)$$

The trajectories of x and θ are shown in Figure 4-2a and Figure 4-2b respectively and the actuation force F_a is plotted in Figure 4-2c.

The maneuver brings the system from a resting position at $x = -5m$ and $\theta = 0$ to a resting position at $x = 0$ and $\theta = 0$ over a time interval of exactly 4 seconds. The peak force amplitude required for the maneuver is approximately 3.6N and the maximum load swing angle is approximately 0.28rad (16°). The optimal drive force essentially accelerates the trolley over the first half the maneuver and decelerates the cart over the last half with identical, but opposite and mirrored forces. The oscillating frequency of the applied force corresponds with the pendular frequency of the suspended load.

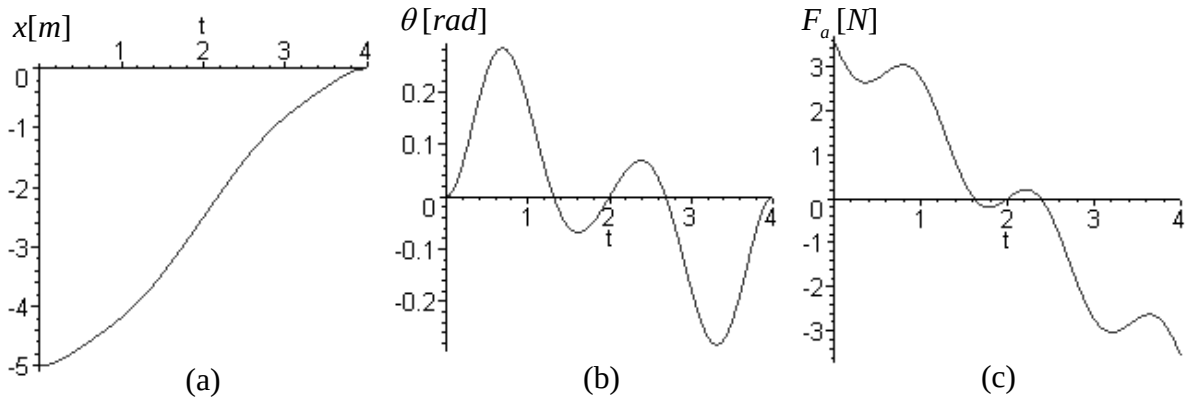

Figure 4-2. Graphs of (a) trolley position, (b) load angle, and (c) trolley force for open-loop, fixed time interval maneuver (case A).

For comparison the same plots of x, θ, and F_a that were presented in [3] are shown in Figure 4-3. This control has an effective maneuver time of $t_f^{3\%} = 6s$, a maximum load rotation angle of 0.73rad (42°), and a peak drive force of approximately 15N.

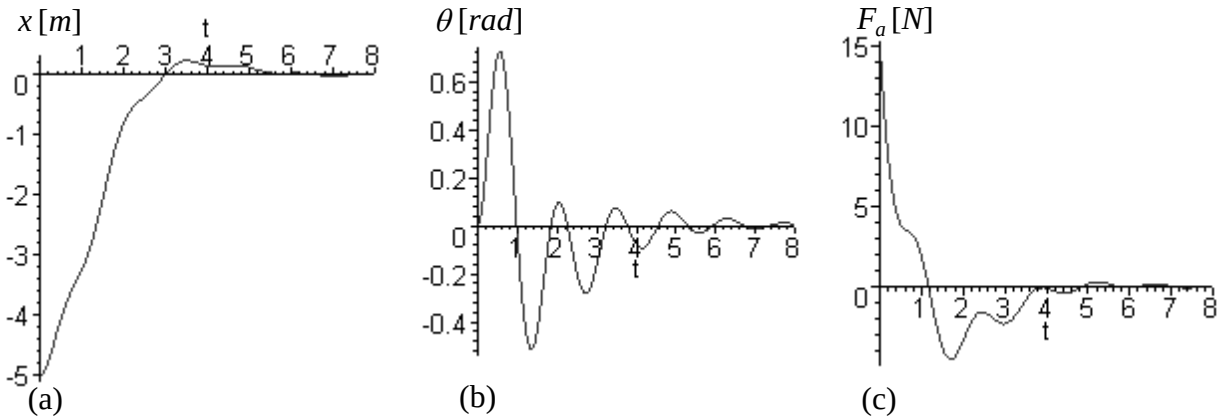

Figure 4-3. Graphs of (a) trolley position, (b) load angle, and (c) trolley force for closed-loop control presented in [3].

Comparing Figure 4-2 and Figure 4-3, the open-loop control effectively performs the maneuver in a shorter period of time ($t_f = 4s$ vs. $t_f^{3\%} = 6s$), with much smaller peak force requirements (3.6*N* vs. 15*N*), and much smaller angles of oscillation (16° vs. 42°). The open-loop control brings the system to a complete stop after 4*s*, while the closed-loop control produces overshoot and the system takes longer to come to effectively come to rest.

If the finite maneuver time for the open-loop control is extended (or shortened), the peak force requirement and maximum swing angle is reduced (or increased) by approximately t_f^{-2}. For example, if the open-loop control is modified to settle over the same effective period of time as the closed-loop control ($t_f = 6s$) the maximum force is reduced to approximately 1.6*N* with a maximum swing of about 7°.

An open-loop control performs a faster and more efficient maneuver. However, such a maneuver is only possible when the initial positions and maneuver times are known in advance. Closed-loop control is necessary for active systems, where any disturbance is to be automatically attenuated (the initial position is unknown). Closed-loop systems are of primary interest in this

thesis and will be considered in the remaining examples. Case B in Section 4.3 demonstrates how the CMSOC method is applied to analyze and simulate a closed-loop control for the gantry crane system to reproduce (approximately) the dynamics produced in [3] that were plotted in Figure 4-3.

4.3 Case B: Time-invariant, closed-loop maneuver that reproduces the dynamics presented in [3]

A closed-loop control can perform the same task as the open-loop control (case A); however, it does so automatically, without prior knowledge of initial conditions. Any disturbance that causes the gantry crane to deviate from its resting configuration at the origin ($x = 0, \theta = 0$) is automatically observed (i.e. by sensors) and the signal is relayed through a set of constant gains to generate a cart-driving force F_a that attenuates the disturbance.

In general, to simulate a closed-loop system analytically the maneuver time t_f becomes theoretically infinite and all disturbances are driven asymptotically to zero. For the gantry crane, this requires that all roots of the characteristic equation (4.14) be non-zero complex numbers in the left half of the complex plane (unlike the open-loop system of case A**,** which contained zero roots and purely imaginary roots). It can be verified that the weightings $Q_{d_{11}}$ and $Q_{d_{22}}$ in the performance index (4.8) must be non-zero for asymptotically stable roots.

Through trial and error, the control system that was given in [3] may be approximately reproduced by choosing the weightings in the performance index (4.8) with the values: $Q_{d_{11}} = 4.5$, $Q_{d_{22}} = 42$, $Q_{v_{11}} = Q_{v_{22}} = 0$, $R_{11} = R_{22} = 1$. Therefore, the characteristic polynomial equation (4.14) has eight roots that take the complex form (3.18), with real and imaginary parts given as:

$$\alpha_1 = 0.853, \qquad \beta_1 = 0.856, \qquad \alpha_2 = 0.513, \qquad \beta_2 = 4.46 \tag{4.23}$$

The parameters α_1 and β_1 respectively, are related to the active damping rate and frequency of the mode related to the rigid body translation of the trolley, whereas the parameters α_2 and β_2 are reflective of the damping and frequency of the higher frequency mode corresponding to the load swinging. Note that the oscillation frequency of the second mode for the damped system is approximately equal to that of the undamped system ($\beta_2 \cong \omega_2$).

Like case A, modal variables η_1 and η_2 are determined by substituting the parameters from (4.23) into an assumed solution form and then solving for the unknown coefficients by comparing similar terms in two of the three optimality/constraint equations (4.9*a*), (4.9*b*), and (4.10), and by substituting the boundary conditions (4.11). Unlike case A, the closed-loop problem requires that only half as many integration constants be obtained, because the coefficients of exponential growth functions ($e^{\alpha_k t}$) are null-valued. The assumed solution functions take the form given in (3.19). The modal variable functions η_1 and η_2 are listed below along with the modal control u_1.

$$\eta_1 = e^{-\alpha_1 t}(-7.70\sin(\beta_1 t) - 7.08\cos(\beta_1 t)) + e^{-\alpha_2 t}(12.6\sin(\beta_2 t) - 0.564\cos(\beta_2 t))/100 \qquad (4.24)$$

$$\eta_2 = e^{-\alpha_1 t}(-0.565\sin(\beta_1 t) + 0.534\cos(\beta_1 t)) + e^{-\alpha_2 t}(0.149\sin(\beta_2 t) - 0.534\cos(\beta_2 t)) \qquad (4.25)$$

$$u_1 = e^{-\alpha_1 t}(-10.3\sin(\beta_1 t) + 11.3\cos(\beta_1 t)) + e^{-\alpha_2 t}(-2.44\sin(\beta_2 t) - 0.686\cos(\beta_2 t)) \qquad (4.26)$$

Using the appropriate transformations from equations (4.22), the modal-space variables in equations (4.24-4.26) can be mapped into corresponding DOFs. It can be verified that the resulting system trajectories and the optimal trolley drive force are practically indistinguishable from the plots shown in Fig. 4-3, which were presented in [3].

The gantry crane system's feedback relationship, in the form of equation (3.22), produces the active trolley driving force from sensor feedback from the trolley's states $(x, \dot{x})$ and suspended load's states $(\theta, \dot{\theta})$ in the form:

$$F_a = -G_{d_{11}}x - G_{d_{12}}L\theta - G_{v_{11}}\dot{x} - G_{v_{12}}L\dot{\theta} \tag{4.27}$$

The states of the suspended load are multiplied by the constant length of the rope L so that all the gains share similar units and for consistency with the system presented in [3]. The closed-loop gains for the gantry crane system discussed in [3] were published as:

$$\boldsymbol{G_d} = [G_{d_{11}} \quad G_{d_{12}}] = [3.00 \quad 0.710], \qquad \boldsymbol{G_v} = [G_{v_{11}} \quad G_{v_{12}}] = [3.69 \quad -0.870] \tag{4.28}$$

Substituting the modal-space transformations (4.22) into equation (4.27), along with the appropriate substitutions of the functions shown in (4.24-4.26), the terms related to the four independent elementary functions can be grouped to obtain:

$$\begin{aligned}
&e^{-\alpha_1 t}\sin(\beta_1 t)\left[-14.6 - 5.85G_{d_{11}} + 8.95G_{v_{11}} - 0.799G_{d_{12}} + 0.0352G_{v_{12}}\right] + \\
&e^{-\alpha_1 t}\cos(\beta_1 t)\left[16.0 - 4.63G_{d_{11}} - 1.06G_{v_{11}} + 0.755G_{d_{12}} - 1.33G_{v_{12}}\right] + \\
&e^{-\alpha_2 t}\sin(\beta_2 t)\left[-3.45 + 0.195G_{d_{11}} + 1.56G_{v_{11}} + 0.211G_{d_{12}} + 3.26G_{v_{12}}\right] + \\
&e^{-\alpha_2 t}\cos(\beta_2 t)\left[-0.970 - 0.374G_{d_{11}} + 1.06G_{v_{11}} - 0.755G_{d_{12}} + 1.33G_{v_{12}}\right] = 0
\end{aligned} \tag{4.29}$$

Equation (4.29) requires that each of the square-bracketed terms be equal to zero for the equation to be satisfied at all times t. Each bracketed term contains an independent linear algebraic relationship producing four equations to be solved for the four unknown gains. This system of equations can be solved to obtain:

$$\boldsymbol{G_d} = [G_{d_{11}} \quad G_{d_{12}}] = [3.00 \quad 0.732], \qquad \boldsymbol{G_v} = [G_{v_{11}} \quad G_{v_{12}}] = [3.66 \quad -0.924] \tag{4.30}$$

Though initial conditions were assumed in determining the trajectories of x and θ and force F_a, it can be verified that the gains in (4.30) remain invariant with respect to changes in these assumed conditions.

Comparing the gains in (4.28) and (4.30) demonstrates that the CMSOC method can closely reproduce the control presented in [3] through careful selection of the weighting parameters in performance index (4.8). However, the dynamic performance of the gantry crane maneuver may be "improved" through a different selection of the performance index weighting parameters. Case C in Section 4.4 demonstrates how the gantry crane maneuver can be modified to produce faster convergence without an increase in the required peak actuation forces.

4.4 Case C – A time-invariant, closed-loop maneuver with improved response

In case B the CMSOC approach was used to demonstrate how the linear gantry crane control system presented in [3] could be reproduced by trial and error selection of the performance index parameters in equation (4.8). It was found that the resulting performance index had zero valued weighting parameters $Q_{v_{11}} = Q_{v_{22}} = 0$; these weighting parameters penalize the velocity states ($\dot{\eta}_1$ and $\dot{\eta}_2$) in the optimization problem. Therefore, the optimal drive force was devoted to reducing the non-zero positions of the trolley and load and no penalty was associated with reducing their non-zero velocities. This is ineffective because the pendulum action of the suspended load oscillates between states of maximum potential energy ($\theta \rightarrow max, \dot{\theta} = 0$) and states of maximum kinetic energy ($\theta = 0, \dot{\theta} \rightarrow max$). Failure to include the velocity states in the performance index produced a maneuver, as shown in case Figure 4-3, that caused the trolley to overshoot its target and result in large persistent load swings. These problems are mitigated by a more careful choice of the performance index weighting parameters in (4.8).

There is a direct relationship between the angle of the load rotation and the second modal variable η_2 ($\theta = \sqrt{2}\eta_2$), such that the load swing angle trajectory is directly affected by varying the weighting values given to the terms containing modal variable η_2 ($Q_{d_{22}}$) and its derivative $\dot{\eta}_2$ ($Q_{v_{22}}$) in the performance index (4.8). On the other hand, the speed at which the cart can be made to approach the final position is affected through variation of the weighting values given to terms containing modal variable variable η_1 ($Q_{d_{11}}$) and its derivative $\dot{\eta}_1$ ($Q_{v_{11}}$).

The effect of various choices of the performance index parameters are studied in detail for the gantry crane system in [22]. Through a trial and error selection process, the weighting parameters $Q_{d_{11}}$, $Q_{d_{22}}$, $Q_{v_{11}}$, and $Q_{v_{22}}$ were varied to study the 'best' combination for producing a quick and effective maneuver with the weighting parameters R_{11} and R_{22} held constant at a value of unity. The 'best' combination was found to be: $Q_{d_{11}} = 6$, $Q_{d_{22}} = 50$, $Q_{v_{11}} = 4$, $Q_{v_{22}} = 50$, and $R_{11} = R_{22} = 1$.

Similar to case B in Section 4.3, the characteristic polynomial equation (4.14) has eight roots that take the complex form (3.18), with real and imaginary parts given as:

$$\alpha_1 = 1.63, \qquad \beta_1 = 0.661, \qquad \alpha_2 = 1.31, \qquad \beta_2 = 1.65 \tag{4.31}$$

In comparison to case B, the damping coefficients α_1 and α_2, have increased by 91-percent and 156-percent respectively. Also the frequency of the higher mode β_2 has decreased by 63-percent to a frequency well below that of the undamped system ($\beta_2 \neq \omega_2$), meaning that the active control has significantly affected the pendular frequency.

Figure 4-4*a* shows the trolley position x, Figure 4-4*b* displays the suspended load rotation θ, and Figure 4-4*c* plots the trolley drive force F_a for 8*s* of the maneuver. The control results in a maximum swing angle of $0.45rad$ (25.8°) and the trolley effectively reaches the target

in $t_f^{3\%} = 3.5s$. The trolley performs the maneuver in a single load swing cycle without persistent oscillations and overshoots upon reaching the target position. The peak trolley drive force is 17.3*N*, which is relatively close in comparison with case B (15*N*).

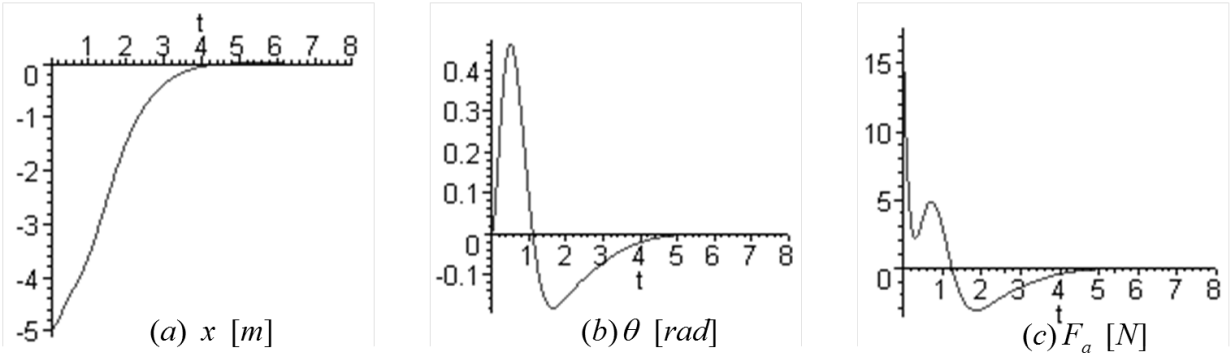

Figure 4-4. Graphs of (a) trolley position, (b) load angle, and (c) trolley force for closed-loop, time-invariant maneuver (case C).

In comparison with the control presented in [3] (see Figure 4-3), the dynamics of case C, shown in Figure 4-4, have several key differences. The trolley reaches the target more quickly, the load swings are smaller and attenuated faster, and the required peak forces are only marginally larger. The closed loop gains in the feedback relationship (4.27) are:

$$\boldsymbol{G_d} = [G_{d_{11}} \quad G_{d_{12}}] = [3.46 \quad 9.10], \qquad \boldsymbol{G_v} = [G_{v_{11}} \quad G_{v_{12}}] = [5.43 \quad 1.79] \tag{4.32}$$

The value of the gains $G_{d_{11}}$ and $G_{v_{11}}$, influencing the proportion of the control force that is related to the trolley position and velocity respectively, are similar in magnitude to case B (see equation (4.28)). However, the value of gains $G_{d_{12}}$ and $G_{v_{12}}$, influencing the proportion of the control force that is related to the load swing angle and velocity respectively, differ significantly (with different orders of magnitude and opposite signs). In case C more effort is applied to attenuate the load swing angle and velocity producing a more efficient overall maneuver.

Case D, in Section 4.5, considers the gantry crane system with an additional actuator located at the center of gravity of the suspended load to illustrate how the CMSOC approach can be applied to fully-actuated systems. It is shown that such a system can perform the control task more quickly and effectively.

4.5 Case D – A time-invariant, closed-loop maneuver of the fully-actuated system.

The CMSOC method can always be extended to the analysis and simulation of fully-actuated systems. This is illustrated by considering the gantry crane system presented in Figure 4-1 with both actuators F_a and F_d acting as real actuators (no dummy actuator). The problem is fully-actuated so there are no additional constraints on the system's motion and hence no Lagrange multipliers needed to enforce them. The optimal trolley drive force F_a and guiding force F_d can be solved for by calculating the inverse dynamics directly from (2.9*b*), which is written as:

$$\boldsymbol{F_a} = \widehat{\boldsymbol{B}}^{-1}\boldsymbol{U} \Rightarrow \begin{bmatrix} F_a \\ F_d \end{bmatrix} = \begin{bmatrix} \frac{M}{\sqrt{M+m}} & \sqrt{\frac{Mm}{M+m}} \\ \frac{m}{\sqrt{M+m}} & -\sqrt{\frac{Mm}{M+m}} \end{bmatrix} \begin{bmatrix} u_1 \\ u_2 \end{bmatrix} \tag{4.33}$$

In the matrix notation (3.15), the optimality equations take the form:

$$\boldsymbol{E_p Y} = [\boldsymbol{E}][\boldsymbol{\eta}] = \boldsymbol{0} \Rightarrow \begin{bmatrix} E_1 & 0 \\ 0 & E_2 \end{bmatrix} \begin{bmatrix} \eta_1 \\ \eta_2 \end{bmatrix} = \boldsymbol{0} \tag{4.34}$$

The matrix components E_1 and E_2 in (4.34) take the form:

$$E_1 = R_{11}D^4 - Q_{v_{11}}D^2 + Q_{d_{11}} \tag{4.35}$$

$$E_2 = R_{22}D^4 + \left(2R_{22}\omega_2^2 - Q_{v_{22}}\right)D^2 + \left(R_{22}\omega_2^4 + Q_{d_{22}}\right) \tag{4.36}$$

The weighting values in equation (4.35) and (4.36) are selected to be identical to case C ($Q_{d_{11}} = 6$, $Q_{d_{22}} = 50$, $Q_{v_{11}} = 4$, $Q_{v_{22}} = 50$, $R_{11} = R_{22} = 1$). The characteristic equation for the

problem in the general form (3.17) is obtained ($E_1E_2|_{D\to r} = 0$) and solved to obtain four roots taking the general form (3.18) with real and imaginary components written as:

$$\alpha_1 = 3.62, \qquad \beta_1 = 2.78, \qquad \alpha_2 = 1.49, \qquad \beta_2 = 0.474 \tag{4.37}$$

Since the system is fully-actuated, each modal variable η_i is independently controlled by a corresponding modal control u_i, which produces uncoupled solution function in the form:

$$\eta_i = e^{-\alpha_i t}\left(c_i^1 sin(\beta_i t) + c_i^2 cos(\beta_i t)\right) \tag{4.38}$$

The four unknown integration constants c_i^j (i = 1,2 and j=1,2) are obtained by directly substituting the four initial conditions given by (4.11). The modal variables in the form (4.38) are mapped into DOF-space through equations (4.22) to obtain the system trajectories x and θ and the control forces applied at the cart $F_a$and at the suspended load F_d. Figure 4-5*a* and Figure 4-5*b* contains graphs of the trolley position and active forces respectively over a time period of 2*s*. A plot of suspended load rotation is trivial, as the suspension rope remains vertical throughout the maneuver ($\theta(t) = 0$). Practically, this means the actuator acting on the suspended load must prevent any swinging of the load while the trolley translates.

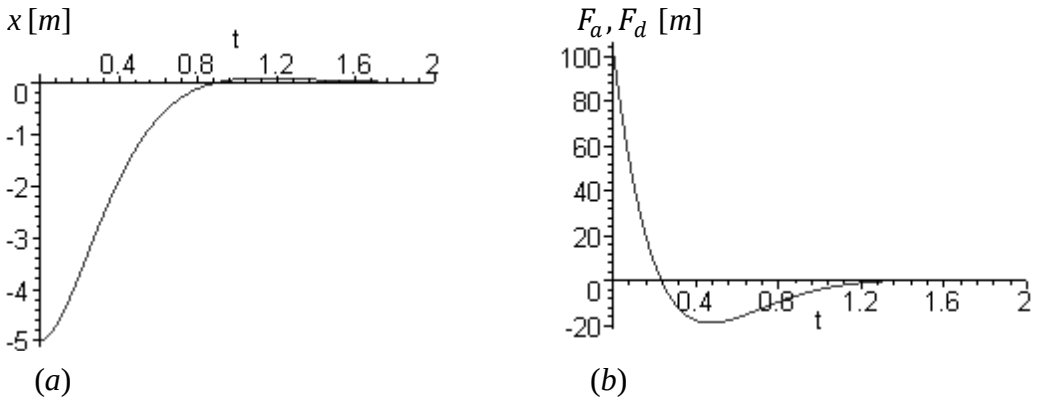

Figure 4-5. Graphs of (a) trolley position and (b) driving forces for the fully-actuated gantry crane system (case D).

The trolley effectively converges with the target position after $t_f^{3\%} = 0.78s$, and the task requires identical forces to drive the trolley and suspended load with a peak force of $104N$. The trolley and suspended load move with identical velocities as a single rigid body, as it does not swing as it travels. The peak forces required are considerably larger than in previous cases; however, these could be reduced by increasing the value assigned to weighting parameters R_{11} and R_{22} in the performance index (4.8).

5. DISTRIBUTED-MASS PLANE FRAME PROBLEM

5.1 Plane Frame Model [21]

In this example, the CMSOC approach is used to analyze and simulate an actively dampened structure consisting of three levels of beams rigidly connected to columns. All three stages of the CMSOC method are implemented and discussed in this example (see flowchart in Figure 3-1). In the structural stage, the effectiveness of certain configurations of actuators are indicated by the controllability parameters λ and κ, introduced in equations (3.5a) and (3.5b), which indicate if excessive attenuation times or prohibitively large force requirements are expected. In the control stage the system response and active forces are calculated confirming the validity of the controllability parameters. Lastly, in the verification stage, the controls are simulated with a transient FEM model to verify that the system response is consistent with the results of the control stage. Also in the verification stage, spillover effects from higher modes are detected.

The distributed-mass three level plane frame structure under consideration is shown in Figure 5-1a. All connections between the beams and columns are assumed to be rigid (angles between intersecting members remain unchanged when loaded) and all members with the exception of the topmost member have identical cross sections and material specifications. The members are modelled based on aluminum material ($E = 71.7GPa$, $\rho = 2800kg/m^3$) with a cross sectional area of $76mm^2$ linear mass of $0.2128kg/m$ and an area moment of inertia of $4585mm^4$. The topmost horizontal member is rigid and weighs $1kg$. The properties of this

frame were chosen somewhat arbitrarily to obtain a particular pattern of vibration modes that are effective at illustrating the CMSOC approach.

An FEM model of the frame was created using the ANSYS software. Two-dimensional beam elements, each of $200mm$ length (five elements per member), make up the bottom eight members of the frame and a rigid mass element was used for the topmost member. The locations of several key nodes that are relevant in future discussions are indicated in Figure 5-1a. The initial displaced configuration of the structure was chosen to provide adequate disturbance of all modes and is represented by the dashed line in this figure. The response of the system will be described by the horizontal and vertical displacements, d_x^p and d_y^p respectively, where the superscript p denotes the node number under consideration. A modal analysis was performed in ANSYS and the resulting modal shapes of the four dominant vibration modes, with natural frequencies $f_i = \omega_i/2\pi$ (i=1,2,3,4), are shown in Figure 5-1b.

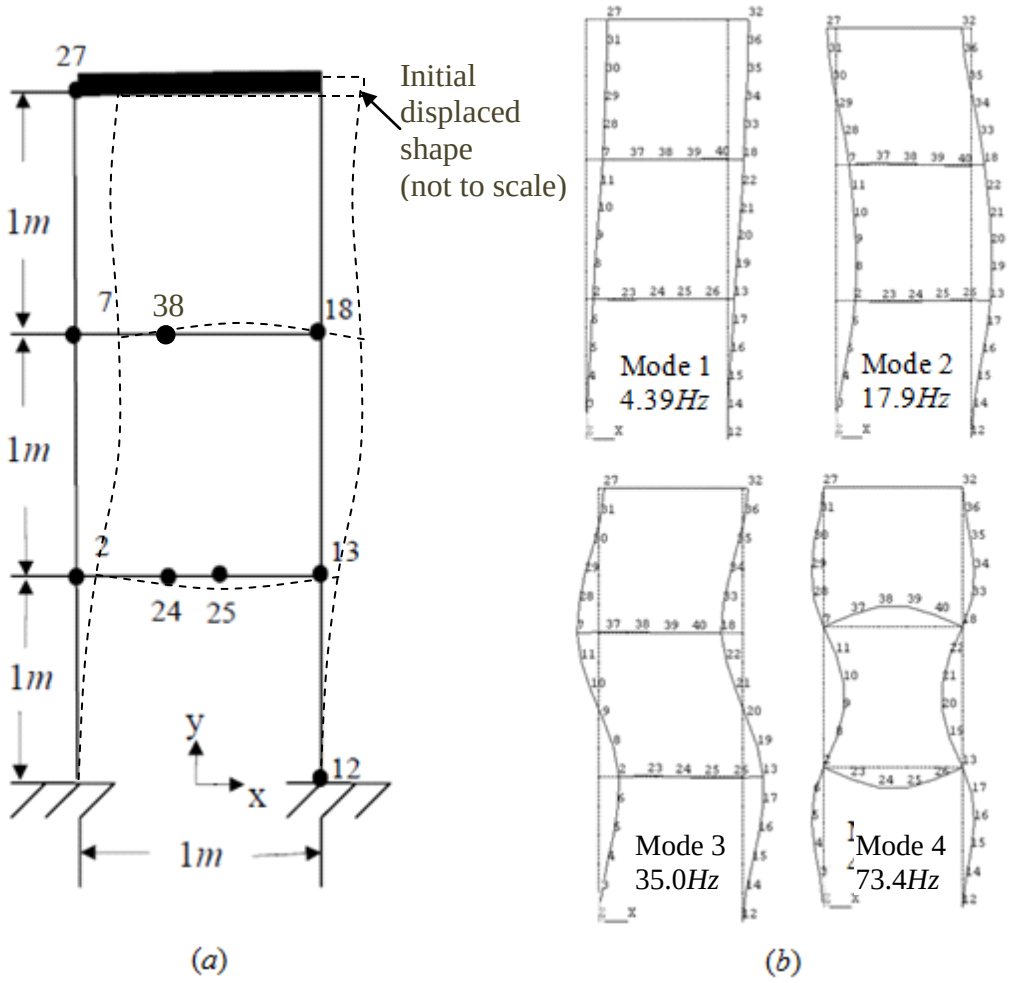

Figure 5-1. (*a*) The plane frame and (*b*) its four dominant mode shapes and frequencies.

The CMSOC method was used to simulate the actively dampened structure for a variety of actuator configurations employing one or two actuators. The dynamics of the frame system was considered for three or four significant modes of vibration. Actuators were assumed to exert equal and opposite axial forces on their points of attachment to the frame. The mass and stiffness of actuators were not considered and all passive damping effects were ignored in the model to emphasize the active damping. In Figure 5-2, the actuator configurations that were examined, as well as the number of modes that were considered, are shown. Each actuator position is labelled by F_i $(i = 1, \dots, 5)$ and the two nodes where they are connected are denoted

accordingly. The effect of actuator configuration on system controllability is the primary motivation for studying each case.

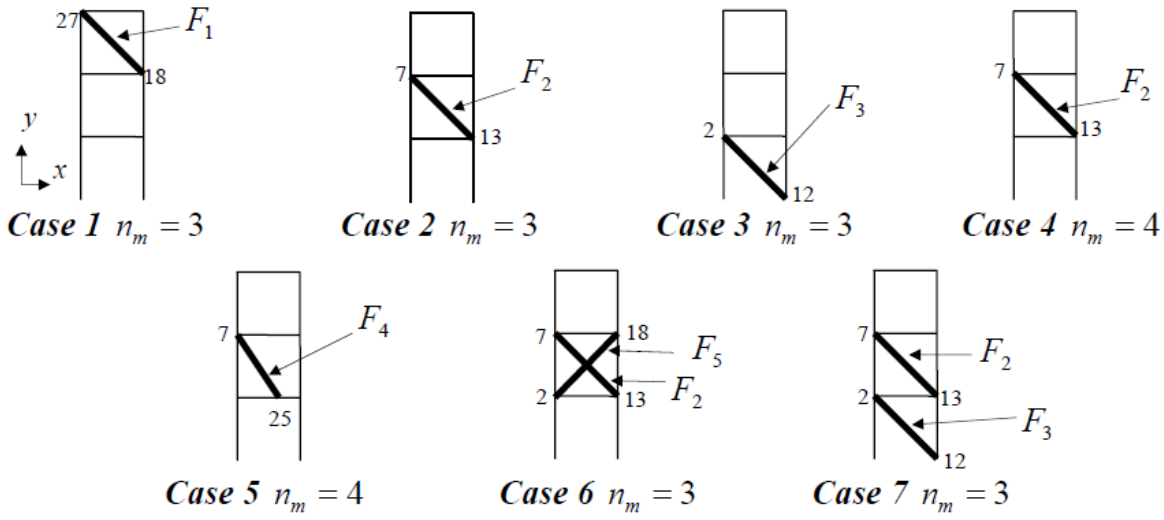

Figure 5-2. Seven cases with different actuator configurations and the number of modes n_m to be considered for each case.

In cases 1, 2, and 3 actuators F_1, F_2, and F_3 act to attenuate the first three modes of vibration, respectively. In cases 4 and 5, actuators F_2 and F_4, respectively, act to attenuate the first four modes of vibration. In cases 6 and 7, two-actuator combinations, F_2-F_5 and F_2-F_3, respectively, attenuate the first three modes of vibration.

The frame structure is assumed to be initially displaced such that the modal variables take initial values of:

$$\eta_1(0) = 0.05, \qquad \eta_2(0) = 0.005, \qquad \eta_3(0) = 0.0045, \qquad \eta_4(0) = 0.004 \tag{5.1a}$$

$$\dot{\eta}_1(0) = \dot{\eta}_2(0) = \dot{\eta}_3(0) = \dot{\eta}_4(0) = 0 \tag{5.1b}$$

Note that these initial displacements may be chosen arbitrarily, but those chosen in (5.1a) were chosen to produce somewhat physically reasonable displacements. In DOF-space the initial

frame position described by (5.1a) and (5.1b) is a stationary deformed shape that is shown by the dotted line in Figure 5-1a (not to scale) with initial displacements of:

$$d_x^{27} = 38.01mm, \qquad d_x^{7} = 28.38mm, \qquad d_y^{24} = -5.740mm \tag{5.2}$$

The optimization problem is defined by the performance index (2.8) with the weighting coefficients taken as: $a = b = c = 1$. In other words, equal weight is given to minimizing the terms relating to the frame's potential energy, kinetic energy, and actuator work respectively. The maneuver time is theoretically infinite ($t_f \to \infty$) because only the time-invariant system is considered.

In Sections 5.2, 5.3, and 5.4, the procedure and results of the structural stage, control stage, and verification stage, respectively, are covered for the cases shown in Figure 5-2. The structural stage and control stage are covered in detail for case 1 only and the results of the remaining cases are listed for discussion. More complete results of the structural stage and control stage for each of the cases are covered in [21]. The verification stage is demonstrated for the actuator configuration shown in case 2.

5.2 Structural Stage

Some results of the structural stage are presented for the seven cases in Table 5-1, but only case 1 is covered in detail. In case 1, the first three dominant modes of vibration are attenuated by a single actuator F_1 located between nodes 18 and 27. The characteristic dimensions of the problem are: $n_a = 1, n_m = 3, n_c = 2, n_t = 5$. Dummy actuators are chosen in the locations of actuators F_2 and F_3, which are located between nodes 7 and 13 and nodes 2 and 12 respectively (see Figure 5-2). The transformation equations (3.1) are:

$$\widehat{\boldsymbol{F}} = \widehat{\boldsymbol{B}}^{-1}\boldsymbol{U} = \begin{bmatrix} \boldsymbol{F_a} \\ \boldsymbol{F_d} \end{bmatrix} = \left[\begin{array}{c|cc} \widetilde{\boldsymbol{B}}_{\boldsymbol{a}} & \widetilde{\boldsymbol{B}}_{\boldsymbol{r}} \\ \boldsymbol{A_a} & \boldsymbol{A_r} \end{array}\right] \begin{bmatrix} \boldsymbol{U_a} \\ \boldsymbol{U_r} \end{bmatrix} = \left[\begin{array}{c|cc} -1.34 & 0.690 & -0.325 \\ -1.87 & 0.127 & 0.383 \\ -2.10 & -0.669 & -0.267 \end{array}\right] \begin{bmatrix} u_1 \\ u_2 \\ u_3 \end{bmatrix} = \begin{bmatrix} F_1 \\ 0 \\ 0 \end{bmatrix} \tag{5.3}$$

The dashed lines appearing on the right hand side of equation (5.3) denote partitions between the sub-matrices and sub-vectors that divide the vectors $\widehat{\boldsymbol{F}}$ and $\boldsymbol{U}$ and matrix $\widehat{\boldsymbol{B}}^{-1}$. The two bottom rows of the matrix $\widehat{\boldsymbol{B}}^{-1}$, containing sub-matrices $\boldsymbol{A_a}$ and $\boldsymbol{A_r}$ are combined and normalized in accordance with (3.3) to obtain:

$$\boldsymbol{A} = \begin{bmatrix} 1 & 0.171 \\ & 1 \quad 0.859 \end{bmatrix} \tag{5.4}$$

Manipulating the sub-matrices in (5.3) in accordance with (3.4) gives the pseudo-transfer matrix $\overline{\boldsymbol{B}}_{\boldsymbol{a}}$. It defines the mapping between the single independent modal control $\boldsymbol{U_a} = u_1$ and the single actuator force $\boldsymbol{F_a} = F_1$ which takes the form:

$$F_1 = \overline{\boldsymbol{B}}_{\boldsymbol{a}}\boldsymbol{U_a} = -7.59u_1 \tag{5.5}$$

The pseudo-transfer matrix $\overline{\boldsymbol{B}}_{\boldsymbol{a}} = -7.59$ takes a scalar value in this case, as it only involves a single actuator. The rate parameter λ and effort parameter κ are obtained from operation (3.5*a*) and (3.5*b*) as:

$$\lambda = |det\boldsymbol{A_r}| = 0.147, \qquad \kappa = |det\overline{\boldsymbol{B}}_{\boldsymbol{a}}| = 7.59 \tag{5.6}$$

Recall that having the rate parameter λ 'close' to unity indicates that the actuator configuration is well positioned to attenuate all modes of vibration with similar attenuation rates. Also, having the effort parameter κ at a 'small' value minimizes the peak force amplitudes. The subjective meaning of the terms 'small' and 'close' will be illustrated in this example. The rate parameter λ and effort parameter κ are summarized for each case in Table 5-1.

Table 5-1. Rate parameter λ and effort parameter κ for cases 1 to 7.

Case Number	Rate Parameter, λ	Effort Parameter, κ
1	0.147	7.59
2	0.171	4.21
3	0.273	5.53
4	393	4.21
5	0.163	5.50
6	0.347	74,500,000
7	0.242	5.20

Cases 1, 2, and 3 are expected to adequately control the first three modes of vibration based on the rate parameter values obtained in Table 5-1. Of these cases, case 3 is expected to have the best overall attenuation rate because it has a rate parameter value closest to unity. In case 4, four modes of vibration are considered and the rate parameter takes an extremely large value. This indicates that poor attenuation of the fourth mode of vibration should be expected. Intuitively, this is because actuator F_2 is poorly positioned with respect to the fourth mode of vibration because it is attached at points that do not undergo displacements in that modal shape. The actuator location in Case 5 is expected to have much better control over all four modes of vibration, as indicated by the rate parameter value similar to those obtained in cases 1, 2, and 3.

Cases 6 and 7 involve two actuators working simultaneously to attenuate the disturbance. Case 6 offers an example of poor positioning of two actuators for controlling the three dominant modes of vibration. The reason is somewhat more complicated than in case 4 and will be discussed later, but note that the problem is indicated by the extremely large effort parameter in Table 5-1. Case 7 is a better configuration of two actuators for controlling the three dominant modes, as reflected by the reduction in the effort parameter to a value more consistent with the first five cases.

5.3 Control Stage

The results of the control stage are discussed in detail for case 1. For the sake of discussion only the plots will be presented for the remaining cases. The optimality and constraint equations for case 1 are written in the form of equations (3.13) and (3.14), respectively, giving:

$$\ddot{\eta}_i + \omega_i^2 \ddot{\eta}_i + 2\omega_i^4 \eta_i = A_{1i}\omega_i^2(\ddot{v}_1 + \omega_i^2 v_1) + A_{2i}\omega_i^2(\ddot{v}_2 + \omega_i^2 v_2), \qquad i = 1,2,3 \qquad (5.7)$$

$$A_{j1}(\ddot{\eta}_1 + \omega_1^2\eta_1) + A_{j2}(\ddot{\eta}_2 + \omega_2^2\eta_2) + A_{j3}(\ddot{\eta}_3 + \omega_3^2\eta_3) = 0, \qquad j = 1,2 \qquad (5.8)$$

The optimality equations (5.7) and the constraint equations (5.8) are written with the differential operator $D^j = d^j/dt^j$ and substituted into the matrix notation (3.15) to obtain a characteristic equation in the form (3.17). The roots of this characteristic equation are complex numbers in the form (3.18) with the real and imaginary components:

$$\begin{array}{lll} \alpha_1 = 7.31 & \alpha_2 = 50.4 & \alpha_3 = 62.2 \\ \beta_1 = 27.7 & \beta_2 = 117 & \beta_3 = 214 \end{array} \qquad (5.9)$$

The modal frequencies $\omega_i = 2\pi f_i$ (frequencies f_i are shown in Figure 5.1*b*) are approximately equal to the parameter β_i given in (5.9), indicating that the active controls do not significantly alter the frame's passive vibration frequencies. The 3-percent settling times for each mode are:

$$t_1^{3\%} = 0.479s, \qquad t_2^{3\%} = 0.0694s, \qquad t_3^{3\%} = 0.0563s \qquad (5.10)$$

The effective settling time t_{ef} is the time required for all controlled modes of vibration to decay to 3-percent of their initial value; therefore the slowest-damped vibration mode governs. In Figure 5-3 the plots of the system dynamics for case 1 confirm visually that oscillations with the second and third frequencies are negligible after approximately 0.07*s*, while those with the first frequency persist until approximately 0.5*s*.

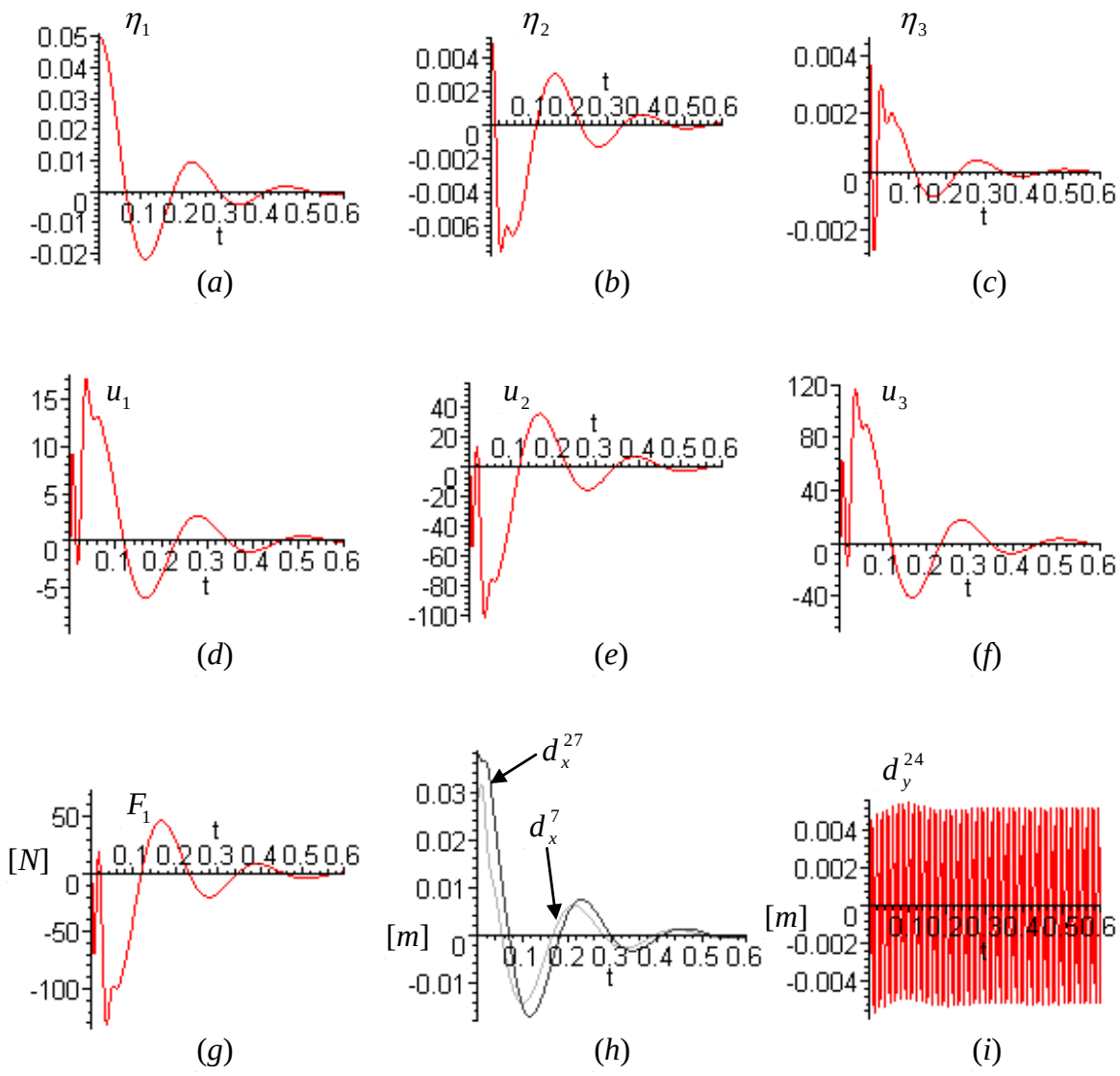

Figure 5-3. (*a*,*b*,*c*) Plots of modal variables, (*d*,*e*,*f*) modal controls, (*g*) actuation force, and (*h*,*i*) displacements over 0.6*s* of the maneuver (case 1).

The dynamic behaviour for case 1 is plotted in Figure 5-3 for the first 0.6*s* of the maneuver. Though only the first three modes of vibration are actively attenuated, the effect of the fourth uncontrolled modal variable is included in the response plots by including the function $\eta_4(t) = \eta_4(0)cos(\omega_4 t)$ when transferring the dynamics of the frame into DOF-space. However,

due to its shape (see Figure 5-1*b*), it does not visibly contribute to the horizontal nodal displacements d_x^{27} and d_x^7 (see Figure 5-3*h*), but it does however have a significant impact on the vertical displacement d_y^{24} (see Figure 5-3*i*). The actuation force F_1 has a peak value of $131N$ (see Figure 5-3*g*).

To solve the dynamics of the system, as shown in the plots of Figure 5-3, the following steps are performed. *Step 1*: The solution functions (3.20) are substituted into the $n_m = 3$ optimality equations (5.7) and $n_c = 2$ constraint equations (5.8) with the numerical values from (5.9). *Step 2*: The method of undetermined coefficients is applied to obtain $2n_m n_t = 30$ linear equations relating thirty unknown integration constants c_{kj}^1 and c_{kj}^2 ($k = 1,2,3$ and $j = 1,2$): $2(n_m)^2 = 18$ constants define the $n_m = 3$ modal variables η_k and $2n_m n_c = 12$ constants define the $n_c = 2$ Lagrange multipliers ν_j. *Step 3*: To render a set of 30 linear equations that can be solved to determine the unknown integration constants, $2n_m = 6$ initial conditions (5.1*a*) and (5.1*b*) (initial conditions pertaining to η_4 are ignored for this case) must replace one set of $2n_m = 6$ equations obtained in the previous step. *Step 4*: The unknown coefficients are solved for and substituted into (3.20) to obtain the desired time varying functions describing the dynamics of modal variables, modal controls, actuation force, and response of any DOF of interest. All steps in this solution process, including the matter of obtaining all unknown integration constants, is handled automatically using the symbolic mathematical capabilities of MAPLE software. A sample of the MAPLE commands used for this example is provided in Appendix A.

Table 5-2 summarizes some key dynamic characteristics for the seven cases shown in Figure 5-2. The modal dampening parameters α_i, frequencies β_i, effective settling times t_{ef}, and peak actuation force amplitudes are given for each case in Table 5-2.

Table 5-2. Modal damping parameters α_i, frequencies β_i, effective settling time t_{ef}, and peak force amplitude(s).

Case #	α_i				β_i				t_{ef} (s)	Peak force(s) (N)
	i=1	2	3	4	i=1	2	3	4		
1	7.31	50.4	62.2	-	27.7	117	214	-	0.479	$F_1 = 131$
2	12.9	9.26	88.7	-	27.5	113	219	-	0.378	$F_2 = 121$
3	10.7	46.1	45.6	-	27.7	114	217	-	0.326	$F_3 = 131$
4	12.9	9.26	88.7	0.0366	27.5	113	219	461	95.6	$F_2 = 330$
5	12.4	7.48	79.0	87.8	27.5	113	222	458	0.468	$F_4 = 240$
6	18.2	26.1	133	-	27.1	115	214	-	0.193	$F_2 = F_5 = 2(10^9)$
7	16.8	45.3	115	-	27.3	116	213	-	0.209	$F_2 = 70, F_3 = 76$

The key dynamic characteristics from Table 5-2 are in agreement with the controllability indicators obtained in the structural stage, listed in Table 5-1. The first three cases attenuate the disturbance with similar damping rates, attenuation times, and force requirements, with case 3 marginally providing the shortest effective settling time of these cases ($t_{ef} = 0.326s$). Case 4, which uses the same actuator as case 2 (F_2), struggles to attenuate the fourth mode of vibration (while damping the first three modes identical to case 2) and requires a larger peak force in doing so. The system oscillates with the fourth mode for $t_{ef} = 95.6s$; this is approximately 250 times longer than it takes to effectively attenuate the other modes. This was expected from the large value of λ in Table 5-1. In case 5, the actuator F_4 is better able to dampen the fourth mode with only a slight reduction in the damping of the other three modes in comparison to case 4. The effective settling time is reduced to $t_{ef} = 0.468s$ and the maximum actuator force amplitude decreases.

Case 6, employing actuators F_2 and F_5, is able to attenuate the three dominant modes of vibration quickly, but the forces required are approximately seven orders of magnitude larger than in cases 1 to 3. This was expected in the structural stage from the large value of κ in Table 5-1. Case 7, employing actuators F_2 and F_3, is better suited to controlling the three modes of

vibration, as it achieves similar damping characteristics as case 6, but with much smaller force requirements. Note that the rate of attenuation is faster and the maximum force requirements are lower in case 7 in comparison to cases 2 and 3, which employed the same actuators acting individually. In all cases the dampened system frequencies β_i are relatively unchanged and approximately equal to the passive system frequencies ω_i ($\omega_i = 2\pi f_i$).

In Figure 5-4, the actuator forces and displacement d_x^7 (horizontal displacement at node 7) are plotted for cases 1, 2, and 3 over a period of 0.6*s*. These plots confirm that cases 1 to 3 are similarly capable of attenuating the frame's first three modes of vibration, with similar peak force requirements.

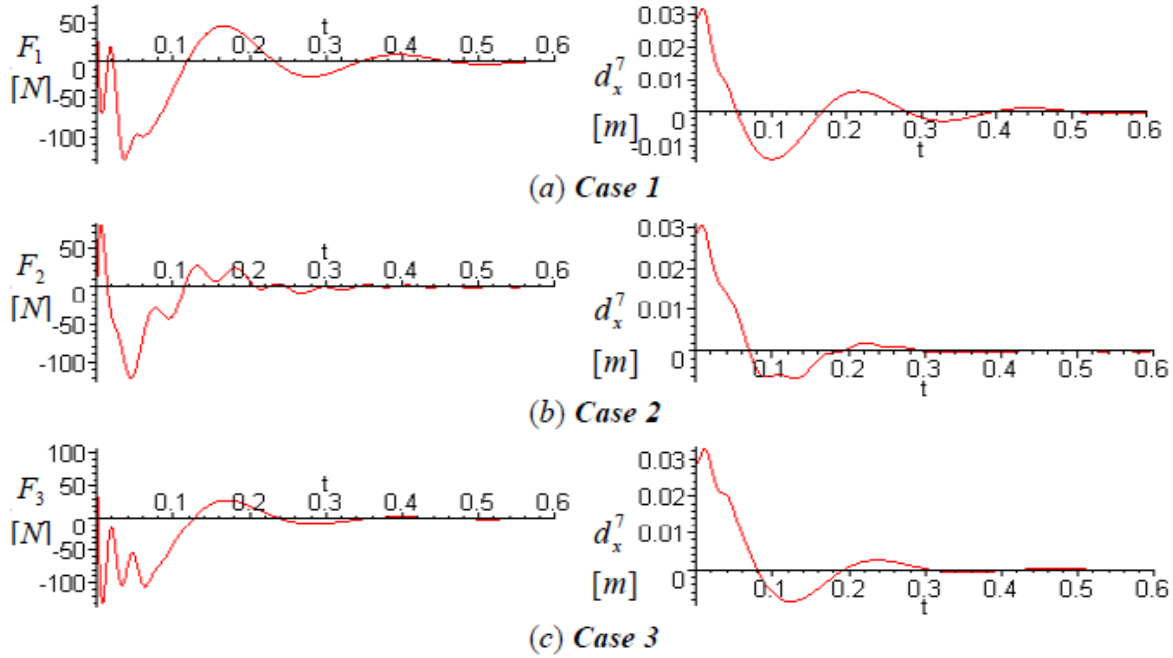

Figure 5-4. Optimal control force (left) and DOF response d_x^7 (right) for (*a*) case 1, (*b*) case 2, and (*c*) case 3.

In Figure 5-5, the displacement responses d_x^7 and d_y^{24} are plotted for case 4 in Figures 5-5*a* and 5-5*b* respectively, over a maneuver time of 0.6*s*. Figure 5-5*c* and 5-5*d* show the active force F_2 over a time period of 0.6*s* and 100*s* respectively. The long time period in Figure 5-5*d* is

shown to better demonstrate the decay period required to dampen the fourth mode to 3-percent of its initial magnitude ($t_4^{3\%} = 95.6s$). Note that in a real structure this mode would dissipate due to passive damping effects, but in these examples such effects were ignored to emphasize active damping.

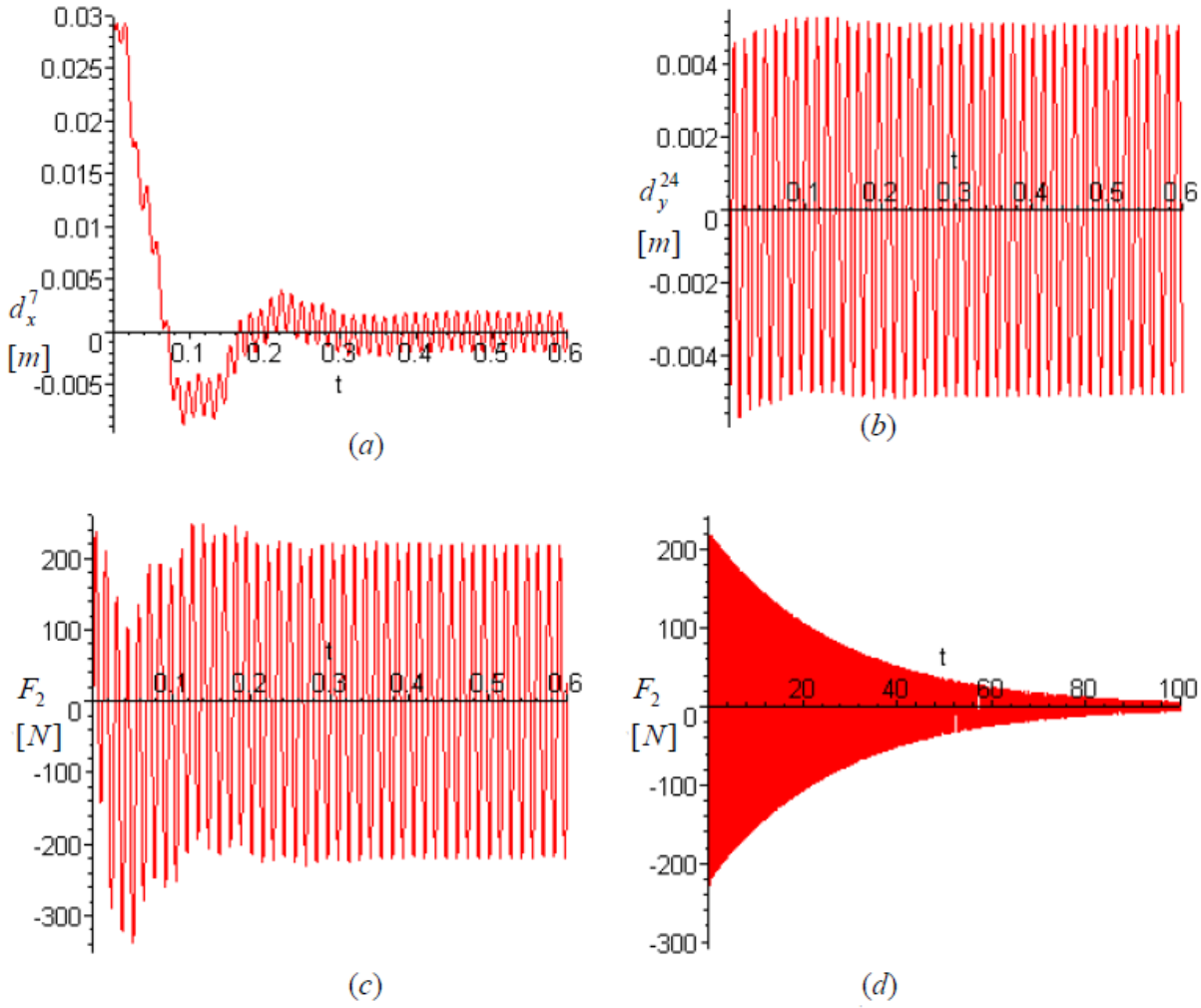

Figure 5-5. (*a*) DOF responses d_x^{27} and (*b*) d_y^{24} and control force F_2 for a period of (*c*) 0.6*s* and (*d*) 100*s* (case 4).

The vertical displacement d_y^{24} is very sensitive to the fourth mode of vibration and the plot in Figure 5.5*b* demonstrates that this mode is very poorly attenuated. Note that the horizontal displacement d_x^7 in Figure 5.5*a* is affected by the fourth mode of vibration, which is

not the case when the fourth mode is left un-attenuated, producing a plot similar to Figure 5-3*h* for case 1. The reason is that, although the location of the DOF d_x^7 is a stationary point in the fourth mode of vibration (see Figure 5-1*b*), when the actuator attempts to control the fourth mode of vibration, its action causes oscillations with the fourth mode frequency at this location of the structure. Essentially the controlled dynamics are dominated by the fourth mode of vibration which vibrates at a frequency of $73.4Hz$ ($461\,rad/s$). After a short initial maneuver time the first three modes of vibration are effectively dampened and the remaining control effort is devoted to attenuating the persistent fourth mode.

Plots similar to those of Figure 5-5 are obtained if actuators F_1 or F_3 is substituted in lieu of actuator F_2 to control the four dominant modes of vibration. Each configuration produces poor controllability over the fourth mode of vibration due to its positioning. In case 5, actuator F_4 is better located to attenuate the fourth mode. Several plots for case 5 are shown in Figure 5-6.

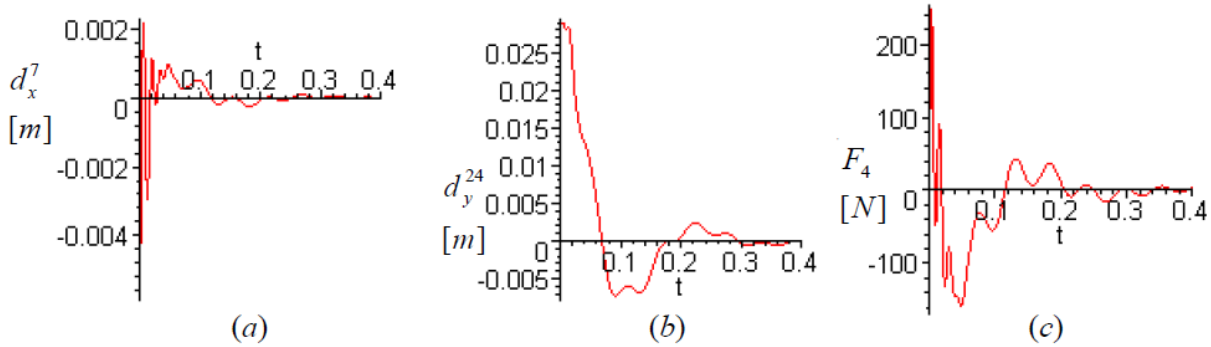

Figure 5-6. DOF responses (*a*) d_x^7 and (*b*) d_y^{24}, and (*c*) control force F_4 (case 5).

The responses d_x^7 and d_y^{24} are shown in Figure 5.6*a* and Figure 5-6*b* and the actuation force F_4 is shown in Figure 5-6*c* over a period of 0.4*s*. Comparing these plots with those of Figure 5-5, the maneuver in case 5 attenuates the fourth mode of vibration in a fraction of the time required for case 4.

Case 1 to 5 each uses a single actuator to control the frame vibrations, however in cases 6 and 7 two actuators are employed to control the three dominant modes of vibration. In case 6, actuators F_2 and F_5 are considered, which produce excessively large forces to attenuate the vibrations. Several plots of the dynamics for case 6 are shown in Figure 5-7.

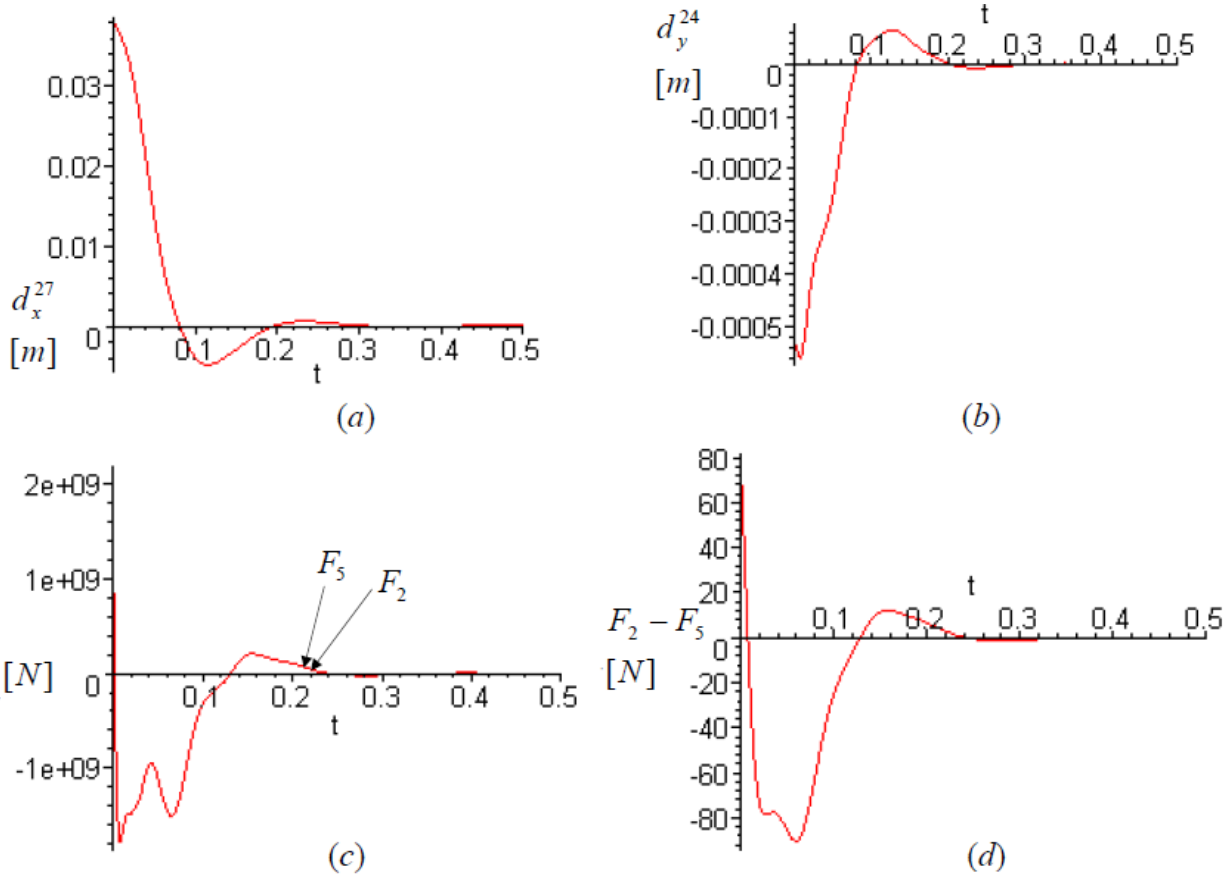

Figure 5-7. DOF responses (*a*) d_x^{27} and (*b*) d_y^{24}, (*c*) actuation forces F_2 and F_5, and (*d*) their difference $F_2 - F_5$ (case 6).

The displacements of DOFs d_x^{27} and d_y^{24} are shown in Figure 5-7*a* and Figure 5-7*b* respectively, over a maneuver time of 0.5*s*. The plots of actuation forces F_2 and F_5 are shown in Figure 5-7*c*, however due to the scale they are indistinguishable so they appear as one single line. Nonetheless, the time-varying actuation forces are distinct, as demonstrated in Figure 5-7*d*, where their difference $F_2 - F_5$ is plotted.

Despite their individually large force amplitudes (approximately $2GN$), actuators F_2 and F_5 produce distinct forces and their difference produces a plot that is somewhat similar to the action of the lone actuator F_2 in case 2 (see Figure 5-4*b*). Also the peak magnitude in plot Figure 5-7*d* is approximately $92N$, which is in the same order of magnitude as the peak force in Case 2 (approximately $121N$).

The large forces resulting from the combination of actuators F_2 and F_5 is due to their positions relative to the modal shapes of the first and second modes of vibration. Recall that actuator F_5 acts upon nodes 2 and 18 and actuator F_2 acts upon nodes 7 and 13 (see Figure 5-2). As the frame vibrates in the first and second modes of vibration the distance between nodes 2 and 18 increases (decreases) in a nearly identical proportion as the decrease (increase) in the distance between node 7 and 13 (see Figure 5.1*b*). Hence, the actuators essentially neutralize each other's action in their attempt to attenuate these modes of vibration. In case 2 the single actuator F_2 performed essentially the same maneuver with forces that were approximately seven orders of magnitude smaller. The addition of actuator F_5 in case 6 is detrimental to the maneuver and should be eliminated or relocated. As shown in Table 5-1, this poor actuator positioning is reflected in the large effort parameter κ.

In the case 7, another two actuator configuration with actuators F_2 and F_3 attenuating the disturbance was considered. It did not generate the counterproductive actuation forces demonstrated in case 6. The time-varying plot of displacement d_x^{27} is shown in Figure 5-8*a* and the plot of d_y^{24} is shown in Figure 5-8*b* over a maneuver time of $0.5s$. The actuation forces F_2 and F_3 are shown in Figure 5-8*c* and Figure 5-8*d* respectively.

Unlike in case 6, the peak actuation forces F_2 and F_3 required for the maneuver are smaller than those required in their individual actuator cases (case 2 and case 3). Note that if the

fourth mode of vibration were considered for either Case 6 or Case 7, then a result similar to Case 4 would be expected, where a very large value of the rate parameter λ would be obtained signalling very slow attenuation of the fourth mode.

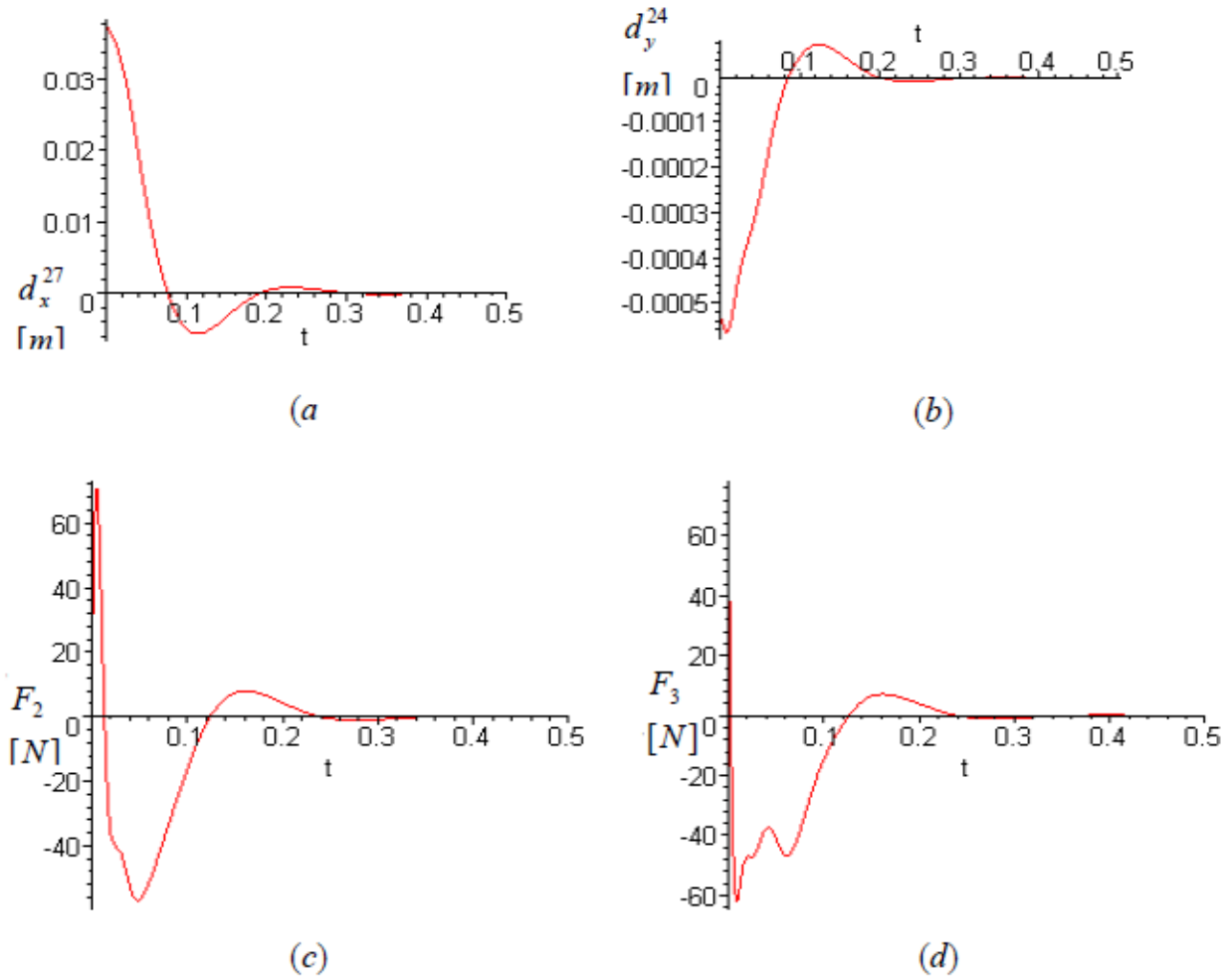

Figure 5-8. DOF responses (*a*) d_x^{27}, (*b*) d_y^{24}, and actuation forces (*c*) F_2, and (*d*) F_3 (case 7).

5.4 Verification Stage

The verification stage takes the actuation forces $\boldsymbol{F_a}(t)$, obtained in the control stage and applies them to the FEM model of the frame in a transient dynamic analysis to check that the resulting time-integrated displacement $\boldsymbol{q_{int}}(t)$ are consistent with those displacements obtained

in the control stage $\boldsymbol{q}(t)$. In this example, ANSYS was used for modelling the transient response of the frame system. The following steps are involved in the verification stage:

1. Input actuation forces from the control stage to FEM model.
2. Initialize the FEM transient analysis.
3. Choose time-integration steps and load steps for the FEM transient analysis.
4. Compare the DOF responses.
5. Check for spillover effects from higher modes of vibration.

A general overview of each of these steps will be considered, however a more detailed handling of the verification stage for this problem is covered in Appendix C.

The frame system of Figure 5-1 with actuator F_2 (case 2 in Figure 5-2) is considered. However, only two modes of vibration will be actively attenuated and the initial conditions are different from those in (5.1*a*) and (5.1*b*); they are:

$$\eta_1(0) = 0.05 \qquad \eta_2(0) = 0.005 \tag{5.11a}$$

$$\dot{\eta}_1(0) = \dot{\eta}_2(0) = 0 \tag{5.11b}$$

Note that the selection of the initial conditions does not affect the procedure and is arbitrary. The solution of the system dynamics is obtained using the same procedure discussed in Section 5.3. The actuator force F_2 and the response d_x^7 obtained from the control stage is plotted in Figure 5-9*a* and Figure 5-9*b* respectively.

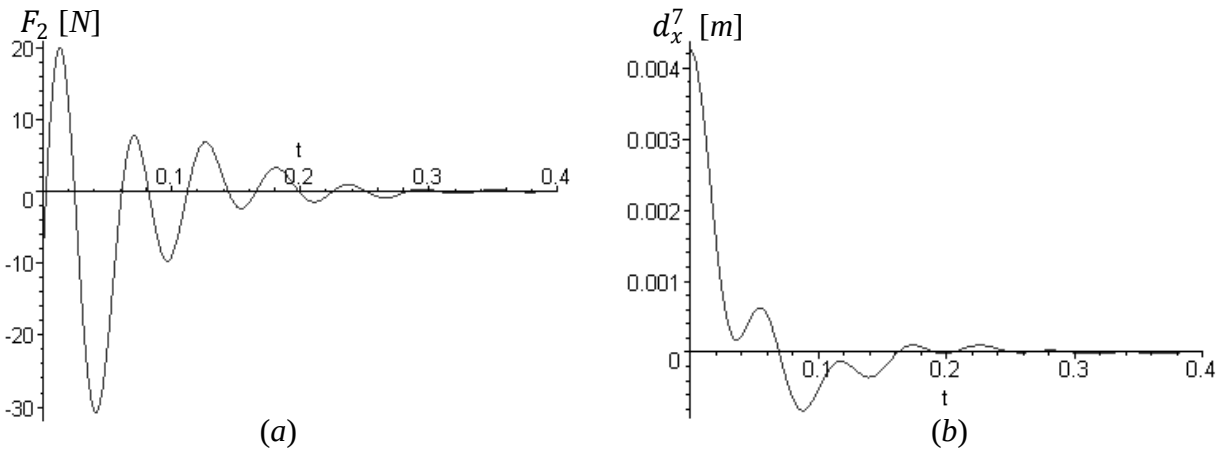

Figure 5-9. (a) Actuator force F_2 and (b) response d_x^7 for initial conditions in equation (5.11) from the control stage.

In the verification stage, the force F_2 in Figure 5-9*a* is applied to the transient FEM model and the resulting response should match the displacement d_x^7 shown in Figure 5-9*b*. Otherwise, there may be spillover effects from higher modes of vibration.

Step 1: Input actuation forces from control stage to FEM model. The actuation force obtained in the control stage is a continuous, time-varying function $F_2(t)$. This continuous function is translated into a discrete form that can be numerically input into the ANSYS program. This operation is easily performed by intermediately using a spreadsheet calculation software, such as the Microsoft EXCEL program, to calculate instantaneous forces $F_2(n\Delta t)$ at all n increments. This data is tabulated over the desired number of increments extending over the desired time period, and then written to a text file. This text file is properly formatted for input to the ANSYS program as an array parameter.

The data from the text file is stored in the ANSYS program as an array parameter of type "table". Parameters of this type are defined by a "primary" variable, which is taken as the time t, and a dependant variable, which is taken as the actuator force at that time. The benefit of

defining forces in this manner is that a looping logic structure can be implemented where each time step in the transient analysis is indexed by the "primary" variable, such that the applied force updates automatically in each load step in the transient solution process. The details of these data manipulation are included in Appendix C.

Step 2: Initialize the FEM transient analysis. The first initializing load step is the most critical to properly approximate the initial conditions of the frame structure as described by equations (5.11). In the first load step, the initial conditions of the problem must be setup; however there are two separate sets of initializing forces to consider: the initial disturbing force vector, $\boldsymbol{F_{dist}}$, and the initial actuation forces, $F_2(0)$.

The initial disturbing forces in vector $\boldsymbol{F_{dist}}$ displace the structure into its initial configuration. In order to do this exactly, all DOFs must be forced into the assumed initial configuration. However, the initial position can be accurately approximated by choosing a more limited number of DOFs to perturb the system into the initial disturbed shape described by (5.11). In this example fourteen DOFs at the upper intersection points of the beams and columns and near the midpoints of each member (at DOFs 2x, 5x, 7x, 9x, 13x, 15x, 18x, 21x, 27x, 27y, 30, 32, 35x, 35y) were selected to produce an initial disturbed shape that deviated in position less than 0.3-percent from the exact initial configuration. Also, the initial actuation force $F_2(0)$ must be applied to the appropriate nodes of the FEM model in this initializing load step; however, this will change the initial configuration of the frame introducing error to the initial load step. A simple method of obtaining the correct initial disturbing forces is to run a static analysis of the frame with the fourteen DOFs acted upon by the forces in vector $\boldsymbol{F_{dist}}$ with displacement constraints in the initial deformed configuration while applying the initial actuation force $F_2(0)$ at the appropriate DOFs. The reactions obtained from this static analysis will provide all the

initial disturbing forces in vector $\boldsymbol{F_{dist}}$. In this manner, the set of initial disturbing forces in vector $\boldsymbol{F_{dist}}$ and the initial actuator force $F_2(0)$ are applied in the first load step. Then, in the following load step all forces are deleted and only the updated actuation force $F_2(n\Delta t)$ is applied to the appropriate DOFs in the subsequent load steps n. This initialization method is discussed more completely, with reference to the ANSYS command code, in Appendix C.

Step 3: Choose Time Steps and Load Steps. The choice of time steps and load steps impacts the accuracy of the transient dynamic FEM model. The time step influences the number of time integrations that are used in computing the system's dynamic response – more steps give better accuracy but at a greater computational cost. On the other hand, the load step influences how often the external actuation forces are updated in the time integration equations. Typically the load steps and time steps are chosen independently (with typically fewer load steps), but for actively dampened systems both the actuation force and the dynamic response of the structure are characterized by the same frequencies so load steps and time steps are also chosen to be similar. This is particularly important early in the attenuation process when the actuation force undergoes large oscillations as seen in Figure 5-9*a*.

To effectively capture sinusoidal oscillations, time steps should be small enough to capture twenty samples per period [30]. Therefore to capture the first two modes of vibration of the frame structure the time steps should be no larger than: $\Delta t = 1/20\,(17.9Hz)^{-1} = 0.00279s$. This recommended time step was found to produce large errors particularly with increasing time, as errors introduced early in the transient process tend to be additive and produce larger errors later in the analysis. Based on some trial and error, described in more detail in Appendix C, the time steps were chosen at 0.0001*s* and the load steps were chosen identically for 0.0001s for

$0 \leq t \leq 0.01s$, but larger load steps of $0.0005s$ were chosen for $0.01s \leq t \leq 0.4s$. This requires a total of 881 load steps to cover the attenuation period of 0.4s.

Step 4: Compare the DOF responses. The response obtained from the transient FEM model, obtained with ANSYS, is compared with the exact solution obtained in the control stage, obtained with MAPLE. Recall that in the control stage two dominant modes of vibration were considered; similarly, using the modal superposition method the FEM transient analysis also considers the superposition of these same two modes. Figure 5-10 shows the displacement response d_x^7 obtained from the FEM transient analysis alongside that obtained from the control stage. The plots are visually indistinguishable, verifying the validity of the dynamic response obtained in the control stage.

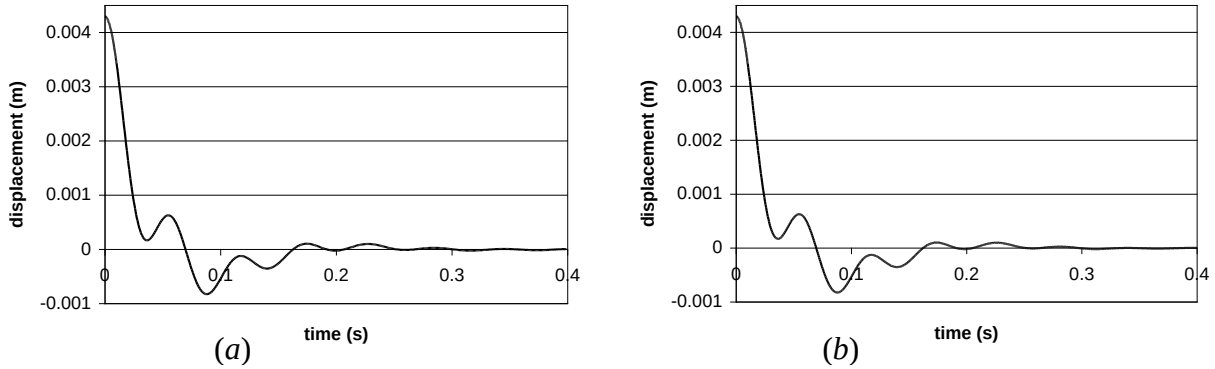

Figure 5-10. Response d_x^7 from the (a) verification stage and (b) the control stage.

Step 5: Check for spillover effects from higher modes of vibration. The implicit assumption in modelling the active attenuation of the frame's first two modes of vibration is that higher modes play an insignificant role in the dynamics. By considering these higher modes in the verification stage, the validity of this assumption is evaluated. To perform this check, the number of additional modes to be considered may be included in a transient analysis based on

the mode superposition method in ANSYS. Alternatively, a full transient analysis where all DOFs are directly integrated in time, can be performed, but at an increased computational cost.

A transient modal superposition analysis was performed with four modes of vibration included in the dynamics. Figure 5-11 shows the displacement response of two selected DOFs on the frame. The response d_x^7 is plotted in Figure 5-11a and the response d_y^{38}, chosen for its sensitivity to the fourth mode of vibration (see Figure 5-1 for location) is plotted in Figure 5-11b. Also, the passive (uncontrolled) response of the structure with four modes considered in the dynamics is included in these plots for comparison.

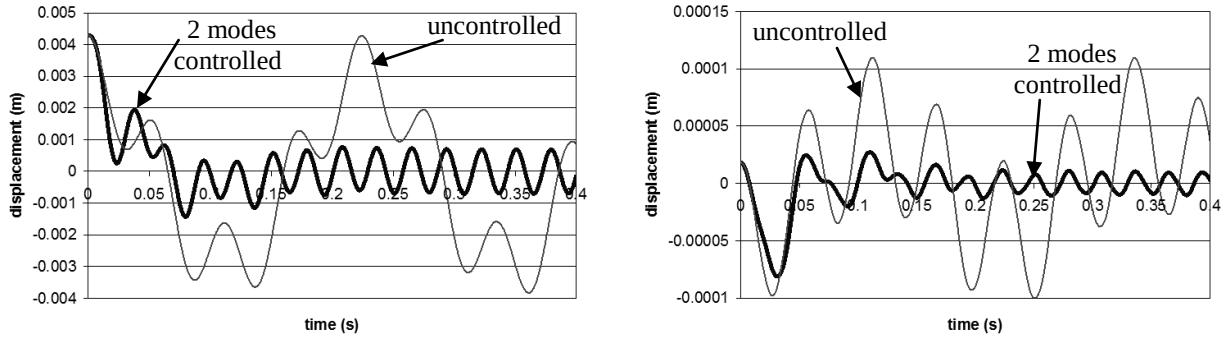

(a) (b)

Figure 5-11. (a) Response d_x^7 and (b) d_y^{38} with two modes actively controlled and four modes considered in the dynamics. Based on FEM transient analysis with control applied from actuator F_2 (thick line) and with no control (thin line).

In both plots in Figure 5-11 a residual vibration mode persists as time progresses and it has a frequency is $35.0Hz$, which can be verified in the figures. Note that the oscillation amplitudes in Figure 5-11a are approximately 100 times larger than those in Figure 5-11b because node 38 undergoes very small displacements (d_y^{38}) in the first three modes of vibration. Also note that the fourth mode of vibration is not visibly present in the plots, even though node 38 is sensitive to vertical displacements in this mode. This result is somewhat expected because the initial disturbance did not deflect the structure into a shape effecting the fourth mode. It is

also evident in Figure 5-11 that the passive (uncontrolled) response of the frame subjected to the same initial disturbance is dominated by the first two modes of vibration. This result is interesting because, due to its placement relative to the third mode of vibration, the actuator F_2 actually excites the third mode of vibration in attempting to dampen the first two modes of vibration. In other words, controlling the first two modes with actuator F_2 resulted in spillover effects on the third mode of vibration.

6. THREE-DIMENSIONAL MAST PROBLEM

6.1 Mast Model [20]

This example demonstrates the CMSOC method for simulating and analyzing active vibration attenuation in a mast structure. Several different positions and actuator locations will be investigated, in search of a "good" configuration for eliminating vibrations. Different configurations will be evaluated in the structural stage by assessing the controllability parameters λ and κ and in the control stage by the forces and responses obtained. The verification stage is not presented for sake of brevity, but can be considered in a similar manner as Chapter 5 to detect spillover effects and verify the system responses as required.

The mast structure shown in Figure 6-1 is based on the geometry and characteristics of an experimental active structure that was discussed in [1] and shown in Figure 1-1. The structure extends into the *z*-direction 1820*mm* with twelve 140*mm* high repeating bays and two irregular half-bays at the fixed end and free end. A 15*mm* thick, 162*mm* diameter steel plate is supported at the free end of the mast by the adjoining members. When viewed along its length (*z*-direction) the centerlines of the three chord members form the points of an isosceles triangle with a base of 140*mm* and a height of 100*mm*. All members are 4*mm* diameter steel members and all their connections are assumed to be rigid. The steel is assumed have a modulus of elasticity of $E = 200GPa$ and density of $\rho = 7800kg/m^3$. The members near the base of the structure that will be considered as potential actuator locations are shown in Figure 6-1 and labelled with the uppercase letters A through E. Point *p*, located at the center of the circular plate supported at the free end of the mast, will be used as a location for observing and plotting the dynamic response

of the structure. To emphasize the active damping in the system all passive damping mechanisms are ignored.

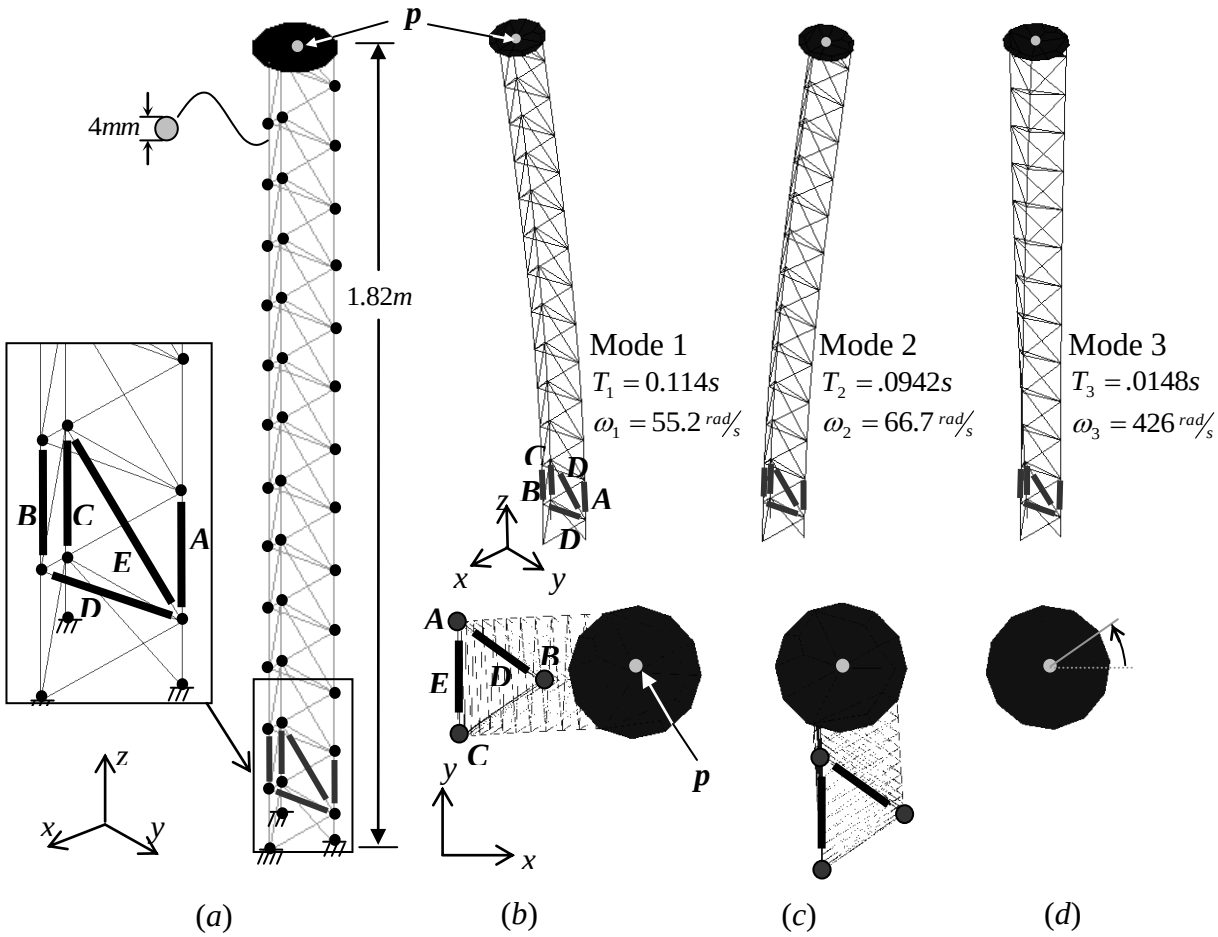

Figure 6-1. (*a*) Mast model and modal shapes of the (*b*) first mode, (*c*) second mode, and (*d*) third mode.

In the Figure 6-1, the first three dominant mode shapes are shown from an isometric perspective as well as a top down view. The first vibration modes is a global flexural bending mode occurring primarily in the *xz*-plane at a radian frequency of $\omega_1 = 55.2 rad/s$ (period of $T_1 = 0.114s$). The second vibration mode is a second flexural bending mode, that oscillates primarily in the *yz*- plane and at a slightly higher frequency of $\omega_2 = 66.7 rad/s$ (period of $T_2 = 0.0942s$). The third vibration mode is a global twisting mode where the mast undergoes

axial rotation at a considerably higher frequency of $\omega_3 = 426 rad/s$ (period of $T_3 = 0.0.0148s$).

In [1] several feedback algorithms were investigated and experimentally tested on the experimental apparatus from which the current model is based. The experimental structure was capable of attenuating the motion of the first two modes ($n_m = 2$) using two actuators ($n_a = 2$) located in positions A and B shown in Figure 6-1. The apparatus employed piezoelectric linear actuators with collocated force transducers to attenuate the vibrations using various feedback control laws. Conveniently, the stiffness and length of the actuators were approximately equal to those of the steel that they replaced. The studies were limited to fully-actuated control systems ($n_m = n_a$) considering two modes of vibration, whereas this example explores the possibility of controlling up to three modes using one, two, or three actuators. The force produced by an actuator is denoted by F_i where i denotes the actuator position (i = A,B,C,D,E).

The task in each case is to bring the mast structure from an initial disturbed state to a resting state using a time-invariant control system. The structural stage and control stage are briefly covered for each case; however the verification stage will not be discussed in this example. The optimization criteria for the process is based on the performance index in the form shown in equation (2.8) with the weighting coefficients selections taken as: $a = 1$, $b = 1$, and $c = 0.1$. Here the actuator work weighting coefficient (c) is weighted at a lower value to obtain faster response times more consistent with those obtained in [1]. The seven cases that are considered in this example are:

1. Two actuators in locations A and B attenuating two dominant modes of vibration.
2. Two actuators in locations D and E attenuating two dominant modes of vibration.
3. One actuator in location A attenuating two dominant modes of vibration.

4. One actuator in location B attenuating two dominant modes of vibration.
5. One actuator in location C attenuating two dominant modes of vibration.
6. Two actuators in locations A and B attenuating three dominant modes of vibration.
7. One actuator in location A attenuating three dominant modes of vibration.

In each case the system is analyzed for an initial disturbance given by:

$$\eta_1(0) = 0.004\,, \qquad \eta_2(0) = 0.004, \qquad \eta_3(0) = 0.001 \tag{6.1a}$$

$$\dot{\eta}_1(0) = \dot{\eta}_2(0) = \dot{\eta}_3(0) = 0 \tag{6.1b}$$

In DOF-space the initial frame position described by (6.1a) and (6.2b) corresponds to a stationary deformed shape with point p at the top of the mast (see Figure 5-1) deflected $2.28mm$ in the x-direction, $2.58mm$ in the y-direction, and rotated 0.548° about the z-axis (counter-clockwise when viewed from the top). Note that in cases 1 to 5, only the first two modes are considered in the dynamic model; hence, initial disturbances causing mast twisting (third mode of vibration) are left un-attenuated.

6.2 Structural Stage

The controllability parameters (κ and λ), obtained in the structural stage of the CMSOC methodology, are shown in Table 6-1 for the seven cases. Details of the solution procedure can be found in [20]. Note that the rate parameter λ does not apply to fully-actuated systems (case 1 and 2) because the modal controls are uncoupled and their rates of attenuation are not affected by changes in actuator positions. Recall that it is generally desirable for an under-actuated system to have a value of the rate parameter λ close to unity to ensure all modes are attenuated adequately. Also the effort parameter κ should be as small as possible for small actuation force amplitudes. Note that these rules are approximate correlations and are only beneficial for comparing various actuator configurations for the same system with the same number of modes

and actuators. For example, a meaningful comparison can be made between the controllability parameters obtained for cases 3 to 5, which all involve single actuator configurations that attenuate the mast's two dominant modes of vibration, but a comparison between cases 6 and 7 is less meaningful because the latter uses two actuators while the former uses only one.

Table 6-1. Dimensions n_m and n_a, rate parameter λ, and effort parameter κ, for cases 1 to 7.

Case Number	Number of Modes, n_m	Number of Actuators, n_a	Rate Parameter, λ	Effort Parameter, κ
1	2	2	-	$45.0(10^3)$
2	2	2	-	$783(10^3)$
3	2	1	0.436	457
4	2	1	11.7	220
5	2	1	0.527	386
6	3	2	0.713	$45.4(10^3)$
7	3	1	0.637	457

In [1] it was shown that good actuator locations are related to the level of strain in the member to be considered for an actuator position. In other words, if an actuator is substituted for a member in the structure that contains a large percentage of the total modal strain energy for a particular mode shape then good attenuation of that mode should be expected. The percentage of strain energy in the members in positions A through E is shown in Table 6-2 for the three dominant modes of vibration. The percentage of modal strain energy is obtained from the FEM program output following the modal analysis.

Table 6-2. Percentage of strain energy in selected members of the mast structure for the first three modes of vibration.

Member	Percentage of strain energy Mode 1	Percentage of strain energy Mode 2	Percentage of strain energy Mode 3
A	2.83	10.2	0.125
B	12.2	0.0630	0.351
C	3.95	9.75	0.0710

D	0.0260	0.0120	1.02
E	0.00200	0.102	3.30

In Table 6-2, members containing a relatively larger percentage of strain energy for a particular mode are in a better position for controlling that mode.

Cases 1 and 2 are fully-actuated systems and produce identical responses (not considering spillover effects on higher modes), but the forces required to produce the same response differ significantly. In Table 6-1, case 2 has a larger value κ and so is expected to use significantly larger forces than in case 1 to attenuate the same disturbance. This result should be expected considering that case 2 uses actuators in positions D and E, which undergo small relative strains in the first two modes (see Table 6-2). Cases 3 to 5 are single actuator systems controlling two modes of vibration; Table 6-1 indicates that Case 4 has a large value of λ and so poor attenuation of one of the modes is expected. Table 6-2 indicates that the actuator in position B is poorly suited for controlling the second mode of vibration, which agrees intuitively with Figure 6-1*b*, as position B effectively lies on the neutral axis of the built-up mast cross section and undergoes considerably smaller strains than the locations A and C. Cases 6 and 7 each consider three dominant modes of vibration in the dynamics and attenuate them with two and one actuator(s), respectively. Table 6-1 indicates that all modes will be attenuated in reasonable times, but Table 6-2 suggests that the third twisting mode of vibration will be attenuated most slowly. In the control stage these observations will be reflected in the dynamics of the structure.

6.3 Control Stage

The control stage of the CMSOC methodology solves the dynamic responses for the seven cases. The mast response is characterized by the modal dampening parameters α_i and

frequencies β_i, the effective settling times, and the peak actuation force amplitudes which are tabulated in Table 6-3.

Table 6-3. Modal damping parameters α_i, frequencies β_i, effective settling time t_{ef}, and peak force amplitude(s) for six cases for the mast example.

Case #	α_i			β_i			t_{ef} (s)	Peak force(s) (kN)
	i=1	2	3	i=1	2	3		
1	12.3	14.8	-	55.2	66.7	-	0.285	$\lvert F_A\rvert = 1.45, \lvert F_B\rvert = 1.25$
2	12.3	14.8	-	55.2	66.7	-	0.285	$\lvert F_D\rvert = 17.0, \lvert F_E\rvert = 14.5$
3	3.79	13.2	-	56.0	66.0	-	0.925	$\lvert F_A\rvert = 1.15$
4	12.2	0.717	-	55.2	66.7	-	4.88	$\lvert F_B\rvert = 1.00$
5	4.51	12.6	-	56.2	65.7	-	0.775	$\lvert F_C\rvert = 1.58$
6	12.1	14.5	25.0	55.2	66.7	426	0.290	$\lvert F_A\rvert = 2.40, \lvert F_B\rvert = 2.80$
7	3.78	13.1	8.98	56.0	66.0	426	0.926	$\lvert F_A\rvert = 2.40$

For cases 1 and 2, the dynamic responses (α_i,β_i, t_{ef} etc.) do not change, but the actuation forces required to produce the response do change. The peak actuation forces required in case 2 significantly exceed that needed in case 1. Comparing cases 3 to 5, case 4 stands out as having poor attenuation of the second mode of vibration and has a long effective attenuation time ($t_{ef} = 4.88s$). Case 6 shows that the third mode of vibration can effectively be controlled using the same two-actuator configuration (F_A and F_B) as case 1 and case 7 demonstrates that a single actuator can control the three dominant modes of vibration although there is some reduction in the attenuation rate when compared to case 6.

The above observations are visually confirmed in the Figures 6-2 to Figure 6-7 which show plots of the actuation force and the system responses over a period of 0.4*s*. The system responses are plotted in terms of the time-varying displacements d_x^p and d_y^p and rotations about the *z*-axis d_{rotz}^p at point *p*. The trajectory that the point *p* follows in the *xy*-plane is also plotted. Figure 6-2 shows the plots for case 1 and Figure 6-3 shows plots for case 2. As expected, the

responses shown in Figures 6-3 and 6-2 are identical, but the actuation forces are much larger for case 2 (Figure 6-3).

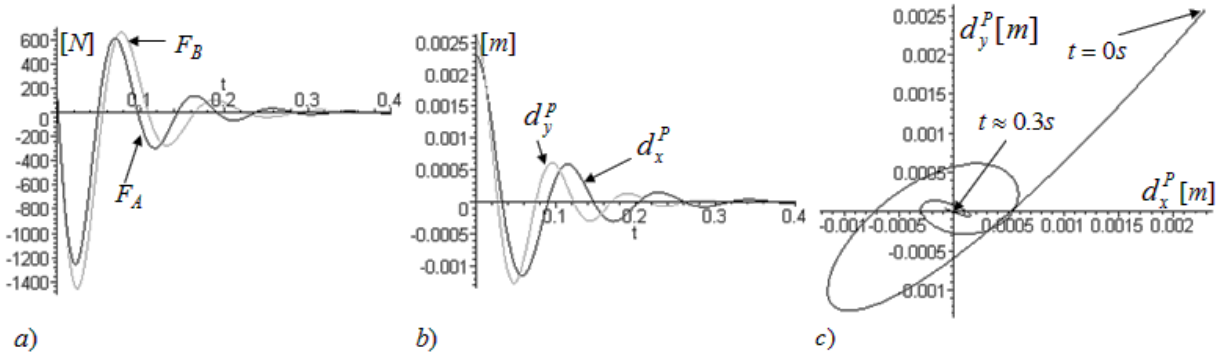

Figure 6-2. (*a*) Attenuation forces F_A and F_B, (*b*) tip deflections d_x^p and d_y^p of point *p* as functions of time, and (*c*) the displacement of point *p* as they appear in the *xy*-plane (case 1).

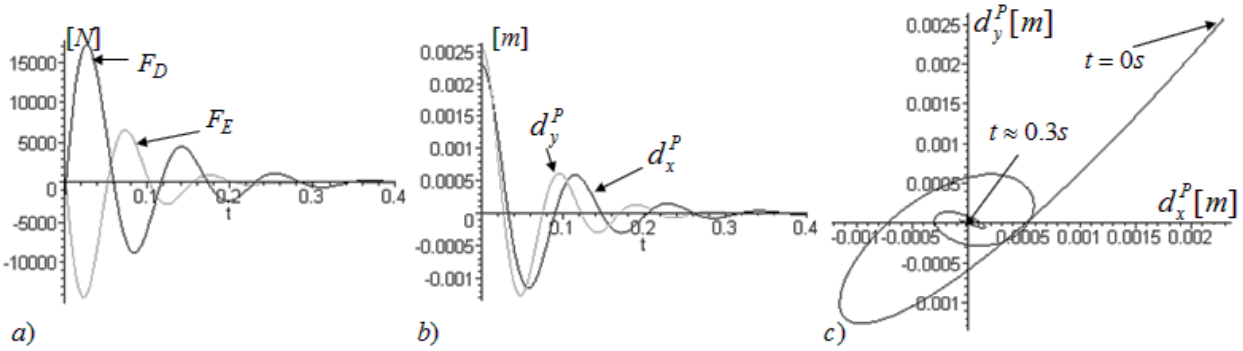

Figure 6-3. (*a*) Attenuation forces F_D and F_E, (*b*) tip deflections d_x^p and d_y^p of point *p* as functions of time, and (*c*) the displacement of point *p* as they appear in the *xy*-plane (case 2).

In Figures 6-4, Figure 6-5, and Figure 6-6 results are shown for cases 3, 4, and 5 respectively. As expected, the plots for case 4 (Figure 6-5) involving force F_B show the effects of the poorly attenuated second mode of vibration, as the mast undergoes more persistent vibrations than cases 3 and 5. Interestingly, in Figure 6-6 it is evident that the tip of the mast begins to deflect around its resting position in a clockwise pattern, consistent with cases 3 and 4; however, the motion switches to a counter-clockwise orbiting pattern after approximately 0.01*s*

of the maneuver. This directional switch requires a larger peak actuation force when compared with cases3 and 5, but the maneuver eliminates the vibrations in the least amount of time.

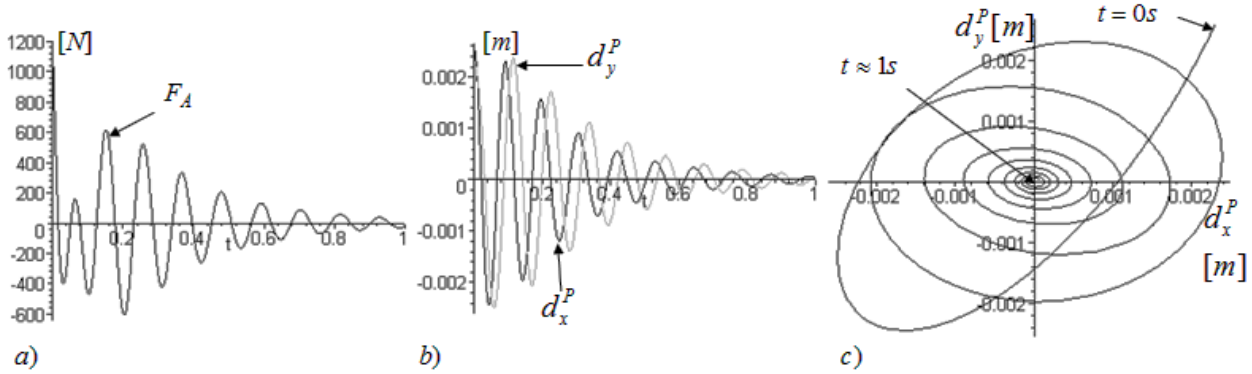

Figure 6-4. (*a*) Attenuation force F_A, (*b*) tip deflections d_x^p and d_y^p of point *p* as functions of time, and (*c*) the displacement of point *p* as they appear in the *xy*-plane (case 3).

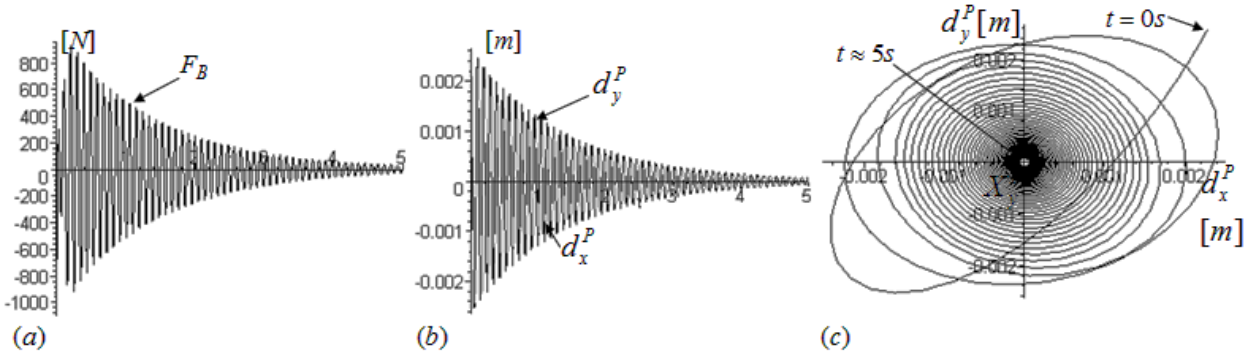

Figure 6-5. (*a*) Attenuation force F_B, (*b*) tip deflections d_x^p and d_y^p of point *p* as functions of time, and (*c*) the displacement of point *p* as they appear in the *xy*-plane (case 4).

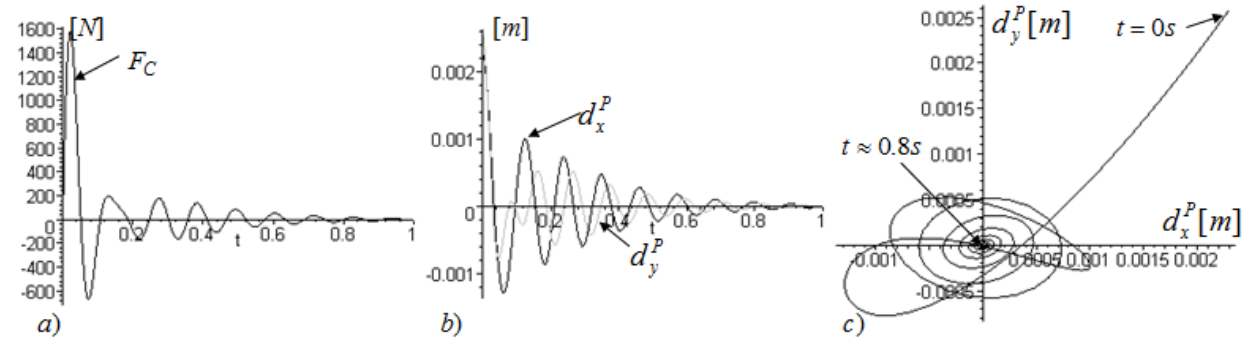

Figure 6-6. (*a*) Attenuation force F_C, (*b*) tip deflections d_x^p and d_y^p of point *p* as functions of time, and (*c*) the displacement of point *p* as they appear in the *xy*-plane (case 5).

In Figures 6-7 and 6-8 plots are shown for case 6 and case 7. In Figure 6-7, one can see the similarity in the tip trajectory of point *p* in comparison to case 1 in Figure 6-2, however in this case the third twisting mode of vibration is also simultaneously attenuated by the same actuators F_A and F_B. In Figure 6-8, a similar tip trajectory as case 3 in Figure 6-4 is produced; however, the third mode of vibration is also simultaneously attenuated. The three modes of vibration are attenuated considerably more quickly with both actuators F_A and F_B in Figure 6-7 than with the solitary actuator F_A in Figure 6-8.

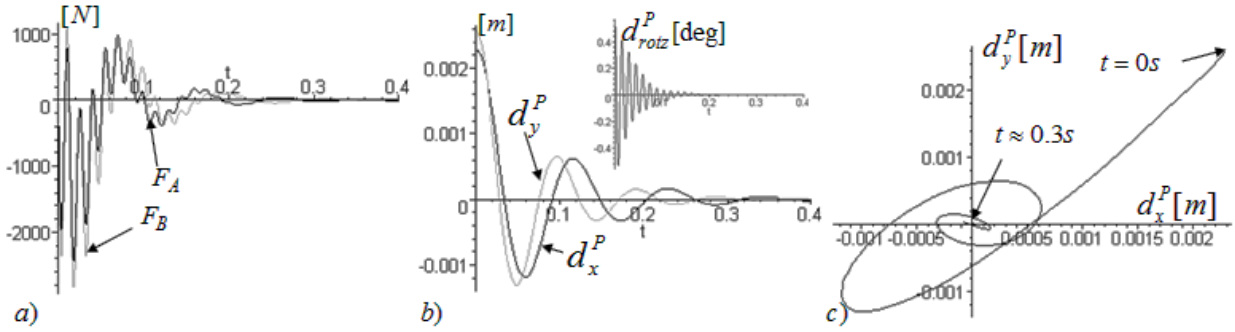

Figure 6-7. (*a*) Attenuation forces F_A and F_B, (*b*) tip deflections d_x^p and d_y^p of point *p* as functions of time, and (*c*) the displacement of point *p* as they appear in the *xy*-plane (case 6). Also, the rotation of point *p* in the *z*-direction d_{rotz}^p is shown inset in graph (*b*).

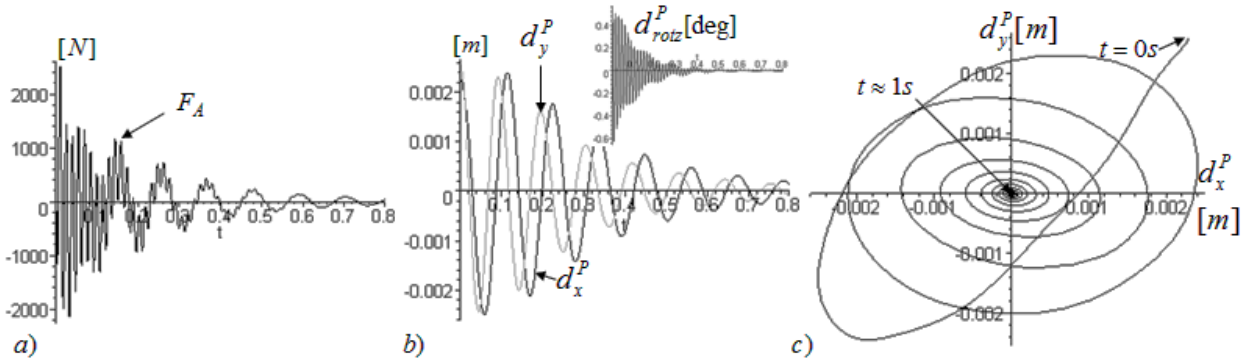

Figure 6-8. (a) Attenuation force F_A, (b) tip deflections d_x^p and d_y^p of point p as functions of time, and (c) the displacement of point p as they appear in the xy-plane (case 6). Also, the rotation of point p in the z-direction d_{rotz}^p is shown inset in graph (b).

7. CONCLUSIONS AND FUTURE WORK

The CMSOC methodology was formulated and demonstrated to show how it can be employed for designing and analyzing the dynamics of actively dampened structures. The methodology is an extension of computational mechanics into the area of control and its advantage is that it can be applied to arbitrary linear structures or mechanical systems involving any number of DOFs that are controlled by any number of actuators. It was implemented on several example systems ranging from very simple, such as the gantry crane, to the more complex, such as the mast structure. The examples served to show how the three stages of the methodology – the structural stage, the control stage, and the verification stage – are well suited for the study of under-actuated linear systems. Each step of the solution is relatively automated by integrating the capabilities of the ANSYS FEM program and the MAPLE mathematical program.

The structural stage involves constructing the FEM model in ANSYS, performing the modal analysis to obtain the number of significant modal shapes and frequencies, transferring this information to MAPLE and then assigning the actuator configurations. This data is automatically manipulated to obtain the system transfer matrix, constraints due to under-actuation, and indicators of poor controllability. If poor controllability is expected than adjustments to the actuator configuration are made to obtain more favourable indicators that suggest that continuing to the control stage is warranted.

The control stage involves inputting the initial conditions and optimization parameters into the MAPLE worksheet, with the information from the structural stage, to calculate the

unknown actuation forces and system response over time. If the actuators are controlled in a closed-loop, than the sensor configuration is input and the corresponding gains are automatically calculated. The potentially large numbers of computationally intensive symbolic calculations are handled automatically in the MAPLE program.

The verification stage involves transferring the actuation forces, obtained in the control stage to the FEM model to obtain the transient time-integrated response of the system for comparison to the system response from the control stage. Any spill-over effects are detected by include higher modes of vibration when performing the transient analysis.

The problem is essentially transformed into a constrained optimization problem, with all the constraints handled by time-dependant Lagrange multipliers. Since the method includes all constraints that may arise due to under-actuation, it avoids difficulties with unstable inverse dynamics often associated with addressing under-actuated problems. Moreover, the method incorporates 'built-in' assessment parameters that can be used to predict controllability issues and quantitatively compare the performance of different actuator configurations.

The strength of the CMSOC method lies in its ability to address the dynamics of essentially any actively dampened structure, with any arbitrary shape and passive dynamic characteristics, and any arbitrary number of actuators. The limitation is that the structure, for the range of motions under consideration, must generally exhibit linear elastic behavior. The methodology does not replace other controller design approaches, as it deals only with idealized systems and has no means to account for inherent 'real world' errors. Therefore its usefulness is primarily in the initial design stages of such systems as it can provide insight into the physical significance of under-actuation and how actuator positioning affects controllability and system performance in actively dampened structures.

Some areas that are of interest to future study are the application of the CMSOC approach when dealing with systems that exhibit two modes with the same frequency (bimodal systems). Also an interesting system to consider would be one that exhibits vibrations with frequencies that are integer multiples of each other, such that actively attenuating the vibrations of a lower frequency mode could excite vibrations of a higher mode with a frequency that is an integer multiple of the lower mode. Another interesting study would be to experimentally test an actively dampened structure to demonstrate how an under-actuated type control system could be designed and implemented using the CMSOC methodology complemented with other control strategies.

LIST OF REFERENCES

[1] Preumont, A. *Vibration Control of Active Structures: An Introduction*, 2nd ed., Kluwer, Dordrecht, Chaps. 3,13, 2002.

[2] Achkire, Y., and Preumont, A., "Active Tendon Control of Cable-Stayed Bridges," *Earthquake Engineering and Structural Dynamics*, Vol. 25, No. 6, pp. 585-597, 1996.

[3] Fantoni, L., and Lozano, R., *Non-linear Control for Underactuated Mechanical Systems*, Springer-Verlag, New York, Chaps. 1-2, 2002.

[4] Szyszkowski, W., and Woods, S., "On Under-Actuated Manipulators and Non-Causal Solution Methods", *The International Journal of Robotics Research* (Submitted 2008).

[5] Craig J.J., *Introduction to Robotics: Mechanics and Control*, Pearson Education, NJ, Chaps 9-10, 2005.

[6] Slotine, J-J., Weiping, L., *Applied Non-linear Control*, Prentice Hall, NJ, 1991.

[7] Bayo E., Papadopoulos, P., Stubbe, J., Serna, M., "Inverse Dynamics and Kinematics of Multi-Link Elastic Robots: An Iterative Frequency Domain Approach," *International Journal of Robotics Research*, Vol. 8, No. 6, pp. 49-62, 1989.

[8] De Jalon, J.G., Bayo, E., *Kinematic and Dynamic Simulation of Multibody Systems-The Real-Time Challenge*, Springer-Verlag, Chap. 12, 1993.

[9] Kwon, D-S., Book, W.J., "A Time-Domain Inverse Dynamic Tracking Control of a Single-Link Flexible Manipulator," *Journal of Dynamic Systems, Measurement, and Control*, Vol. 116, pp. 193-200, 1994.

[10] Karihaloo, B.L., Parbery, R.D., "Optimal Control of a Dynamical System Representing a Gantry Crane," *Journal of Optimization Theory and Applications*, Vol. 36, No. 3, pp. 409-417, 1982.

[11] Spong, M.W., "The Swing Up Control Problem for the Acrobot," *IEEE Control Systems Magazine*, Vol. 15, No. 1, 1995.

[12] Do, K.D., Pan, J., "Global Tracking Control of Underactuated Ships with Nonzero Off-Diagonal Terms in their System Matrices," *42nd IEEE Conference on Decision and Control, USA*, IEEE Control Systems Society, Vol. 1, pp. 1250-1255, 2003.

[13] Saimek, S., Li, P.Y., "Motion Planning and Control of a Swimming Machine," *The International Journal of Robotics Research*, Vol. 23, No. 1, pp. 27-53, 2004.

[14] Horvat, D., "Applications of Optimal Control to Advanced Automotive Suspension Design," *Journal of Dynamic Systems, Measurement, and Control*, Vol. 115, No. 331, pp. 328-342, 1993.

[15] Ju, F., Chao, Y.S., Cui, F.S., "Dynamic Response of Tower Crane Induced by the Pendulum Motion of the Payload," *International Journal of Solids and Structures*, Vol. 43, pp. 376-389, 2006.

[16] Saleh, A., Adeli, H., "Algorithms for Solution of the Riccati Equation," *Control, Optimization, and Smart Structures*, J. Wiley&Sons Inc., New York, Chap. 5, 1999.

[17] Bathe, K.J., *Finite Element Procedures*, Prentice Hall, Englewood Cliffs, NJ, Chap. 9.3, 1996.

[18] Calfield, R.A., Meirovitch, L., "Integrated Structural Design and Vibration Suppression Using Independent Modal Space Control," *AIAA Journal*, Vol. 32, No. 10, pp. 2053-2060, 1994.

[19] Szyszkowski, W., Dhotre, N., "A Procedure for Solving Under-Actuated Optimal Attenuation of Vibrations by Means of Symbolic Operators," *Journal of Vibration and Control*, Vol. 15, No. 5, pp. 739-771, 2009.

[20] Woods, S., Szyszkowski, W., "Simulating Active Vibration Attenuation in Underactuated Spatial Structures," *Journal of Guidance, Control, and Dynamics*, Vol. 32, No. 4, pp. 1246-1253, 2009.

[21] Woods, S., Szyszkowski, W., "Analysis and Simulation of Optimal Vibration Attenuation for Underactuated Mechanical Systems," *AIAA Journal*, Vol. 47, No. 12, pp. 2821-2835.

[22] Woods, S., Szyszkowski, W., "Optimal Manoeuvres of Underactuated Linear Mechanical Systems: Controlling Gantry Crane Operations," *Mathematical Problems in Engineering* (submitted 2012).

[23] Junkins, J.L., Kim, Y.D., *Introduction to Dynamics and Control of Flexible Structures*, AIAA Series, Washington DC, 1993.

[24] Meirovitch, L., Baruh, H., "Control of Self-Adjoint Distributed-Parameter Systems," *AIAA Journal*, Vol. 5, No. 1, pp. 60-66, 1980.

[25] Oz, H., Meirovitch, L., "Optimal Modal-Space Control of Flexible Gyroscopic Systems," *AIAA Journal*, Vol. 3, No. 3, pp. 218-226, 1980.

[26] Lammering, R., Jia, J., Rogers, C.A., "Optimal Placement of Piezoelectric Actuators in Adaptive Truss Structures," *Journal of Sound and Vibration*, Vol. 171, No. 1, pp. 67-85.

[27] Zhang, X., "Integrated Optimal Design of Flexible Mechanisms and Vibration Control," *International Journal of Mechanical Sciences*, Vol. 46, No. 11, pp. 1607-1620, 2004.

[28] Kirk, D.E., *Optimal Control Theory*, Dover Publications, New York, 1998.

[29] Zill, D.G., Cullen, M.R., *Advanced Engineering Mathematics*, PWS Publications, Boston, 1992.

[30] Ansys Support Documentation, Release 11.0, 2007.

APPENDIX A: MAPLE PROGRAM

This appendix presents the maple commands that were used for solving the active dampening structure presented in Chapter 5 and shown in Figure 5-1*a*. The commands and outputs are shown for case 1 in Chapter 5, which uses the single actuator F_1 to control the frames first three dominant modes of vibration.

3 Level Frame Structure with Actuator F1

```
> restart;with(linalg):
```

Structural Stage

Input Modal Frequencies and Modal Shapes from ANSYS (modal shape data written to text file for ease of input)

```
> omega1:=27.565; omega2:=112.306; omega3:=219.968;
```

$$\omega 1 := 27.565$$
$$\omega 2 := 112.306$$
$$\omega 3 := 219.968 \quad \textbf{(2.1)}$$

```
> phi := ImportMatrix
  ("C:\\Users\\Simon\\Desktop\\MSc\\thesis\\Appendix
  A\\mode123.txt", source = delimited, delimiter = ",", format
  = rectangular, datatype = float[4], transpose = false,
  skiplines = 0);
```

$$\phi := \begin{bmatrix} 111 \text{ x } 3 \text{ Matrix} \\ \text{Data Type: } float_4 \\ \text{Storage: rectangular} \\ \text{Order: Fortran\_order} \end{bmatrix} \quad \textbf{(2.2)}$$

```
> phi_tran:=transpose(phi):
```

Assemble Actuator Configuration Matrix, B. Relate actuator forces to nodes of structure. Actuators F2 and F3 act as dummy actuators

```
> rt:=1/(2)^.5:
```

```
> Bmat:=matrix([[0,0,-rt],[0,-rt,0],[0,0,rt],[0,rt,0],[rt,0,0],
  [-rt,0,0],[0,0,rt],[0,rt,0],[0,0,-rt],[0,-rt,0],[-rt,0,0],
  [rt,0,0]]);
```

$$Bmat := \begin{bmatrix} 0 & 0 & -0.7071067814 \\ 0 & -0.7071067814 & 0 \\ 0 & 0 & 0.7071067814 \\ 0 & 0.7071067814 & 0 \\ 0.7071067814 & 0 & 0 \\ -0.7071067814 & 0 & 0 \\ 0 & 0 & 0.7071067814 \\ 0 & 0.7071067814 & 0 \\ 0 & 0 & -0.7071067814 \\ 0 & -0.7071067814 & 0 \\ -0.7071067814 & 0 & 0 \\ 0.7071067814 & 0 & 0 \end{bmatrix} \quad (2.3)$$

```
> phi_tran_redu:=matrix([[phi_tran[1,2],phi_tran[1,7],phi_tran
  [1,12],phi_tran[1,13],phi_tran[1,18],phi_tran[1,27],phi_tran
  [1,39],phi_tran[1,44],phi_tran[1,49],phi_tran[1,50],phi_tran
  [1,55],phi_tran[1,64]],[phi_tran[2,2],phi_tran[2,7],phi_tran
  [2,12],phi_tran[2,13],phi_tran[2,18],phi_tran[2,27],phi_tran
  [2,39],phi_tran[2,44],phi_tran[2,49],phi_tran[2,50],phi_tran
  [2,55],phi_tran[2,64]],[phi_tran[3,2],phi_tran[3,7],phi_tran
  [3,12],phi_tran[3,13],phi_tran[3,18],phi_tran[3,27],phi_tran
  [3,39],phi_tran[3,44],phi_tran[3,49],phi_tran[3,50],phi_tran
  [3,55],phi_tran[3,64]]]);
```

$$phi\_tran\_redu := [[0.256029993, 0.592750013, 0., 0.256029993, 0.592750013, 0.780439973, 0.000388009998, 0.000611989992, 0., -0.000388009998, -0.000611989992, 0.000697050011], [0.937929988, 0.664830029, 0., 0.937929988, 0.664830029, -0.430579990, -0.000821280002, -0.00192970003, 0., 0.000821209978, 0.00192960002, -0.00255450001], [0.938799977, -1.02020001, 0., 0.938799977, -1.02020001, 0.253479987, 0.000564449991, 0.00146509998, 0., -0.000564539980, -0.00146529998, 0.00255550002]] \quad (2.4)$$

```
> phi_redu:=transpose(phi_tran_redu):
```

Matrix manipulations to obtain psuedo transfer matrix and constraint matrix and assess controllability parameters, kappa and lambda.

```
> Bhat:=evalm(phi_tran_redu&*Bmat);
```

$$Bhat := \begin{bmatrix} -0.1317912124 & -0.2373899028 & -0.1807661798 \\ 0.7714011153 & 0.1911656459 & -0.6637973877 \\ -0.8977846283 & 1.386657348 & -0.6634327037 \end{bmatrix} \quad (2.5)$$

```
> Bhat_inv:=inverse(Bhat);
```

$$Bhat\_inv := \begin{bmatrix} -1.340734809 & 0.6895179818 & -0.3245856352 \\ -1.871339370 & 0.1264563160 & 0.3833599025 \\ -2.096995486 & -0.6687747870 & -0.2667989978 \end{bmatrix} \quad (2.6)$$

```
> Ba_tilda:=matrix([[Bhat_inv[1,1]]]);
```

$$Ba\_tilda := \begin{bmatrix} -1.340734809 \end{bmatrix} \quad (2.7)$$

```
> Br_tilda:=matrix([[Bhat_inv[1,2],Bhat_inv[1,3]]]);
```

$$Br\_tilda := \begin{bmatrix} 0.6895179818 & -0.3245856352 \end{bmatrix} \quad (2.8)$$

```
> Aa:=matrix([[Bhat_inv[2,1]],[Bhat_inv[3,1]]]);
```

$$Aa := \begin{bmatrix} -1.871339370 \\ -2.096995486 \end{bmatrix} \quad (2.9)$$

```
> Ar:=matrix([[Bhat_inv[2,2],Bhat_inv[2,3]],[Bhat_inv[3,2],
  Bhat_inv[3,3]]]);
```

$$Ar := \begin{bmatrix} 0.1264563160 & 0.3833599025 \\ -0.6687747870 & -0.2667989978 \end{bmatrix} \quad (2.10)$$

```
> Ba_bar:=evalm(Ba_tilda-Br_tilda&*inverse(Ar)&*Aa);
```

$$Ba\_bar := \begin{bmatrix} -7.587759319 \end{bmatrix} \quad (2.11)$$

```
> kappa:=det(Ba_bar);
```

$$\kappa := -7.587759319 \quad (2.12)$$

Matrix manipulations for normalizing the constraint matric to obtain A_bar

```
> matrix([[Bhat_inv[2,1],Bhat_inv[2,2],Bhat_inv[2,3]],[Bhat_inv
  [3,1],Bhat_inv[3,2],Bhat_inv[3,3]]]);
```

$$\begin{bmatrix} -1.871339370 & 0.1264563160 & 0.3833599025 \\ -2.096995486 & -0.6687747870 & -0.2667989978 \end{bmatrix} \quad (2.13)$$

```
> addrow(%,1,2,-%[2,1]/%[1,1]):
```

```
> addrow(%,1,2,-%[2,1]/%[1,1]):
```

```
> addrow(%,2,1,-%[1,3]/%[2,3]):
```

```
> A_bar:=matrix([[%[1,1]/%[1,1],%[1,2]/%[1,1],%[1,3]/%[1,1]],[%
[2,1]/%[2,2],%[2,2]/%[2,2],%[2,3]/%[2,2]]]);
```

$$A\_bar := \begin{bmatrix} 1.000000000 & 0.1708465412 & -0. \\ -1.233836918\ 10^{-19} & 1.000000000 & 0.8592273591 \end{bmatrix} \quad (2.14)$$

```
> Ar_bar:=matrix([[%[1,2],%[1,3]],[%[2,2],%[2,3]]]);
```

$$Ar\_bar := \begin{bmatrix} 0.1708465412 & -0. \\ 1.000000000 & 0.8592273591 \end{bmatrix} \quad (2.15)$$

```
> lambda:=det(Ar_bar);
```

$$\lambda := 0.1467960224 \quad (2.16)$$

```
> A_bar_tran:=transpose(A_bar):
```

Control Stage

Input optimization parameters to obtain performance index weighting parameters

```
> a:=1 ; b:=1; c:=1 ;zeta1:=0;zeta2:=0;zeta3:=0;
```

$$a := 1$$
$$b := 1$$
$$c := 1$$
$$\zeta 1 := 0$$
$$\zeta 2 := 0$$
$$\zeta 3 := 0 \quad (3.1)$$

```
> Qd1:=a*omega1^2;
```

$$Qd1 := 759.829225 \quad (3.2)$$

```
> Qd2:=a*omega2^2;
```

$$Qd2 := 12612.63764 \quad (3.3)$$

```
> Qd3:=a*omega3^2;
```

$$Qd3 := 48385.92102 \quad (3.4)$$

```
> Qv1:=b;
```

$$Qv1 := 1 \quad (3.5)$$

```
> Qv2:=b;
```

$$Qv2 := 1 \quad (3.6)$$

```
> Qv3:=b;
```

$$Qv3 := 1 \quad (3.7)$$

```
> R1:=1/(c*omega1^2);
```

$$R1 := 0.001316085203 \quad (3.8)$$

```
> R2:=1/(c*omega2^2);
```

$$R2 := 0.00007928555696 \quad (3.9)$$

```
> R3:=1/(c*omega3^2);
```

$$R3 := 0.00002066716886 \quad (3.10)$$

Input initial conditions

```
> eta_initial:=matrix(3,1,[0.05,0.005,0.0045]);
```

$$eta\_initial := \begin{bmatrix} 0.05 \\ 0.005 \\ 0.0045 \end{bmatrix} \quad (3.11)$$

```
> x_initial:=evalm(phi&*eta_initial):
```

```
> x_initial[27,1];x_initial[7,1];x_initial[2,1];x_initial
  [24+37,1];x_initial[25+37,1];
```

$$\begin{aligned} &0.03800975864 \\ &0.02837075076 \\ &0.02171574949 \\ &-0.0005298989893 \\ &0.0005298804851 \end{aligned} \quad (3.12)$$

Writing characteristic equation and obtaining roots

```
> Ebar:=matrix([[E1,0,0,-D11,0],[0,E2,0,-D21,-D22],[0,0,E3,0,-
  D32],[D11,D21,0,0,0],[0,D22,D32,0,0]]);
```

$$Ebar := \begin{bmatrix} E1 & 0 & 0 & -D11 & 0 \\ 0 & E2 & 0 & -D21 & -D22 \\ 0 & 0 & E3 & 0 & -D32 \\ D11 & D21 & 0 & 0 & 0 \\ 0 & D22 & D32 & 0 & 0 \end{bmatrix} \quad (3.13)$$

```
> D_curl:=det(%);
```

$$D\_curl := E1\, D21^2\, D32^2 + E2\, D32^2\, D11^2 + D22^2\, E3\, D11^2 \quad (3.14)$$

```
> D11:=A_bar[1,1]*(D^2+omega1^2);
```

$$D11 := 1.000000000\, D^2 + 759.8292250 \quad (3.15)$$

```
> D21:=A_bar[1,2]*(D^2+omega2^2);
```

$$D21 := 0.1708465412\, D^2 + 2154.825516 \quad (3.16)$$

```
> D22:=A_bar[2,2]*(D^2+omega2^2);
```

$$D22 := 1.000000000\, D^2 + 12612.63764 \quad (3.17)$$

```
> D32:=A_bar[2,3]*(D^2+omega3^2);
```

$$D32 := 0.8592273591\, D^2 + 41574.50714 \quad (3.18)$$

```
> DELTA:=0;
```

$$DELTA := 0 \quad (3.19)$$

```
> E1:=R1*D^4+(2*omega1^2*R1-Qv1-R1*DELTA^2)*D^2+(R1*omega1^4+
  Qd1);
```

$$E1 := 0.001316085203\, D^4 + 1.000000000\, D^2 + 1519.658450 \quad (3.20)$$

```
> E2:=R2*D^4+(2*omega2^2*R2-Qv2-R2*DELTA^2)*D^2+(R2*omega2^4+
  Qd2);
```

$$E2 := 0.00007928555696\, D^4 + 1.000000000\, D^2 + 25225.27527 \quad (3.21)$$

```
> E3:=R3*D^4+(2*omega3^2*R3-Qv3-R3*DELTA^2)*D^2+(R3*omega3^4+
```

```
Qd3);
```

$$E3 := 0.00002066716886\,D^4 + 1.000000000\,D^2 + 96771.84205 \quad (3.22)$$

```
> D_curl;
```

$$(0.001316085203\,D^4 + 1.000000000\,D^2 + 1519.658450)\,(0.1708465412\,D^2 + 2154.825516)^2\,(0.8592273591\,D^2 + 41574.50714)^2 + (0.00007928555696\,D^4 + 1.000000000\,D^2 + 25225.27527)\,(0.8592273591\,D^2 + 41574.50714)^2\,(1.000000000\,D^2 + 759.8292250)^2 + (1.000000000\,D^2 + 12612.63764)^2\,(0.00002066716886\,D^4 + 1.000000000\,D^2 + 96771.84205)\,(1.000000000\,D^2 + 759.8292250)^2 \quad (3.23)$$

```
> sol:=[solve(D_curl,D)];
```

$$sol := [-50.43651831 - 116.6371111\,I,\ 50.43651831 + 116.6371111\,I,\ -62.20241237 - 213.7142012\,I,\ 62.20241237 + 213.7142012\,I,\ -7.307830489 - 27.68201977\,I,\ 7.307830489 + 27.68201977\,I,\ -7.307830489 + 27.68201977\,I,\ 7.307830489 - 27.68201977\,I,\ -62.20241237 + 213.7142012\,I,\ 62.20241237 - 213.7142012\,I,\ -50.43651831 + 116.6371111\,I,\ 50.43651831 - 116.6371111\,I] \quad (3.24)$$

```
> alpha2:=abs(Re(sol[12]));alpha1:=abs(Re(sol[8]));alpha3:=abs
(Re(sol[4]));
```

$$\alpha 2 := 50.43651831$$

$$\alpha 1 := 7.307830489$$

$$\alpha 3 := 62.20241237 \quad (3.25)$$

```
> t1ef:=3.5/alpha1;t2ef:=3.5/alpha2;t3ef:=3.5/alpha3;
```

$$t1ef := 0.4789383123$$

$$t2ef := 0.06939416354$$

$$t3ef := 0.05626791415 \quad (3.26)$$

```
> beta2:=abs(Im(sol[12]));beta1:=abs(Im(sol[8]));beta3:=abs(Im
(sol[4]));
```

$$\beta 2 := 116.6371111$$

$$\beta 1 := 27.68201977$$

$$\beta 3 := 213.7142012 \quad (3.27)$$

Writing solution functions, eta and nu

```
> eta1:=exp(-alpha1*t)*(c11_1*sin(beta1*t)+c11_2*cos(beta1*t))+
  exp(-alpha2*t)*(c21_1*sin(beta2*t)+c21_2*cos(beta2*t))+exp(-
  alpha3*t)*(c31_1*sin(beta3*t)+c31_2*cos(beta3*t));
```

$$\eta 1 := e^{-7.307830489\,t}\,(c11\_1\sin(27.68201977\,t) + c11\_2\cos(27.68201977\,t)) + e^{-50.43651831\,t}\,(c21\_1\sin(116.6371111\,t) + c21\_2\cos(116.6371111\,t)) + e^{-62.20241237\,t}\,(c31\_1\sin(213.7142012\,t) + c31\_2\cos(213.7142012\,t)) \quad \textbf{(3.28)}$$

```
> eta2:=exp(-alpha1*t)*(c12_1*sin(beta1*t)+c12_2*cos(beta1*t))+
  exp(-alpha2*t)*(c22_1*sin(beta2*t)+c22_2*cos(beta2*t))+exp(-
  alpha3*t)*(c32_1*sin(beta3*t)+c32_2*cos(beta3*t));
```

$$\eta 2 := e^{-7.307830489\,t}\,(c12\_1\sin(27.68201977\,t) + c12\_2\cos(27.68201977\,t)) + e^{-50.43651831\,t}\,(c22\_1\sin(116.6371111\,t) + c22\_2\cos(116.6371111\,t)) + e^{-62.20241237\,t}\,(c32\_1\sin(213.7142012\,t) + c32\_2\cos(213.7142012\,t)) \quad \textbf{(3.29)}$$

```
> eta3:=exp(-alpha1*t)*(c13_1*sin(beta1*t)+c13_2*cos(beta1*t))+
  exp(-alpha2*t)*(c23_1*sin(beta2*t)+c23_2*cos(beta2*t))+exp(-
  alpha3*t)*(c33_1*sin(beta3*t)+c33_2*cos(beta3*t));
```

$$\eta 3 := e^{-7.307830489\,t}\,(c13\_1\sin(27.68201977\,t) + c13\_2\cos(27.68201977\,t)) + e^{-50.43651831\,t}\,(c23\_1\sin(116.6371111\,t) + c23\_2\cos(116.6371111\,t)) + e^{-62.20241237\,t}\,(c33\_1\sin(213.7142012\,t) + c33\_2\cos(213.7142012\,t)) \quad \textbf{(3.30)}$$

```
> nu1:=exp(-alpha1*t)*(c14_1*sin(beta1*t)+c14_2*cos(beta1*t))+
  exp(-alpha2*t)*(c24_1*sin(beta2*t)+c24_2*cos(beta2*t))+exp(-
  alpha3*t)*(c34_1*sin(beta3*t)+c34_2*cos(beta3*t));
```

$$\nu 1 := e^{-7.307830489\,t}\,(c14\_1\sin(27.68201977\,t) + c14\_2\cos(27.68201977\,t)) + e^{-50.43651831\,t}\,(c24\_1\sin(116.6371111\,t) + c24\_2\cos(116.6371111\,t)) + e^{-62.20241237\,t}\,(c34\_1\sin(213.7142012\,t) + c34\_2\cos(213.7142012\,t)) \quad \textbf{(3.31)}$$

```
> nu2:=exp(-alpha1*t)*(c15_1*sin(beta1*t)+c15_2*cos(beta1*t))+
  exp(-alpha2*t)*(c25_1*sin(beta2*t)+c25_2*cos(beta2*t))+exp(-
  alpha3*t)*(c35_1*sin(beta3*t)+c35_2*cos(beta3*t));
```

$$\nu 2 := e^{-7.307830489\,t}\,(c15\_1\sin(27.68201977\,t) + c15\_2\cos(27.68201977\,t)) + e^{-50.43651831\,t}\,(c25\_1\sin(116.6371111\,t) + c25\_2\cos(116.6371111\,t)) + e^{-62.20241237\,t}\,(c35\_1\sin(213.7142012\,t) + c35\_2\cos(213.7142012\,t)) \quad \textbf{(3.32)}$$

Differentiating Solution Functions

```
> eta1_d1:=diff(eta1,t):

> eta1_d2:=diff(eta1_d1,t):

> eta1_d3:=diff(eta1_d2,t):

> eta1_d4:=diff(eta1_d3,t):

> eta2_d1:=diff(eta2,t):

> eta2_d2:=diff(eta2_d1,t):

> eta2_d3:=diff(eta2_d2,t):

> eta2_d4:=diff(eta2_d3,t):

> eta3_d1:=diff(eta3,t):

> eta3_d2:=diff(eta3_d1,t):

> eta3_d3:=diff(eta3_d2,t):

> eta3_d4:=diff(eta3_d3,t):

> nu1_d1:=diff(nu1,t):

> nu1_d2:=diff(nu1_d1,t):

> nu2_d1:=diff(nu2,t):

> nu2_d2:=diff(nu2_d1,t):
```

Solving Optimality and constraint equations

optimality eq. 1

```
> optim1:=eta1_d4+omega1^2*eta1_d2+2*omega1^4*eta1-(A_bar_tran
  [1,1]*omega1^2*(nu1_d2+omega1^2*nu1)):

> alphaterms1:=coeff(optim1,exp(-alpha1*t)):
```

```
> xe1:=coeff(alphaterms1,sin(beta1*t));
```

$$xe1 := 9.575243951\ 10^{5}\ c11\_1 - 35665.9226\ c14\_1 - 2.694375648\ 10^{5}\ c11\_2 - 3.074200784\ 10^{5}\ c14\_2 \tag{3.33}$$

```
> xe2:=coeff(alphaterms1,cos(beta1*t));
```

$$xe2 := 9.575243951\ 10^{5}\ c11\_2 - 35665.9226\ c14\_2 + 2.694375648\ 10^{5}\ c11\_1 + 3.074200784\ 10^{5}\ c14\_1 \tag{3.34}$$

```
> alphaterms2:=coeff(optim1,exp(-alpha2*t)):
> xe3:=coeff(alphaterms2,sin(beta2*t));
```

$$xe3 := -2.33453779\ 10^{7}\ c21\_1 + 7.826654425\ 10^{6}\ c24\_1 - 2.513227191\ 10^{8}\ c21\_2 - 8.939800818\ 10^{6}\ c24\_2 \tag{3.35}$$

```
> xe4:=coeff(alphaterms2,cos(beta2*t));
```

$$xe4 := -2.33453779\ 10^{7}\ c21\_2 + 7.826654425\ 10^{6}\ c24\_2 + 2.513227191\ 10^{8}\ c21\_1 + 8.939800818\ 10^{6}\ c24\_1 \tag{3.36}$$

```
> alphaterms3:=coeff(optim1,exp(-alpha3*t)):
> xe5:=coeff(alphaterms3,sin(beta3*t));
```

$$xe5 := 1.010143834\ 10^{9}\ c31\_1 + 3.118703132\ 10^{7}\ c34\_1 - 2.202723709\ 10^{9}\ c31\_2 - 2.020163867\ 10^{7}\ c34\_2 \tag{3.37}$$

```
> xe6:=coeff(alphaterms3,cos(beta3*t));
```

$$xe6 := 1.010143834\ 10^{9}\ c31\_2 + 3.118703132\ 10^{7}\ c34\_2 + 2.202723709\ 10^{9}\ c31\_1 + 2.020163867\ 10^{7}\ c34\_1 \tag{3.38}$$

optimality eq. 2

```
> optim2:=eta2_d4+omega2^2*eta2_d2+2*omega2^4*eta2-(A_bar_tran
  [2,1]*omega2^2*(nu1_d2+omega2^2*nu1)+A_bar_tran[2,2]*
  omega2^2*(nu2_d2+omega2^2*nu2)):
> alphaterms1:=coeff(optim2,exp(-alpha1*t)):
> ye1:=coeff(alphaterms1,sin(beta1*t));
```

$$ye1 := 3.095103531\ 10^{8}\ c12\_1 - 2.564188022\ 10^{7}\ c14\_1 - 1.500872072\ 10^{8}\ c15\_1 + 4.526102236\ 10^{6}\ c12\_2 - 8.718230452\ 10^{5}\ c14\_2 - 5.102959879\ 10^{6}\ c15\_2 \quad (3.39)$$

```
> ye2:=coeff(alphaterms1,cos(beta1*t));
```

$$ye2 := 3.095103531\ 10^{8}\ c12\_2 - 2.564188022\ 10^{7}\ c14\_2 - 1.500872072\ 10^{8}\ c15\_2 - 4.526102236\ 10^{6}\ c12\_1 + 8.718230452\ 10^{5}\ c14\_1 + 5.102959879\ 10^{6}\ c15\_1 \quad (3.40)$$

```
> alphaterms2:=coeff(optim2,exp(-alpha2*t)):
```

```
> ye3:=coeff(alphaterms2,sin(beta2*t));
```

$$ye3 := 1.625607115\ 10^{8}\ c22\_1 - 3.34485879\ 10^{6}\ c24\_1 - 1.95781475\ 10^{7}\ c25\_1 - 1.118680326\ 10^{8}\ c22\_2 - 2.535268488\ 10^{7}\ c24\_2 - 1.483944873\ 10^{8}\ c25\_2 \quad (3.41)$$

```
> ye4:=coeff(alphaterms2,cos(beta2*t));
```

$$ye4 := 1.625607115\ 10^{8}\ c22\_2 - 3.34485879\ 10^{6}\ c24\_2 - 1.95781475\ 10^{7}\ c25\_2 + 1.118680326\ 10^{8}\ c22\_1 + 2.535268488\ 10^{7}\ c24\_1 + 1.483944873\ 10^{8}\ c25\_1 \quad (3.42)$$

```
> alphaterms3:=coeff(optim2,exp(-alpha3*t)):
```

```
> ye5:=coeff(alphaterms3,sin(beta3*t));
```

$$ye5 := 8.31644260\ 10^{8}\ c32\_1 + 6.290362779\ 10^{7}\ c34\_1 + 3.681878916\ 10^{8}\ c35\_1 - 1.887592170\ 10^{9}\ c32\_2 - 5.729051351\ 10^{7}\ c34\_2 - 3.353331775\ 10^{8}\ c35\_2 \quad (3.43)$$

```
> ye6:=coeff(alphaterms3,cos(beta3*t));
```

$$ye6 := 8.31644260\ 10^{8}\ c32\_2 + 6.290362779\ 10^{7}\ c34\_2 + 3.681878916\ 10^{8}\ c35\_2 + 1.887592170\ 10^{9}\ c32\_1 + 5.729051351\ 10^{7}\ c34\_1 + 3.353331775\ 10^{8}\ c35\_1 \quad (3.44)$$

optimality eq. 3

```
> optim3:=eta3_d4+omega3^2*eta3_d2+2*omega3^4*eta3-(A_bar_tran
  [3,2]*omega3^2*(nu2_d2+omega3^2*nu2)):
```

```
> alphaterms1:=coeff(optim3,exp(-alpha1*t)):
```

```
> ze1:=coeff(alphaterms1,sin(beta1*t));
```

$$ze1 := 4.648245393\ 10^{9}\ c13\_1 - 1.981982776\ 10^{9}\ c15\_1 + 1.899965131\ 10^{7}\ c13\_2 - 1.682067209\ 10^{7}\ c15\_2 \quad (3.45)$$

```
> ze2:=coeff(alphaterms1,cos(beta1*t));
```

$$ze2 := 4.648245393\ 10^{9}\ c13\_2 - 1.981982776\ 10^{9}\ c15\_2 - 1.899965131\ 10^{7}\ c13\_1 + 1.682067209\ 10^{7}\ c15\_1 \quad (3.46)$$

```
> alphaterms2:=coeff(optim3,exp(-alpha2*t)):
> ze3:=coeff(alphaterms2,sin(beta2*t));
```

$$ze3 := 4.131132292\ 10^{9}\ c23\_1 - 1.551791250\ 10^{9}\ c25\_1 + 3.090239488\ 10^{8}\ c23\_2 - 4.891465091\ 10^{8}\ c25\_2 \quad (3.47)$$

```
> ze4:=coeff(alphaterms2,cos(beta2*t));
```

$$ze4 := 4.131132292\ 10^{9}\ c23\_2 - 1.551791250\ 10^{9}\ c25\_2 - 3.090239488\ 10^{8}\ c23\_1 + 4.891465091\ 10^{8}\ c25\_1 \quad (3.48)$$

```
> alphaterms3:=coeff(optim3,exp(-alpha3*t)):
> ze5:=coeff(alphaterms3,sin(beta3*t));
```

$$ze5 := 3.700393204\ 10^{9}\ c33\_1 - 2.73614360\ 10^{8}\ c35\_1 - 9.36485104\ 10^{8}\ c33\_2 - 1.105344653\ 10^{9}\ c35\_2 \quad (3.49)$$

```
> ze6:=coeff(alphaterms3,cos(beta3*t));
```

$$ze6 := 3.700393204\ 10^{9}\ c33\_2 - 2.73614360\ 10^{8}\ c35\_2 + 9.36485104\ 10^{8}\ c33\_1 + 1.105344653\ 10^{9}\ c35\_1 \quad (3.50)$$

constraint eq 1

```
> Const1:=A_bar[1,1]*(eta1_d2+omega1^2*eta1)+A_bar[1,2]*
  (eta2_d2+omega2^2*eta2):
> alphaterms1:=coeff(Const1,exp(-alpha1*t)):
> te1:=coeff(alphaterms1,sin(beta1*t));
```

$$te1 := 46.9393930\ c11\_1 + 404.5910162\ c11\_2 + 2033.030755\ c12\_1 + 69.12297572\ c12\_2 \quad (3.51)$$

```
> te2:=coeff(alphaterms1,cos(beta1*t));
```

$$te2 := 46.9393930\ c11\_2 - 404.5910162\ c11\_1 + 2033.030755\ c12\_2 - 69.12297572\ c12\_1 \quad (3.52)$$

```
> alphaterms2:=coeff(Const1,exp(-alpha2*t)):
```

```
> te3:=coeff(alphaterms2,sin(beta2*t));
```

$$te3 := -10300.54409\,c21\_1 + 11765.53958\,c21\_2 + 265.198992\,c22\_1 + 2010.101742\,c22\_2 \quad (3.53)$$

```
> te4:=coeff(alphaterms2,cos(beta2*t));
```

$$te4 := -10300.54409\,c21\_2 - 11765.53958\,c21\_1 + 265.198992\,c22\_2 - 2010.101742\,c22\_1 \quad (3.54)$$

```
> alphaterms3:=coeff(Const1,exp(-alpha3*t)):
```

```
> te5:=coeff(alphaterms3,sin(beta3*t));
```

$$te5 := -41044.79046\,c31\_1 + 26587.07774\,c31\_2 - 4987.349164\,c32\_1 + 4542.310272\,c32\_2 \quad (3.55)$$

```
> te6:=coeff(alphaterms3,cos(beta3*t));
```

$$te6 := -41044.79046\,c31\_2 - 26587.07774\,c31\_1 - 4987.349164\,c32\_2 - 4542.310272\,c32\_1 \quad (3.56)$$

constraint eq 2

```
> Const2:=A_bar[2,2]*(eta2_d2+omega2^2*eta2)+A_bar[2,3]*
  (eta3_d2+omega3^2*eta3):
```

```
> alphaterms1:=coeff(Const2,exp(-alpha1*t)):
```

```
> le1:=coeff(alphaterms1,sin(beta1*t));
```

$$le1 := 11899.74781\,c12\_1 + 404.5910162\,c12\_2 + 40961.97269\,c13\_1 + 347.6356705\,c13\_2 \quad (3.57)$$

```
> le2:=coeff(alphaterms1,cos(beta1*t));
```

$$le2 := 11899.74781\,c12\_2 - 404.5910162\,c12\_1 + 40961.97269\,c13\_2 - 347.6356705\,c13\_1 \quad (3.58)$$

```
> alphaterms2:=coeff(Const2,exp(-alpha2*t)):
```

```
> le3:=coeff(alphaterms2,sin(beta2*t));
```

$$le3 := 1552.26433\,c22\_1 + 11765.53958\,c22\_2 + 32071.13179\,c23\_1 + 10109.27350\,c23\_2 \quad (3.59)$$

```
> le4:=coeff(alphaterms2,cos(beta2*t));
```

$$le4 := 1552.26433\ c22\_2 - 11765.53958\ c22\_1 + 32071.13179\ c23\_2 - 10109.27350\ c23\_1 \quad (3.60)$$

```
> alphaterms3:=coeff(Const2,exp(-alpha3*t)):
```

```
> le5:=coeff(alphaterms3,sin(beta3*t));
```

$$le5 := -29191.98205\ c32\_1 + 26587.07774\ c32\_2 + 5654.83417\ c33\_1 + 22844.34459\ c33\_2 \quad (3.61)$$

```
> le6:=coeff(alphaterms3,cos(beta3*t));
```

$$le6 := -29191.98205\ c32\_2 - 26587.07774\ c32\_1 + 5654.83417\ c33\_2 - 22844.34459\ c33\_1 \quad (3.62)$$

initial condition equations

```
> bc1:=eval(eta1,t=0)=eta_initial[1,1];
```

$$bc1 := 1.\ c11\_2 + 1.\ c21\_2 + 1.\ c31\_2 = 0.05 \quad (3.63)$$

```
> bc2:=eval(eta2,t=0)=eta_initial[2,1];
```

$$bc2 := 1.\ c12\_2 + 1.\ c22\_2 + 1.\ c32\_2 = 0.005 \quad (3.64)$$

```
> bc3:=eval(eta3,t=0)=eta_initial[3,1];
```

$$bc3 := 1.\ c13\_2 + 1.\ c23\_2 + 1.\ c33\_2 = 0.0045 \quad (3.65)$$

```
> bc4:=eval(eta1_d1,t=0)=0;
```

$$bc4 := -7.307830489\ c11\_2 + 27.68201977\ c11\_1 - 50.43651831\ c21\_2 + 116.6371111\ c21\_1 - 62.20241237\ c31\_2 + 213.7142012\ c31\_1 = 0 \quad (3.66)$$

```
> bc5:=eval(eta2_d1,t=0)=0;
```

$$bc5 := -7.307830489\ c12\_2 + 27.68201977\ c12\_1 - 50.43651831\ c22\_2 + 116.6371111\ c22\_1 - 62.20241237\ c32\_2 + 213.7142012\ c32\_1 = 0 \quad (3.67)$$

```
> bc6:=eval(eta3_d1,t=0)=0;
```

$$bc6 := -7.307830489\ c13\_2 + 27.68201977\ c13\_1 - 50.43651831\ c23\_2 + 116.6371111\ c23\_1 - 62.20241237\ c33\_2 + 213.7142012\ c33\_1 = 0 \quad (3.68)$$

Solving for unknown integration constants

```
> solve({te1,te2,te3,te4,te5,te6,ye1,ye2,ye3,ye4,ye5,ye6,ze1,
  ze2,ze3,ze4,ze5,ze6,bc1,bc2,bc3,bc4,bc5,bc6,le1,le2,le3,le4,
  le5,le6},{c11_1,c11_2,c21_1,c21_2,c31_1,c31_2,c12_1,c12_2,
```

```
c22_1,c22_2,c32_1,c32_2,c13_1,c13_2,c23_1,c23_2,c33_1,c33_2,
c14_1,c14_2,c24_1,c24_2,c34_1,c34_2,c15_1,c15_2,c25_1,c25_2,
c35_1,c35_2});
```

$$\{c11\_1 = 0.01325584211,\ c11\_2 = 0.05015344029,\ c12\_1 = -0.01032541814,\ c12\_2 = 0.001129003559,\ c13\_1 = 0.002991890409,\ c13\_2 = -0.0004045786891,\ c14\_1 = -0.1659079849,\ c14\_2 = 0.01657937480,\ c15\_1 = 0.007020643382,\ c15\_2 = -0.0009179363132,\ c21\_1 = 0.0007400557345,\ c21\_2 = -0.0004916131340,\ c22\_1 = -0.0009165539895,\ c22\_2 = 0.006790770545,\ c23\_1 = -0.002035085233,\ c23\_2 = -0.001306410283,\ c24\_1 = -0.01839633081,\ c24\_2 = -0.004217661676,\ c25\_1 = -0.004283737026,\ c25\_2 = -0.004422913612,\ c31\_1 = -0.0004235268123,\ c31\_2 = 0.0003381728422,\ c32\_1 = 0.002629067382,\ c32\_2 = -0.002919774104,\ c33\_1 = 0.002208725527,\ c33\_2 = 0.006210988972,\ c34\_1 = 0.03514007631,\ c34\_2 = -0.003802150879,\ c35\_1 = -0.02085816333,\ c35\_2 = 0.007295233449\} \quad (3.69)$$

```
> assign(%);
```

Defining Functions

```
> etaMat:=matrix(3,1,[eta1,eta2,eta3]):

> etaMat_d1:=matrix(3,1,[diff(eta1,t),diff(eta2,t),diff(eta3,t)
]):

> uMat:=matrix(3,1,[eta1_d2+omega1^2*eta1,eta2_d2+omega2^2*
eta2,eta3_d2+omega3^2*eta3]):

> Fact:=evalm(Bhat_inv&*uMat):

> Fa1:=Fact[1,1]:Fa2:=Fact[2,1]:Fa3:=Fact[3,1]:

> xMat:=evalm(phi&*etaMat):
```

Solving modal gains

```
> Er1:=Fa1+G11d*eta1+G11v*eta1_d1+G21d*eta2+G21v*eta2_d1+G31d*
eta3+G31v*eta3_d1:

> collect_alpha1:=coeff(Er1,exp(-alpha1*t)):

> i1:=coeff(collect_alpha1,sin(beta1*t));
```

$$i1 := -158.6892796 + 0.01325584211\ G11d - 1.485219973\ G11v - 0.01032541814\ G21d + 0.04420330666\ G21v + 0.002991890409\ G31d - 0.01066467268\ G31v \quad (3.70)$$

```
> i2:=coeff(collect_alpha1,cos(beta1*t));
```

$$i2 := 22.83173914 + 0.05015344029\ G11d + 0.0004356433\ G11v + 0.001129003559\ G21d - 0.2940789957\ G21v - 0.0004045786891\ G31d + 0.08577816193\ G31v \quad (3.71)$$

```
> collect_alpha2:=coeff(Er1,exp(-alpha2*t)):
```

```
> i3:=coeff(collect_alpha2,sin(beta2*t));
```

$$i3 := 101.7296241 + 0.0007400557345\ G11d + 0.02001450113\ G11v - 0.0009165539895\ G21d - 0.7458280664\ G21v - 0.002035085233\ G31d + 0.2550185349\ G31v \quad (3.72)$$

```
> i4:=coeff(collect_alpha2,cos(beta2*t));
```

$$i4 := 27.64427310 - 0.0004916131340\ G11d + 0.1111132178\ G11v + 0.006790770545\ G21d - 0.4494070324\ G21v - 0.001306410283\ G31d - 0.1714756762\ G31v \quad (3.73)$$

```
> collect_alpha3:=coeff(Er1,exp(-alpha3*t)):
```

```
> i5:=coeff(collect_alpha3,sin(beta3*t));
```

$$i5 := -200.1240934 - 0.0004235268123\ G11d - 0.04592794941\ G11v + 0.002629067382\ G21d + 0.4604628569\ G21v + 0.002208725527\ G31d - 1.464764603\ G31v \quad (3.74)$$

```
> i6:=coeff(collect_alpha3,cos(beta3*t));
```

$$i6 := 19.87911880 + 0.0003381728422\ G11d - 0.1115488610\ G11v - 0.002919774104\ G21d + 0.7434860282\ G21v + 0.006210988972\ G31d + 0.0856975144\ G31v \quad (3.75)$$

```
> solve({i1,i2,i3,i4,i5,i6},{G11d,G11v,G21d,G21v,G31d,G31v});
```

$$\{G11d = 423.8937990,\ G11v = -151.1040783,\ G21d = 1348.218826,\ G21v = 151.4094039,\ G31d = -21842.42558,\ G31v = -114.9295123\} \quad (3.76)$$

```
> assign(%);
```

plots

```
> plot(eta1,t=0..0.6):
```

```
> plot(eta2,t=0..0.6,numpoints=800):
> plot(eta3,t=0..0.6,numpoints=800):
> plot(uMat[1,1],t=0..0.6):
> plot(uMat[2,1],t=0..0.6):
> plot(uMat[3,1],t=0..0.6):
> plot(Fa1,t=0..0.6):
> plot(Fa2,t=0..0.6):
> plot(Fa3,t=0..0.6):
> plot({xMat[27,1],xMat[7,1]},t=0..0.6,numpoints=1000):
>
```

APPENDIX B: ON OBTAINING GAINS

This appendix presents a detailed discussion on how gains may be obtained when using the CMSOC method. The method can be easily carried out using the MAPLE program, for which the necessary program commands are given in Appendix A for the plane frame problem.

In modal-space, a system's output vector $\boldsymbol{y}$ must be written in terms of modal variables by substituting (2.9*a*) into (3.21) to obtain:

$$\boldsymbol{y} = \boldsymbol{C_d}\boldsymbol{\Phi}\boldsymbol{\eta} + \boldsymbol{C_v}\boldsymbol{\Phi}\dot{\boldsymbol{\eta}} = [\boldsymbol{C_d}\boldsymbol{\Phi} \quad \boldsymbol{C_v}\boldsymbol{\Phi}]\begin{bmatrix}\boldsymbol{\eta}\\ \dot{\boldsymbol{\eta}}\end{bmatrix} = \widetilde{\boldsymbol{C}}\boldsymbol{N} \tag{A.1}$$

The matrix $\widetilde{\boldsymbol{C}} = [\boldsymbol{C_d}\boldsymbol{\Phi} \quad \boldsymbol{C_v}\boldsymbol{\Phi}]$, of size $n_s \times 2n_m$, will be referred to as the modal observability matrix because it transfers the modal state vector $\boldsymbol{N} = [\boldsymbol{\eta}^T \quad \dot{\boldsymbol{\eta}}^T]^T$ into the output vector $\boldsymbol{y}$. It indicates how well suited a particular sensor location is for measuring various modes of vibration in the system.

Actuation forces can be related to the modal state vector by substituting the output vector in the form (A.1) into the feedback equation (3.22) to yield the equations:

$$\boldsymbol{F_a} = \boldsymbol{G}\widetilde{\boldsymbol{C}}\boldsymbol{N} = -\boldsymbol{G_d}\boldsymbol{\Phi}\boldsymbol{\eta} - \boldsymbol{G_v}\boldsymbol{\Phi}\dot{\boldsymbol{\eta}} = -\boldsymbol{g_d}\boldsymbol{\eta} - \boldsymbol{g_v}\dot{\boldsymbol{\eta}} \tag{A.2}$$

The modal gains matrices $\boldsymbol{g_d}$ and $\boldsymbol{g_v}$ contain $2n_a n_m$ components $g_{d_{ij}}$and $g_{v_{ij}}$, where $i = 1, \dots, n_m$ and $j = 1, \dots, n_a$. In modal-space the feedback relation (A.2) can be substituted into equations (3.1) and (2.12) to obtain:

$$\boldsymbol{I}\ddot{\boldsymbol{\eta}} + \left(\boldsymbol{\Delta} + \widehat{\boldsymbol{B}}\boldsymbol{g_v}\right)\dot{\boldsymbol{\eta}} + \left(\boldsymbol{\Omega} + \widehat{\boldsymbol{B}}\boldsymbol{g_d}\right)\boldsymbol{\eta} = \boldsymbol{0} \tag{A.3}$$

To obtain the n_a actuation forces F_{a_j} contained in vector $\boldsymbol{F_a}$ the solution functions (3.20) are substituted into equations (3.4) with the appropriate substitution from (2.12) to obtain:

$$F_{a_j} = \sum_{k=1}^{n_m} e^{-\alpha_k t}\left[\tilde{c}_{kj}^1 sin(\beta_k t) + \tilde{c}_{kj}^2 cos(\beta_k t)\right] \tag{A.4}$$

It can be shown through appropriate mathematical substitutions that the coefficients $\tilde{c}_{kj}^1$ and $\tilde{c}_{kj}^2$ are related to the integration constants c_{kj}^1 and c_{kj}^2 in (3.20) and to the gains in (A.2) by:

$$\tilde{c}_{kj}^1 = \sum_{i=1}^{n_m}\left\{g_{v_{ij}}(\alpha_k c_{ki}^1 + \beta_k c_{ki}^2) - g_{d_{ij}} c_{ki}^1\right\} \tag{A.5a}$$

$$\tilde{c}_{kj}^2 = \sum_{i=1}^{n_m}\left\{g_{v_{ij}}(\alpha_k c_{ki}^2 - \beta_k c_{ki}^1) - g_{d_{ij}} c_{ki}^2\right\} \tag{A.5b}$$

The algebraic equations contained in (A.5*a*) and (A.5*b*) contain $2n_m n_a$ equations that can be solved for an equal number of unknown gains $g_{d_{ij}}$ and $g_{v_{ij}}$ contained in modal gains matrices $\boldsymbol{g_d}$ and $\boldsymbol{g_v}$, respectively. These gains are independent of the initial conditions despite the fact that these conditions were used in calculating the integration constants c_{ki}^1 and c_{ki}^2.

It is possible to obtain the gains $\boldsymbol{g_d}$ and $\boldsymbol{g_v}$ without intermediately calculating the integration constants that are dependent on initial conditions as described above. This is performed by substituting the solution functions (3.20) into equations (A.3) and then using the method of undetermined coefficients to obtain $2n_m n_a$ algebraic equations from which all unknown gains $g_{d_{ij}}$ and $g_{v_{ij}}$ may be determined (without consideration for initial conditions).

In order to obtain constant modal gains in matrices $\boldsymbol{g_d}$ and $\boldsymbol{g_v}$ all system states, which includes the positions and velocities of all n_m modal variables ($2n_m$ states in total), must be observed by sensors. In other words, each state that is to be controlled using a constant gain feedback relation must be observed, which requires that the number of sensors must be equal in number to the modes of vibration that are to be controlled ($n_s = n_m$). If fewer than the required

$2n_m$ states are observed than the modal gains must vary with time to satisfy the feedback relation (A.2).

The modal state vector $\boldsymbol{N}$ is determined by manipulating equations (A.1) to obtain:

$$\boldsymbol{N} = \begin{bmatrix} \boldsymbol{\eta} \\ \dot{\boldsymbol{\eta}} \end{bmatrix} = \left(\widetilde{\boldsymbol{C}}^T \widetilde{\boldsymbol{C}}\right)^{-1} \widetilde{\boldsymbol{C}}^T \boldsymbol{y} \tag{A.6}$$

The existence of operation (A.6) is required for the system with $n_s = n_m$ position and velocity sensors to be considered observable (i.e. $\left(\widetilde{\boldsymbol{C}}^T \widetilde{\boldsymbol{C}}\right)^{-1}$ must be defined). Formally, the gains matrix $\boldsymbol{G}$ transferring the sensor output vector $\boldsymbol{y}$ into to the actuation force vector $\boldsymbol{F_a}$, in accordance with equations (3.22), may then be obtained from:

$$\boldsymbol{G} = [\boldsymbol{g_d} \quad \boldsymbol{g_v}]\left(\widetilde{\boldsymbol{C}}^T \widetilde{\boldsymbol{C}}\right)^{-1} \widetilde{\boldsymbol{C}}^T \tag{A.7}$$

APPENDIX C: PERFORMING THE VERIFICATION STAGE

This appendix presents the complete details for performing the verification stage using the ANSYS FEM program, the MAPLE program, and the EXCEL program. In this appendix the results of the verification stage are provided for the three level plane frame problem described in Section 5.4.

C.1 Overview of the Frame Problem

The frame structure under consideration is consistent with that of Chapter 5, which is shown in Figure 5-1*a*. Figure C-1*a* and C-1*b* shows the actuator that is employed in this example along with the first four dominant mode shapes. The solution for the problem with the single actuator exerting the actuation force, $F_{act}(t)$, on nodes 7 and 13 to control the first two modes of vibration is considered. This structural stage and control stage of this solution were covered in detail in Chapter 5.

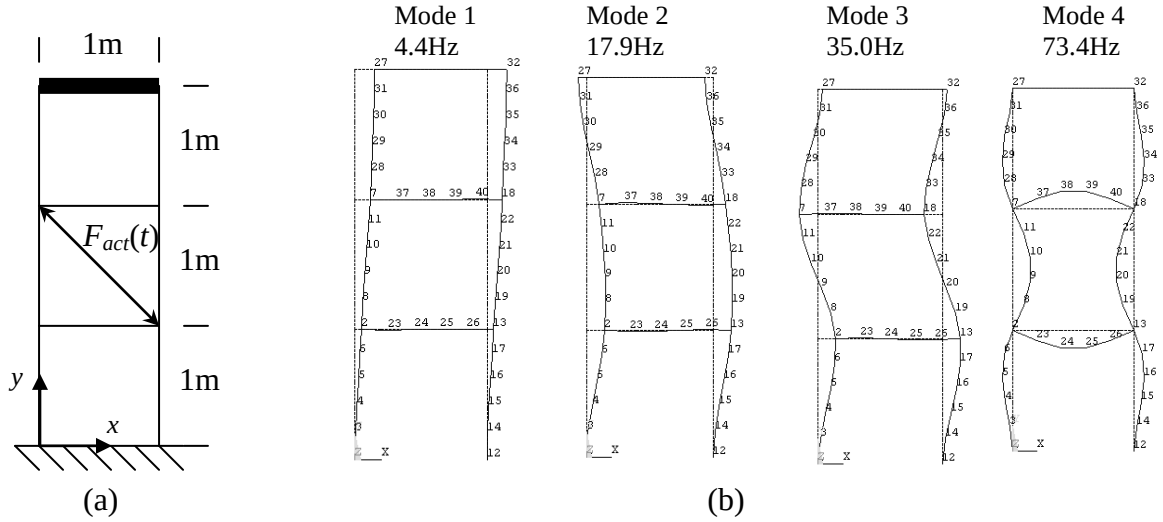

Figure C-1. (a) Frame structure and (b) its four dominant mode shapes.

The analytical solution of the optimal attenuation problem, subjected to the initial disturbance described by $\eta_1(0) = 0.005$ and $\eta_2(0) = 0.002$ From this solution the trajectory of the actuation force, $F_{act}(t)$, as well as the response of response of node 7 in the x direction, d_x^7, are obtained; these functions are plotted in Fig. 2a and 2b, respectively.

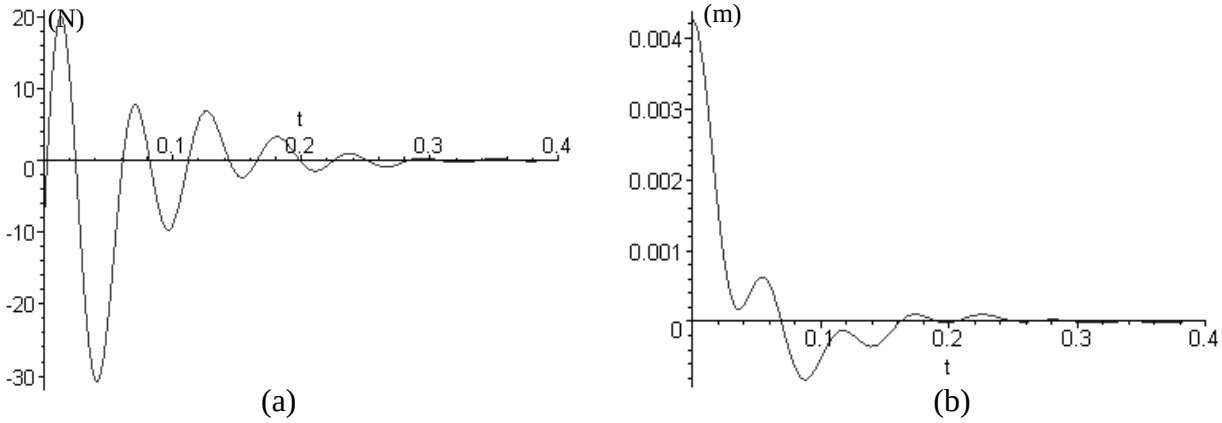

Figure C-2. (a) Actuator force histogram, Fact(t), and (b) the displacement response, d_x^7 (t).

These analytical solutions, characterized by the plots of Figure C-2, are checked in the verification stage, covered in the following discussion. The ANSYS model should produce a nearly identical response, d_x^7, when subjected to the force, $F_{act}(t)$. However, the first step in this verification process is to transfer the function, $F_{act}(t)$, obtained analytically from the MAPLE program, into a discrete form, $F_{act}(n\Delta t)$, that can be implemented in ANSYS (where Δt is a chosen time step for discretization and n=0,1,2…).

C.2 Transferring Optimal Control Forces from MAPLE to ANSYS

The function $F_{act}(t)$ is obtained in MAPLE and input into a two column table of increasing time steps, Δt, and the corresponding actuation force, $F_{act}(n\Delta t)$, at that particular increment time increment n. This task is accomplished using the formulaic and automatic cell-referencing capabilities of EXCEL, as demonstrated in Figure C-3. Additional columns

representing the respective components of $F_{act}(n\Delta t)$ at nodes 7 and 13 are also included in this table. Subsequently, the columns of time and nodal forces are copied to text files that can easily be input into the ANSYS program, which is also shown in Figure C-3.

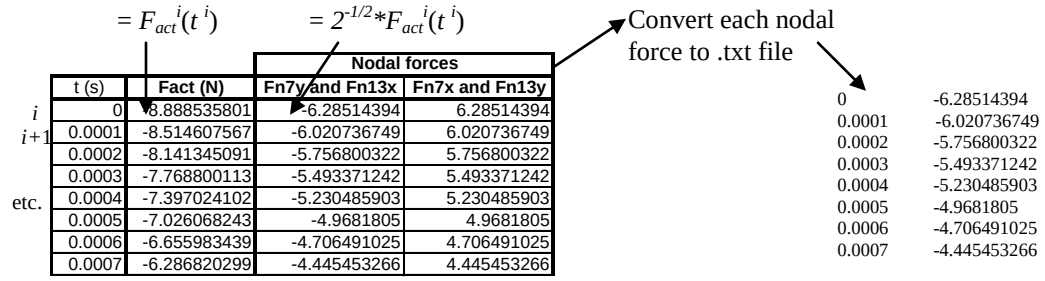

Figure C-3. Data manipulations involved in transferring forces from MAPLE to ANSYS.

Only the first eight time steps are shown in Figure C-3, whereas the entire table actually consists of 581 entries – up to a final time of 0.4s. Also note that the time increment, Δt, was chosen as 0.0001s, for $0 < t < 0.01$s; 0.0005, for $0.0105 < t < 0.1$s; and 0.001, for $0.101 < t < 0.4$s. Time increments are lengthened as time increases because $\boldsymbol{F_{act}}(t)$ becomes less transient, and so fewer time steps are needed to accurately describe the trajectory as time progresses. This chosen number of data points is still computationally economic – the text files created are under 15kB and can be read very quickly by the ANSYS program into array parameters of type "TABLE" (as oppose to type 'ARRAY', see [30]).

The advantage of storing the time varying discrete nodal actuation forces as 'TABLE' parameters lies in the capability of denoting the advancing time increment column as a 'primary variable' so that the accompanying 'dependant variable' column automatically adjusts in correspondence with global changes in the primary variable. In this manner the entire table is applied as a nodal force boundary condition and its value automatically updates as time advances in the transient solution process – this permits the use of looping structures to automatically

perform each load step in the transient analysis without the need for manually changing the applied actuation forces. Another attribute that makes 'TABLE' parameters attractive is that values are automatically linearly interpolated if the current global value of the primary variable falls in between tabulated entries.

C.3 Initializing the ANSYS Transient Analysis

The first initializing load step is the most critical and most difficult step in the ANSYS dynamic simulation of an active attenuation problem. In the first load step, the initial conditions of the problem must be written; however in the vibrating frame problem, there are two separate sets of initializing forces to consider: the initial disturbing forces, $\boldsymbol{F}_{dist}$, and the initial actuation force, $F_{act}(0)$. The difficulty lies in choosing the correct order of application of these initial forces.

The forces, $\boldsymbol{F}_{dist}$, displace the structure into the initial deformed configuration that was assumed in the analytical solution, as described by the initial modal conditions, $\eta_1(0) = 0.005$ and $\eta_2(0) = 0.002$. The following degrees of freedom were constrained to deform the frame into this assumed initial configuration: 2x, 5x, 7x, 9x, 13x, 15x, 18x, 21x, 27x, 27y, 30x, 32x, 32y, 35x. By assigning the appropriate initializing forces, $\boldsymbol{F}_{dist}$, at these DOFs the exact initial configuration can be accurately approximated (all DOFs must be constrained to obtain this exactly). The chosen selection of DOFs ensures that deviations in unconstrained DOFs are generally less than 0.3% from the exact initial configuration. Refer to the ANSYS command code in Section X for the numerical values of the forces, $\boldsymbol{F}_{dist}$.

The method requires that the initial actuation force components at nodes 7 and 13 are applied when running a static analysis of the frame with the selected DOFs constrained in the deformed configuration. This procedure determines the initializing forces, $\boldsymbol{F}_{dist}$, that are required

at each selected DOF to create the assumed disturbed configuration. In this manner, the set of initial disturbing forces to set the initial conditions, $\boldsymbol{F_{dist}}$, and the non-zero force, $F_{act}(0)$ (consisting of four nodal force components), are applied in the first step at time = 0, while still producing the correct initial disturbed configuration. Then, in the following load step all forces are deleted, and only the nodal actuation force components are applied in the subsequent load steps.

Note that this initializing load step method pertains to a modal superposition ANSYS dynamic analysis; a slight modification must be made when performing a full dynamic analysis. In a full dynamic analysis both initial conditions are applied in a similar manner, only they are applied in two static sub-steps over a small time interval and not at time = 0. Consequently, actuation forces must be correspondingly time shifted by the amount of this first time step. This modified procedure is also demonstrated in Section X. With the correct initial load steps determined, the remaining problem is to choose appropriate time steps and load steps to accurately model the attenuation process.

C.4 Choosing Time Steps and Load Steps

The choice of time steps and load steps has a significant impact on the accuracy of the dynamic FEM model of the attenuation process. Generally, the time step influences the number of Newmark time integrations that are used in computing the system's dynamic response – more steps give better accuracy but at a greater computational cost. On the other hand, the load step influences how often the external actuation forces are updated in the time integration equations. Although typically the load steps and time steps are chosen independently (with typically far fewer load steps), the active attenuation problem is an exception because both the actuation force, $F_{act}(t)$, and the dynamic response of the structure, $\boldsymbol{x}(t)$, involve the same oscillation frequencies. Therefore the choice of time steps and load steps should be similar, particularly in the early

stages of attenuation, when $F_{act}(t)$ is changing most rapidly. In the ANSYS help documentation it is suggested that to effectively capture sinusoidal oscillations time steps should be small enough to capture twenty samples per period [30]. According to this suggestion the time step for the frame structure, modeled dynamically by its first two modes, should be no larger than: $\Delta t = (1/17.9)/20 = 0.00279\,\text{s}$. However, this suggested step was too large, which is evident in Figure C-4, where even smaller time steps (i.e. Δt=0.001 or 0.0005) failed to accurately reproduce the response of the exact MAPLE solution.

In Fig. 4, the *x*-displacement response of node 7, d_x^7, is plotted for time and load steps of 0.001s, 0.0005s, and 0.0001s alongside the exact MAPLE response that was previously shown in Figure C-2. The time steps are chosen to be equal to the load steps because choosing smaller time steps, while leaving load steps unchanged, did not change the overall response, suggesting that the solution accuracy was primarily limited by the time length of load steps.

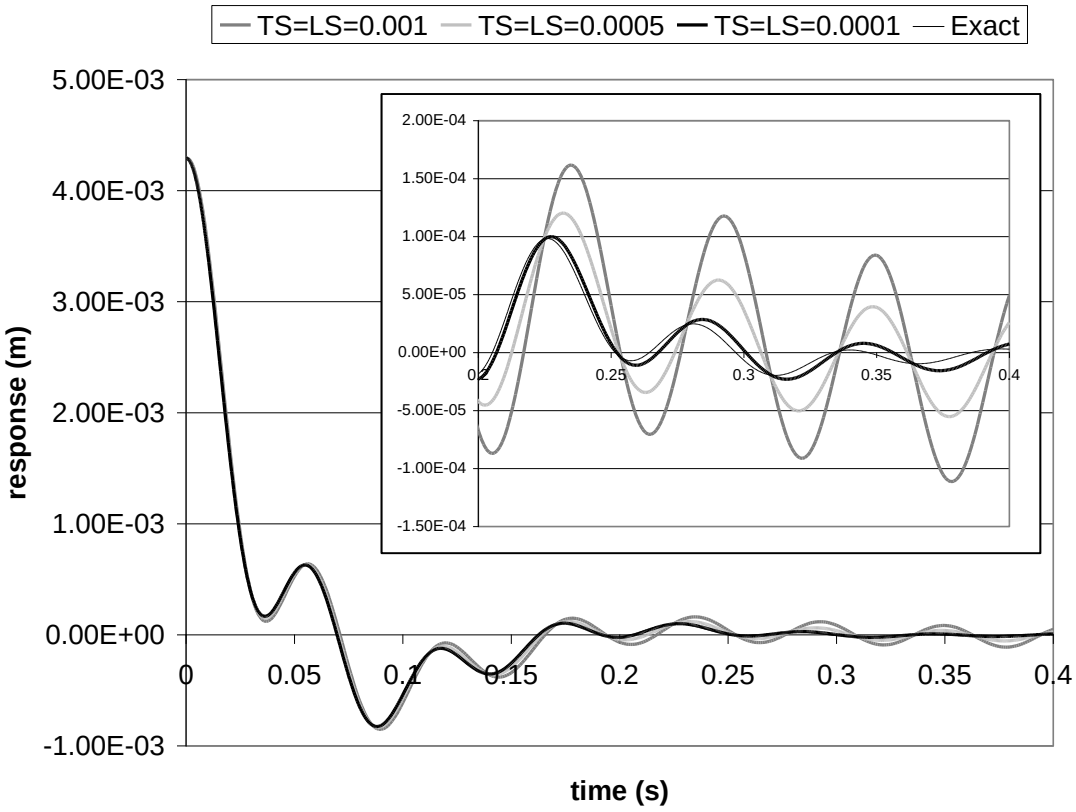

Figure C-4. Plots of d_x^7 (*t*), obtained from FEM for several different time and load steps compared to the exact response. The inset graph shows the last half of the attenuation period.

As expected, Figure C-4 demonstrates that choosing smaller time steps and load steps yields a response closer to the exact response. Also notable in this figure is the fact that errors tend to accumulate as time progresses – in the first 0.03s all curves are nearly indistinguishable but as time progresses the differences between the exact and FEM response grows much larger, especially for the larger time steps. This problem is compounded by the fact that the variation in time of $F_{act}(t)$ is greatest at the beginning of the attenuation period, thus the numerical errors associated with representing it by discrete straight line segments will be most significant during this initial phase. Therefore, initially small errors in d_x^7 (*t*) propagate into large errors at later times, and consequently result in the FEM response failing to reach an attenuated state. This suggests that load steps need to be smallest during the first moments of the attenuation period

and can be increased as time progresses.

In confirmation of this last point, the response, d_x^7 (t), that was obtained with a constant load step of 0.0001s (requiring 4001 load steps in total) was essentially identical to that obtained by using a step of 0.0001s only in the first 100 load steps and then switching to load steps of 0.001s for the remainder of the attenuation period (requiring only 491 load steps in total). Although both produce the same result, the latter solution is computationally much more economic. In the following sections, a common load step scheme is used to perform the ANSYS simulations of the frame structure; however, higher modes of vibration are also of interest so a more computationally expensive load step scheme is chosen as follows: 0.0001s for $0 \le t \le 0.01s$ and 0.0005s for $0.01 < t \le 0.4s$. This requires a total of 881 load steps to cover the attenuation period of 0.4s, as is shown in the ANSYS command code of Section X.

C.5 Comparing the Response of the ANSYS model to the exact MAPLE Solution

The ANSYS FEM response and the exact MAPLE response of the frame model were compared in the previous section as a means of investigating the effect of time steps on the solution; however, this comparison will now be explicitly addressed. To verify the exact response obtained from MAPLE with the first two modes of vibration considered, the mode superposition method must be used to perform the FEM analysis, and these same two modes should be superposed to approximate the dynamic motion. Figure C-5 shows the response, d_x^7, obtained from FEM and that obtained analytically in MAPLE. These plots are essentially identical, verifying that the actuation force, $F_{act}(t)$, does indeed produce the actively dampened response, d_x^7.

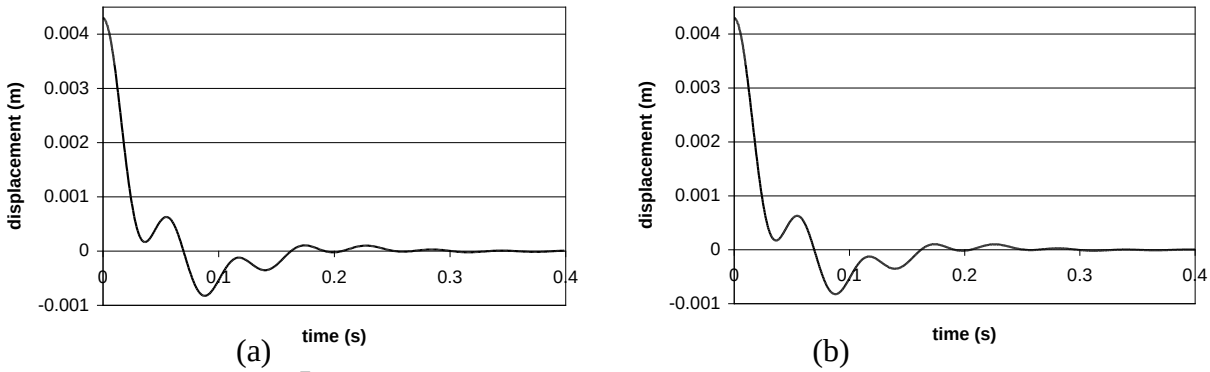

Figure C-5. Response, d_x^7, for the (a) FEM model and (b) analytical model.

C.6 Effect of Higher Modes on Frame' Response

The assumption in solving the active attenuation problem for only the first two modes of vibration is that all higher modes are insignificant. However, by considering these higher modes in the FEM model, the validity of this assumption may be evaluated by checking if the uncontrolled, higher frequency vibration modes are significant in the displacement response. There are two methods of considering these residual vibration modes in ANSYS. One option is to simply use the extra higher frequency modes in the mode superposition method, or another option is to use a full transient analysis, where all DOFs are directly integrated in time, which essentially picks up all modes of vibration (that may be described by the finite number of DOFs).

First, consider a mode superposition solution, where four modes of vibration are included. Figure C-6*a* shows the response, d_x^7, and Figure C-6*b* shows the *y*-displacement response of node 38, d_y^{38}(chosen to capture the motion of the fourth mode). Also, the uncontrolled response of the structure is included in these plots for comparison. On reviewing Figure C-6, it is apparent that one residual mode has a significant effect on the frame's response. These relatively large amplitude residual vibrations are caused by the third mode of vibration, which can be

checked by observing that the residual vibration frequency in both Figure C-6*a* and Figure C-6*b* is 35.0Hz. Note that the oscillations in Figure C-6*a* are roughly 100 times smaller than those in Figure C-6*b* because the first three mode shapes involve no significant relative changes in d_y^{38}. Also note that the fourth mode of vibration is not present in the frame's response, even in the response of d_y^{38}– a DOF that undergoes significant relative deflection in the fourth mode shape. However, this result is not surprising, as the assumed initial disturbed configuration is unable to excite the fourth mode of vibration. One last observation from Figure C-6 is that the free response, as expected, is completely dominated by the first two modes of vibration.

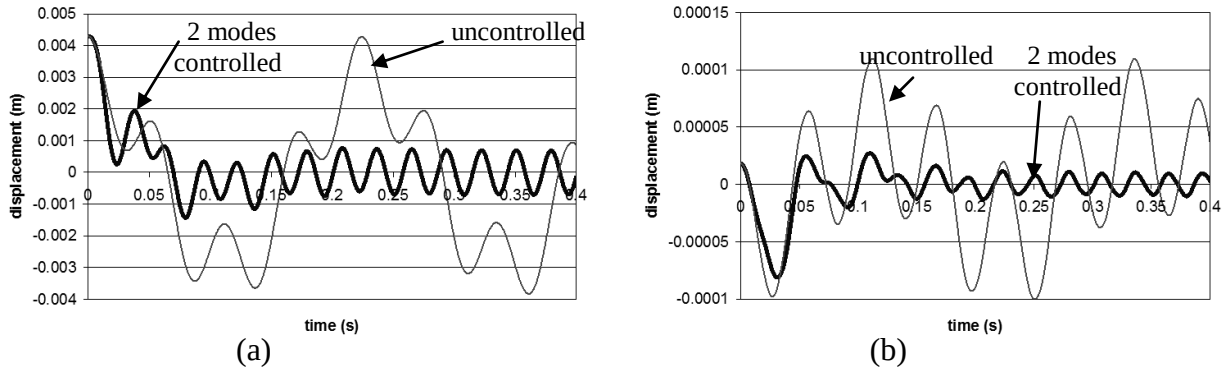

(a) (b)

Figure C-6. (*a*) Response, d_x^7, and response, d_y^{38}, (node 38 in *y*-direction) obtained by superposing first four modes of vibration. Uncontrolled responses are also shown.

To confirm that the system dynamics are accurately modeled in FEM by superposing only the first four vibration modes, a full dynamic analysis is performed to check for any significant presence of higher modes in the response. In Figure C-7 the responses obtained from superposing the first four modes are compared to those obtained in the full DOF analysis. In Figure C-7*a*, there is no distinguishable difference in the response of d_x^7, but in Figure C-7*b* one can see the slight affect of higher vibration modes in the full DOF response of d_y^{38}. Differences are so slight that for practical purposes the mode superposition method provides an equivalent

response at a reduced computational cost. In fact three modes would likely be adequate to model the structures response, as it provides agreement with the full method to an order well below 10^{-6}m.

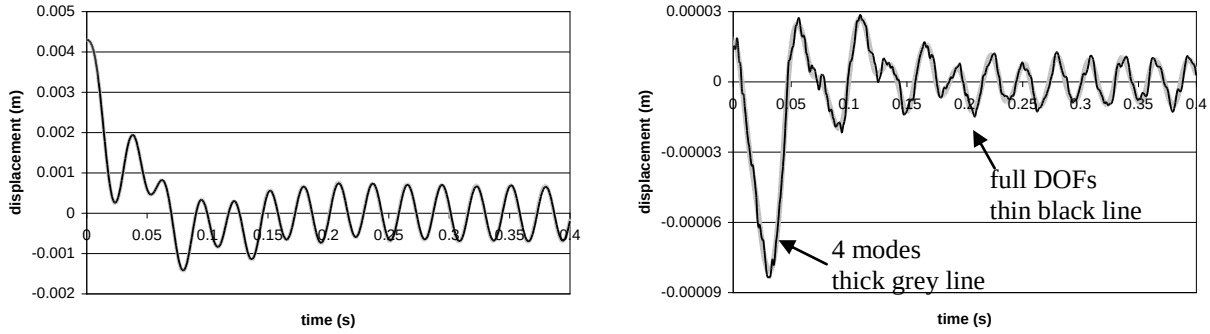

(a) (b)

Figure C-7: (a) Displacement response $X_{7x}(t)$ and (b) $X_{38y}(t)$, obtained by superposing first four modes of vibration compared with those obtained by the full DOF analysis.

C.7 ANSYS Input Codes

The ANSYS input code for performing the modal analysis and performing the modal superposition transient dynamic analysis with four modes considered is:

```
fini
/clear

/filnam,m_t1_bc1
/prep7
/title,truss
et,1,beam3
!acel,,9.8
r,1,76e-6,4585.33e-12,20e-3
r,2,0.0357/100,1.01501e-4,0.2132
mp,ex,1,7.17e10
mp,dens,1,2800
mp,gxy,1,7.17e10/2.6
k,1
k,2,1
k,3,,1
```

```
k,4,1,1
k,5,,2
k,6,1,2
k,7,,3
k,8,1,3
real,1
l,1,3
l,3,5
l,2,4
l,4,6
l,3,4
l,5,7
l,6,8
l,5,6
esize,,5
lmesh,all
real,2
l,7,8
esize,,1
lmesh,all
finish
!initial displacements
!d,2,ux,.00315601
!d,5,ux,.00178415
!d,7,ux,.00429341
!d,9,ux,.00391305
!d,13,ux,.00315601
!d,15,ux,.000941175
!d,18,ux,.00429341
!d,21,ux,.00417508
!d,27,ux,.00304104
!d,27,uy,-.162375e-5
!d,30,ux,.00344938
!d,32,ux,.00304104
!d,32,uy,.162335e-5
!d,35,ux,.00344938

/solu    !modal analysis
d,1,all
d,12,all
antype,modal
modopt,lanb,4
solve
save
```

```
finish

/solu
antype,trans
trnopt,msup,4
outpr,nsol
outres,nsol
deltim,.0001
f,2,fx,4.4721
f,5,fx,1.3528
f,7,fx,-1.7978+6.28514394
f,7,fy,-6.28514394
f,9,fx,2.8826
f,13,fx,12.096-6.28514394
f,13,fy,6.28514394
f,15,fx,1.1068
f,18,fx,3.6931
f,21,fx,2.7329
f,27,fx,-4.3442
f,30,fx,0.24252
f,32,fx,-4.4114
f,35,fx,.42924
f,27,fy,4.2308
f,32,fy,-2.1365
lswrite

fdele,all

*do,k,1,800
 time,.0005*k
 !F,7,fx,%F2_neg%
 !F,7,fy,%F2%
 !F,13,fx,%F2%
 !F,13,fy,%F2_neg%
 !kbc,0
 lswrite
*enddo

save
lssolve,1,801
finish
/solu
expass,on
numexp,all
```

```
solve
finish
```

The ANSYS input code for performing the full transient analysis is:

```
fini
/clear

/filnam,full
/prep7
/title,truss
et,1,beam3
r,1,76e-6,4585.33e-12,20e-3
r,2,0.0357/100,1.01501e-4,0.2132
mp,ex,1,7.17e10
mp,dens,1,2800
mp,gxy,1,7.17e10/2.6
k,1
k,2,1
k,3,,1
k,4,1,1
k,5,,2
k,6,1,2
k,7,,3
k,8,1,3
real,1
l,1,3
l,3,5
l,2,4
l,4,6
l,3,4
l,5,7
l,6,8
l,5,6
esize,,5
lmesh,all
real,2
l,7,8
esize,,1
lmesh,all
finish
!initial displacements
!d,2,ux,.00315601
!d,5,ux,.00178415
```

```
!d,7,ux,.00429341
!d,9,ux,.00391305
!d,13,ux,.00315601
!d,15,ux,.000941175
!d,18,ux,.00429341
!d,21,ux,.00417508
!d,27,ux,.00304104
!d,27,uy,-.162375e-5
!d,30,ux,.00344938
!d,32,ux,.00304104
!d,32,uy,.162335e-5
!d,35,ux,.00344938

!get optimal force from textfile
*dim,F2,table,581,1,1,time
*tread,F2,'F2','txt','E:\ME858\project\'
*dim,F2_neg,table,581,1,1,time
*tread,F2_neg,'F2_neg','txt','E:\ME858\project\'

/solu
antype,trans
trnopt,full
outpr,nsol
outres,nsol
deltim,.0001
timint,off
d,1,all
d,12,all
f,2,fx,4.4721
f,5,fx,1.3528
f,7,fx,-1.7978+6.28514394 !initial actuation force added
f,7,fy,-6.28514394        !initial actuation force added
f,9,fx,2.8826
f,13,fx,12.096-6.28514394 !initial actuation force added
f,13,fy,6.28514394        !initial actuation force added
f,15,fx,1.1068
f,18,fx,3.6931
f,21,fx,2.7329
f,27,fx,-4.3442
f,30,fx,0.24252
f,32,fx,-4.4114
f,35,fx,.42924
f,27,fy,4.2308
f,32,fy,-2.1365
```

```
time,.0001
nsubst,2
kbc,1
lswrite

timint,on
fdele,all

*do,k,2,100
 time,.0001*k
 F,7,fx,%F2_neg%
 F,7,fy,%F2%
 F,13,fx,%F2%
 F,13,fy,%F2_neg%
 kbc,0
 lswrite
*enddo

*do,k,11,400
 time,.001*k
 F,7,fx,%F2_neg%
 F,7,fy,%F2%
 F,13,fx,%F2%
 F,13,fy,%F2_neg%
 kbc,0
 lswrite
*enddo

save
lssolve,1,491
finish
```